FACTORS AFFECTING ASPHALTENES STABILITY

A Dissertation

by

ABHISHEK PUNASE

Submitted to the Office of Graduate and Professional Studies of
Texas A&M University
in partial fulfillment of the requirements for the degree of

DOCTOR OF PHILOSOPHY

Chair of Committee,	Berna Hascakir
Committee Members,	Hisham Nasr-El-Din
	Hadi Nasrabadi
	Yuefeng Sun
Head of Department,	Daniel Hill

May 2017

Major Subject: Petroleum Engineering

ABSTRACT

Asphaltenes represent the heaviest and the most polar fraction of crude oil. Asphaltenes precipitation within the reservoir pores or production flow lines can severely hamper petroleum extraction process. Although the effect of temperature and pressure on asphaltenes deposition is well known, how the oil composition affects the asphaltenes precipitation mechanism requires more clarity. Thus, interaction of asphaltenes with other crude oil fractions and reservoir elements like rock minerals, clays, and reservoir brines were investigated in this work and their impact on overall asphaltenes stability was assessed.

This dissertation analyzes the effect of solubility, electrical charges, and polarity of asphaltenes on its overall stability. Impact of each of these phenomena are described under three distinct sections of this study. In the first part, the effect of asphaltenes solubility and the mutual interaction between different crude oil fractions on asphaltenes stability were evaluated through elemental analysis and stability parameters (ΔPS and Colloidal Instability Index) of 11 crude oil and bitumen samples. In the second part, presence of inorganic minerals originating from reservoir rocks, clays, and reservoir brines on asphaltenes surface was confirmed using Scanning Electron Microscopy (SEM) – Energy Dispersive Spectroscopy (EDS) analyses. The charge distribution on asphaltenes' surface was also studied by measuring electrical properties of the asphaltenes-deionized water supernatant. Finally, in the third part, polarity of asphaltenes and other crude oil fractions were estimated indirectly through dielectric constant measurement using an in-house-built cylindrical capacitor.

It was observed that all three phenomena (solubility, electric charges, and polarity) contributes towards overall asphaltenes stability. However, combined assessment of solubility and polarity aspects yields better estimation of asphaltenes stability. Using the integrated approach, intermolecular forces acting between asphaltenes clusters and other crude oil fractions can be holistically understood. Moreover, strong electrostatic force between charge carrying inorganic minerals present on asphaltenes surface can also influence asphaltenes stability.

Through this dissertation, combined impact of asphaltenes solubility and polarity as well as the contribution of electrical charges induced by the inorganic mineral content of asphaltenes on overall asphaltenes stability are analyzed and described for the first time in literature.

DEDICATION

I dedicate this thesis to my parents, sister, brother-in-law, grandfather (nanaji), family members, and all my friends who have supported and guided me throughout my life.

ACKNOWLEDGEMENTS

Firstly, I would like to express by sincere gratitude towards Dr. Berna Hascakir for providing me with the opportunity to conduct research under her supervision. I thank her for the continuous guidance, support, and encouragement that she provided me throughout the course of this research. Her patience, belief, and involvement have helped me tremendously in my research and I am extremely grateful for having her as my advisor and mentor.

I would also like to extend my deepest gratitude to Dr. Hisham Nasr-El-Din for his supervision as an advisor during my MS and as a guide through my PhD program. His advices and instructions kept me motivated and focused. I am also grateful to Dr. Hadi Nasrabadi and Dr. Yuefeng Sun for serving on my research committee and providing their valuable inputs towards improving my research.

A special thanks to Andreas Prakoso for helping me conduct this research. His support is immensely appreciated. Moreover, I would like to acknowledge the contribution of all the members of the Heavy Oil, Oil shales, Oil sands, and Carbonate Analysis and Recovery Methods (HOCAM) research group for their help and support. My friends and colleagues also deserve thanks for their constant encouragement during the course of my research and for making my time at Texas A&M University an enjoyable one.

Finally, I would like to extend my heartfelt gratitude to my parents, sister, brother-in-law and entire family for their constant support and faith in me.

CONTRIBUTORS AND FUNDING SOURCES

Contributors

This work was supervised by a dissertation committee consisting of Professor Berna Hascakir (advisor), Professor Hisham Nasr-El-Din, and Professor Hadi Nasrabadi of the Department of Petroleum Engineering and Professor Yuefeng Sun of the Department of Geology and Geophysics.

The elemental analysis and solubility profile experiments in Chapter 2 of this dissertation were conducted by Dr. Ceasar Ovalles and Dr. Estrella Rogel of Chevron Energy Technology Company.

All other work conducted for the dissertation was completed by the student independently.

Funding Sources

Graduate study was supported by a fellowship from Texas A&M University and a dissertation research fellowship from Dr. Berna Hascakir's research fund.

NOMENCLATURE

a	Radius of the inner solid cylinder of the capacitor in capacitance design for dielectric constant measurement, cm
API	American Petroleum Institute
ASTM	American Society for Testing and Materials
b	Radius of the co-axial outer cylinder of the capacitor in capacitance design for dielectric constant measurement, cm
C	Capacitance, F
C_{air}	Capacitance of air, F
C_{sample}	Capacitance of sample, F
CHN	Carbon, Hydrogen, and Nitrogen
CII	Colloidal Instability Index
DAO	Deasphalted Oil
dgts	Digits
EDS	Energy Dispersive Spectroscopy
ELSD	Evaporative Light Scattering Detector
EOR	Enhanced Oil Recovery
F	Farad
FE-SEM	Field Emission – Scanning Electron Microscope
FTIR	Fourier Transform InfraRed
H/C	Hydrogen to Carbon ratio by weight
HPLC	High Performance Liquid Chromatography

ICP	Inductively Coupled Plasma
L	Length of the capacitor cylinders in capacitance design for dielectric constant measurement, cm
NaCl	Sodium Chloride
nC5	n-pentane
nC7	n-heptane
ND	Non-detectable
OAP	Onset Asphaltenes Precipitation
PAH	Polycyclic Aromatic Hydrocarbon
pF	Pico-Farad, 10^{-12} F
ppm	Parts per million
rdg	Reading
SARA	Saturates, Aromatics, Resins, and Asphaltenes
SEM	Scanning Electron Microscopy
TDS	Total Dissolved Solids
wt.%	Weight percent
ΔPS	Asphaltenes stability parameter
ρ	Density, g/cm^3
ε_o	Permittivity of vacuum, $8.85x10^{-12}$ F/m
ε_r	Dielectric Constant
μ	Viscosity, cP
μF	micro-Farad, 10^{-6} F

μg/L	Microgram per liter
μS	microsiemens
v	Volume Fraction

TABLE OF CONTENTS

Page

TABLE OF FIGURES

Page

TABLE OF TABLES

Page

1. INTRODUCTION*

Asphaltenes represent the heaviest and the most polar fraction of the crude oil, which remains insoluble in normal alkanes (aliphatic hydrocarbons) but soluble in aromatic solvents (Speight 1991; Li and Firoozabadi 2010; Hoepfner et al. 2013). It consist of complex aliphatic hydrocarbon molecules attached to aromatic and naphthenic rings containing heteroatoms like sulfur, nitrogen, oxygen, and metals (Speight 1991). Maintaining the stability of asphaltenes within the crude oil is important because once destabilized, the polar sides of asphaltenes clusters can interact with each other, and can potentially lead to agglomeration and precipitation of heavy asphaltenes clusters (Speight 1991; Bestougeff and Byramjee 1994). Thermodynamic changes and crude oil compositional variations can result in different interactive environments for asphaltenes and destabilize or precipitate them out (Speight and Long 1996; Peramanu et al. 2001; Buenrostro-Gonzalez et al. 2004; Mullins et al. 2007).

---

*Part of this chapter is reprinted with permission from:
1. "A Mechanistic Understanding of Asphaltenes Precipitation from Varying-Saturate-Concentration Perspectives" by Andreas Prakoso, Abhishek Punase, and Berna Hascakir, 2015. SPE Proceedings, Copyright [2015] by Society of Petroleum Engineers.
2. "Determination of Stability of Asphaltenes through Physicochemical Characterization of Asphaltenes" by Andreas Prakoso, Abhishek Punase, Kristina Klock et al., 2016. SPE Publications, Copyright [2016] by Society of Petroleum Engineers.
3. "The Polarity of Crude Oil Fractions Affects Asphaltenes Stability" by Abhishek Punase, Andreas Prakoso, and Berna Hascakir, 2016. SPE Proceedings, Copyright [2016] by Society of Petroleum Engineers.
4. "Stability Determination of Asphaltenes through Dielectric Constant Measurements of Polar Oil Fractions" by Abhishek Punase and Berna Hascakir, 2017. Energy and Fuels, 31 (1), 65-77, Copyright [2017] by American Chemical Society.
5. "A Mechanistic Understanding of Asphaltenes Precipitation from Varying-Saturate-Concentration Perspectives" by Andreas Prakoso, Abhishek Punase, and Berna Hascakir, 2017. SPE Production and Operations, Copyright [2017] by Society of Petroleum Engineers.

Asphaltenes precipitation can have several detrimental consequences that can significantly reduce the amount of oil production and make the transportation and processing of crude oil more challenging (Leontaritis 1989; Kokal and Sayegh 1995; Amin et al. 2005). Within the reservoir, asphaltenes precipitation can damage the formation by plugging the reservoir pores, alter the wettability towards more oil-wet condition, and increase the viscosity of in-situ oil due to emulsion or sludge formation (Gaspar and Travalloni-Louvisse 1993; Leontaritis et al. 1994; Khalifeh et al. 2013; Seifried et al. 2013; Uetani 2014). Moreover, asphaltenes precipitation within the flow-lines can also cause severe flow assurance issues (Leontaritis 1989; Akbarzadeh et al. 2007). Treatment of the problems associated with asphaltenes deposition is very expensive and may lead to further damage, if the operation fails (Becker 2000; Cenegy 2001). Thus, it is essential to have an in-depth understanding of asphaltenes stability to mitigate the asphaltenes precipitation-related issues.

Most of the studies conducted on asphaltenes stability and molecular structure suggest that the asphaltenes molecules, at stable condition, exist as dispersed colloids which do not coagulate or precipitate due to its balanced net surface charges (Pfeiffer and Saal 1940; Yen 1992; Gawrys and Kilpatrick 2005; Eyssautier et al., 2011). Moreover, some of the recently developed theories and models consider polarity associated with the asphaltenes molecules to be the primary reason for asphaltenes precipitation and formation of nano-aggregates (Goual and Firoozabadi 2002; Akbarzadeh et al. 2007; Mullins 2009; Mullins et al. 2013). Additionally, interaction between different crude oil components and reservoir constituents like clays, rock

minerals, and reservoir brine has also been shown to impact the overall stability of asphaltenes (Mukhametshina et al. 2015; Kar et al. 2015a; Demir et al. 2016a). Therefore, it is imperative to holistically analyze the behavior of asphaltenes in its natural state.

Due to the non-unique and complex molecular composition of crude oils, characterization of individual molecular structures is not practical (Borton et al. 2010; Schuler et al. 2015). Therefore, classification of crude oil into Saturates, Aromatics, Resins, and Asphaltenes (SARA) fractions is a widely used characterization technique (Kharrat et al. 2007). Saturates fraction is composed of straight, cyclic, or branched alkane chains with no double or triple bonds between the carbon atoms. Aromatics fraction incorporates aromatic hydrocarbons with possible traces of oxygen, sulfur, and nitrogen in the molecule. Resins are similar to asphaltenes, but are soluble in higher molecular weight n-alkanes (Jewell et al. 1972). Saturates and aromatics are considered as the non-polar fractions of the crude oil while resins and asphaltenes constitute the polar fractions (Fan and Buckley 2002). However, recent studies have proposed the presence of polar sides within saturate and aromatics fractions (Waldo et al. 1991; Liu et al. 2010; Gaspar et al. 2012, Prakoso et al. 2015). As asphaltenes are soluble in aromatic hydrocarbons and insoluble in normal alkanes, it is expected that while aromatics fraction of crude oil stabilize the asphaltenes, saturates fraction of crude oils will disturb asphaltenes stability (Jamaluddin et al. 1996; Loeber et al. 1998; Wang and Buckley 2003, Wiehe et al. 2012; Punase and Hascakir 2016; Kar et al. 2016). Onset Asphaltenes Precipitation (OAP) tests using regular alkane (n-pentane) and aromatic (toluene)

solvents as well as the crude oil's own saturates and aromatics fractions are conducted to assess the solvent power of different crude oil fractions (Prakoso et al. 2015). Moreover, determination of solubility parameter is also used to evaluate the impact of crude oil composition on asphaltenes stability.

Interaction of crude oil fractions with inorganic reservoir components is reported to generate superficial electrical charges (Demir et al. 2016a; Punase et al. 2017). Asphaltenes are the heaviest fraction of crude oils and their interaction with reservoir rock and salts are inevitable (Speight 1991; Mullins 1998). Even in asphaltenes separation process, crude oil is not charged directly through the percolation column comprising of clay or silica to prevent the irreversible interaction between the asphaltenes fines and the adsorption materials (Jewell et al. 1972; Speight 1991). This interaction is not chemical but physical and occurs when asphaltenes or the reservoir fines are dispersed in each other and as they create electrically charged surfaces (Schuler et al. 2015; Punase et al. 2017). The attractive or repulsive forces between the electrically charged sites may influence the overall stability of asphaltenes. However, the impact of electrical charges on asphaltenes stability has not been investigated yet.

Furthermore, the elements having different electronegativity or asymmetrical bond structure within crude oil fractions can create an unequal distribution of electrons, thus, generating dipoles with partial negative (δ^-) and partial positive (δ^+) charges (Smyth 1929; Pauling 1931; Sidgwick 1936; Nelson et al. 1967). The product of charge density and distance between the centers of positive and negative charges within the molecule is defined as the dipole moment (Feynman et al. 1964). Since the

determination of charge density and charge separation for a mixture of complex molecules like asphaltenes is difficult, direct measurement of polarity or dipole moment is very challenging. Thus, indirect assessment of polarity through measurement of dielectric constant, refractive index, and density is commonly used (Goual and Firoozabadi 2002; Wattana et al. 2005). Due to the limitations associated with dielectric spectroscopic techniques, most of the research related to asphaltenes polarity measurement have been conducted on its dispersed solution in solvents like benzene, xylene, and toluene (Swanson 1942; Maruska and Rao 1987; Halvorson 1997; Ese et al. 1998; Goual and Firoozabadi 2002). Large variation in the reported dielectric constant necessitates a more accurate determination of dielectric properties of pure state solid asphaltenes.

This study investigates the impact of asphaltenes solubility and polarity, as well as the contribution of superficial electrical charge attached to asphaltenes cluster on the overall stability of asphaltenes.

2. PART 1: EFFECT OF SOLUBILITY OF ASPHALTENES ON ASPHALTENES STABILITY*

Abstract

Complex molecular structure, high impurity content, and self-association tendency of asphaltenes makes determination of its phase behavior very difficult. Since, asphaltenes phase behavior is indicative of asphaltenes stability within bulk oil, it is very important to understand its stability. Various production and flow assurance challenges related to precipitation of unstable asphaltenes can be prevented by proper comprehension of asphaltenes stability. This study provides a data set on 11 different asphaltenes which helps us to understand the complicated nature of the components of asphaltenes and crude oils which play an important role in maintaining the stability of asphaltenes. In addition to the physical and chemical characterization, elemental analysis and ΔPS parameter which is the indication of the solubility of asphaltenes in different solvents of the bulk oil samples were measured and evaluated. The results from this study show that the presence of paraffinic wax and water within the crude oil samples along with impurities in the form of reservoir fines can greatly affect the stability of asphaltenes. Organometallic content of crude oil destabilizes asphaltenes, whereas high fines content increases the stability of asphaltenes.

---

*Part of this chapter is reprinted with permission from "Determination of Stability of Asphaltenes through Physicochemical Characterization of Asphaltenes" by Andreas Prakoso, Abhishek Punase, Kristina Klock et al., 2016. SPE Publications, Copyright [2016] by Society of Petroleum Engineers.

Introduction

Asphaltenes are complex hydrocarbon molecules with high heteroatom content (Speight 1991). The change in pressure and temperature conditions of reservoir may result in asphaltenes precipitation which might plug the reservoir pores and/or production and transportation pipelines (Speight 1991). The changes in oil composition due to the interaction with the injected Enhanced Oil Recovery (EOR) fluids may also trigger the asphaltenes flocculation. Precipitation of asphaltenes may also be induced with the presence of clays in the reservoir rock (Mukhametshina et al. 2015; Kar et al. 2015a). Additionally, reservoir salinity may also have an influence on asphaltenes stability, as asphaltenes aggregation tendencies may depend on the type of ions in the reservoir brine and asphaltenes (Demir et al. 2016a). The contribution of all reservoir components on asphaltenes stability is complicated and can be determined through dielectric constant measurements (Punase et al. 2016), dipole moment estimations (Goual and Firoozabadi 2002), zeta potential measurements (Prakoso et al. 2015), onset asphaltenes precipitation tests (Hammami et al. 2000), refractive index measurements (Buckley 1999), and solubility profile analysis (Rogel et al. 2010). Each method follows different procedure by targeting the estimation of different behaviors of asphaltenes in bulk oil. While there are several debates on the asphaltenes molecular structures and their presence within crude oils, these authors believe that all factors (polarity, solvent power, and electrical charges within the crude oil) contribute to determine the asphaltenes stability. However, it is also possible that only one factor might dominate the overall stability of asphaltenes. The non-hydrocarbon component of asphaltenes and

their molecular bonding state has been determined as the dominating factor (Speight 1991). Hence, it is important to first ascertain the non-hydrocarbon components through elemental analysis of asphaltenes to develop a better understanding towards the stability of asphaltenes (Khayan 1984; Meyer and de Witt 1990). Hydrogen and carbon content along with the Hydrogen to Carbon (H/C) ratio determines the aliphatic/aromatic nature of the crude oil molecules (Speight 2014). Still, it should be noted that even hydrogen and carbon may have both organic (hydrocarbons) and inorganic origins (i.e.; bicarbonate and carbonate). Hence, not only the elemental but also the molecular level characterization is necessary. However, due to complex nature of the crude oils and asphaltenes, the characterization of the individual molecular structures is not practical (Borton et al. 2010; Schuler et al. 2015). Still, some fractionation methods can be implemented. Saturates, Aromatics, Resins, and Asphaltenes (SARA) fractionation is a widely used fractionation method for this purpose (Kharrat et al. 2007). SARA fractionation groups the similar chemical structures within the crude oil according to their solubility in different solvents. Since asphaltenes are soluble in aromatic hydrocarbons and insoluble in normal alkanes, it is expected that while aromatics fraction of crude oil stabilize the asphaltenes, saturates fraction of crude oils will disturb asphaltenes stability (Prakoso et al. 2015; Kar et al. 2016). However, since the solubility parameter of saturates and aromatics fractions are not known, their impact on the overall stability of asphaltenes remains unclear.

This study highlights the importance of analyzing asphaltenes in its natural state with the presence of water, brine, and reservoir fines. Interaction of these elements with

asphaltenes can impact its overall solubility and stability. Simple correlations are developed to understand the impact of elemental composition of crude oil as well as the interaction of asphaltenes with other crude oil fractions and reservoir fines on asphaltenes behavior.

Experimental Procedure

11 different crude oil and bitumen samples from Canada, Colombia, Indonesia, Mexico, USA, and Venezuela were first characterized with their viscosity; API gravity; the amount of Saturates, Aromatics, Resins, and Asphaltenes (SARA) fractions; and carbon, hydrogen, nitrogen (CHN), and metal contents. Brookfield DV-III Ultra rheometer was used to measure the viscosity of the samples at ambient temperature (22.3 °C). The density values were measured at standard conditions using Anton Paar DMA 4100 Density Meter. The ASTM (ASTM D2007-11) method (using n-pentane) was followed to determine SARA fractions of each crude oil sample based on their solubility in different solvents and adsorption affinity towards the attapulgus clay and silica gel. A schematic representation of the SARA process followed based on the ASTM D2007-11 method is shown in Fig. 2.1.

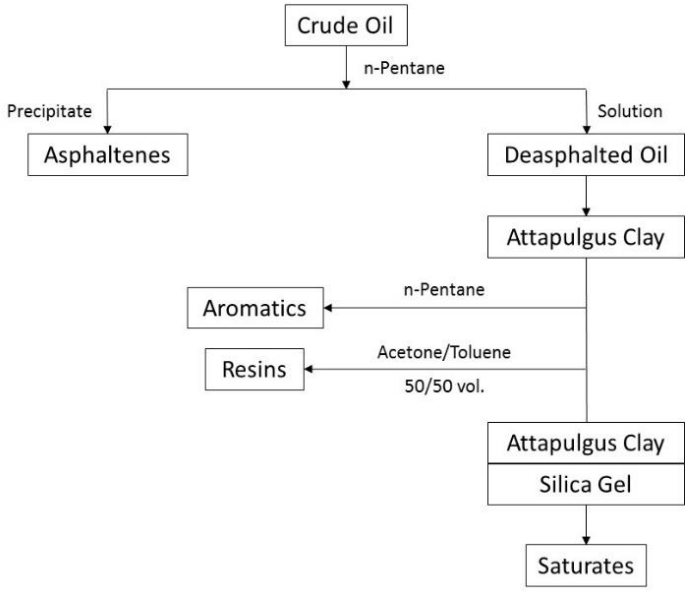

Fig. 2.1 – SARA fractionation process based on ASTM D2007-11 method.

From the schematic, it can be observed that the crude oil is initially treated with n-pentane to separate asphaltenes from other crude oil fractions (called as deasphalted oil). This procedure is carried out to prevent the interaction between polar asphaltenes fraction with the adsorption materials. Saturates being the non-polar fraction of deasphalted oil, when washed with n-pentane, flows through the adsorption columns without getting adsorbed and is collected at the bottom of the assembly. Aromatics fraction on the other hand, can contain heteroatoms and have partial polarity associated with it leading to its adsorption onto the attapulsgus clay. Thus, the upper column is attached to an extraction assembly refluxing toluene and aromatics fraction is recovered. For extraction of resins fraction, which is the most polar fraction within the deasphalted oil, continuous rinsing of attapulgus clay with 50/50 volume percent mixture of toluene and acetone is carried out. The solvent mixture cleans the entire sand column and yields entire adsorbed resins fraction.

Standard combustion method, using a Leco CHN analyzer Carlo Erba model was used to estimate the carbon, hydrogen, and nitrogen content in the test sample. The metal content of samples was determined by Thermo Intrepid Inductively Coupled Plasma (ICP).

Evaluation of the asphaltenes stability within the crude oil is difficult due to unknowns associated with asphaltenes fraction of crude oil (Speight 1991). Due to the non-unique molecular composition of asphaltenes, it is difficult to assess its natural stable state. Several studies suggest that the asphaltenes exist as dispersed colloids which do not coagulate or precipitate due to its balanced net surface charges (Pfeiffer and Saal 1940; Yen 1992; Gawrys and Kilpatrick 2005; Eyssautier et al. 2011). However, some recently developed theories consider the asphaltenes polarity to be primarily influence its stability (Punase et al. 2016; Guoal and Firoozabadi 2002; Akbarzadeh et al. 2007; Mullins 2009; Mullins et al. 2013). The varying views pertaining to asphaltenes molecular structure and interaction tendency makes the evaluation of asphaltenes stability within the crude oil extremely challenging. One method which provides good estimation of the asphaltenes stability is the solubility profile of crude oils (Rogel et al. 2010). The solubility profile of asphaltenes measures the solubility distribution of asphaltenes molecules and relates their solubility properties towards their tendencies to precipitate. The asphaltenes solubility profile involves the precipitation of asphaltenes in a column packed with an inert material using n-heptane as the mobile phase. After maltenes have eluted, the mobile phase is changed gradually from pure n-heptane to 90/10 methylene chloride/methanol and then to 100% methanol. Detection and

quantification of the eluent is conducted by using Alltech Evaporative Light Scattering Detector (ELSD) 2000 detector and HP series 1100 High Performance Liquid Chromatography (HPLC) chromatograph. The solubility profiles were analyzed to obtain a ΔPS parameter, which represents the time taken for the elution of the middle 50% area (between 25% and 75%) distribution of the solubility profile. Since ΔPS is calculated by the time taken for the elution of the sample, it has a unit minutes. Higher ΔPS parameter value indicates higher instability of asphaltenes (Rogel et al. 2010). Fig. 2.2 is provided as an example to describe the interpretation of solubility profiles and calculation of the ΔPS parameters for samples C2, C3, C6, and C5.

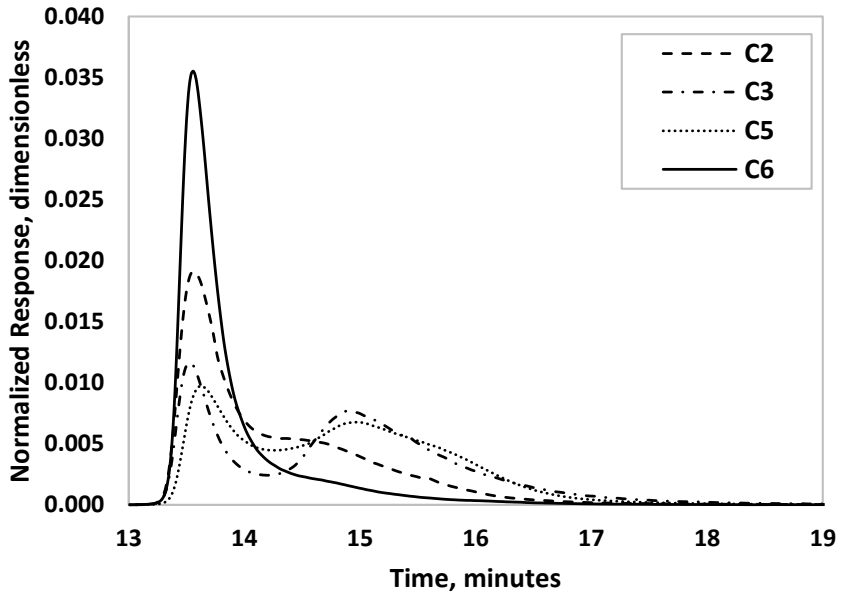

Fig. 2.2 – Asphaltenes solubility profile comparison for samples C2, C3, C6, and C5.

Figure reprinted with permission from "Determination of Stability of Asphaltenes through Physicochemical Characterization of Asphaltenes" by Andreas Prakoso, Abhishek Punase, Kristina Klock et al., 2016. SPE Publications, Copyright [2016] by Society of Petroleum Engineers.

In the above figure, the distribution of normalized absorbance of the sample constituents on to the chromatography column with respect to elution time is described. As the distribution extends further to the right, the sample is expected to contain heavier molecules or more strongly-bonded molecules (more polar) which require longer time to dissolve. Thus, two distinct types of distribution can be observed; unimodal (one peak in the graph) and bimodal (two peaks in the graph) distribution. Unimodal distribution denotes similar solubility behavior for the all of the components within the sample. On the other hand, bimodal distribution means that there are two different groups of molecules which are insoluble within one another. In Fig. 2.2, samples C2 and C6 display unimodal distribution with sample C2 having a small shoulder, whereas sample C3 and C5 show bimodal distribution. Solubility profile of sample C3 shows the most apparent separation within the two peaks, which was expected due to the presence of wax within the sample that is fundamentally different from the average asphaltenes molecules and will be discussed in details in the later sections. The solubility profile of crude oils was measured for all 11 samples and the results are given in Fig. 2.3.

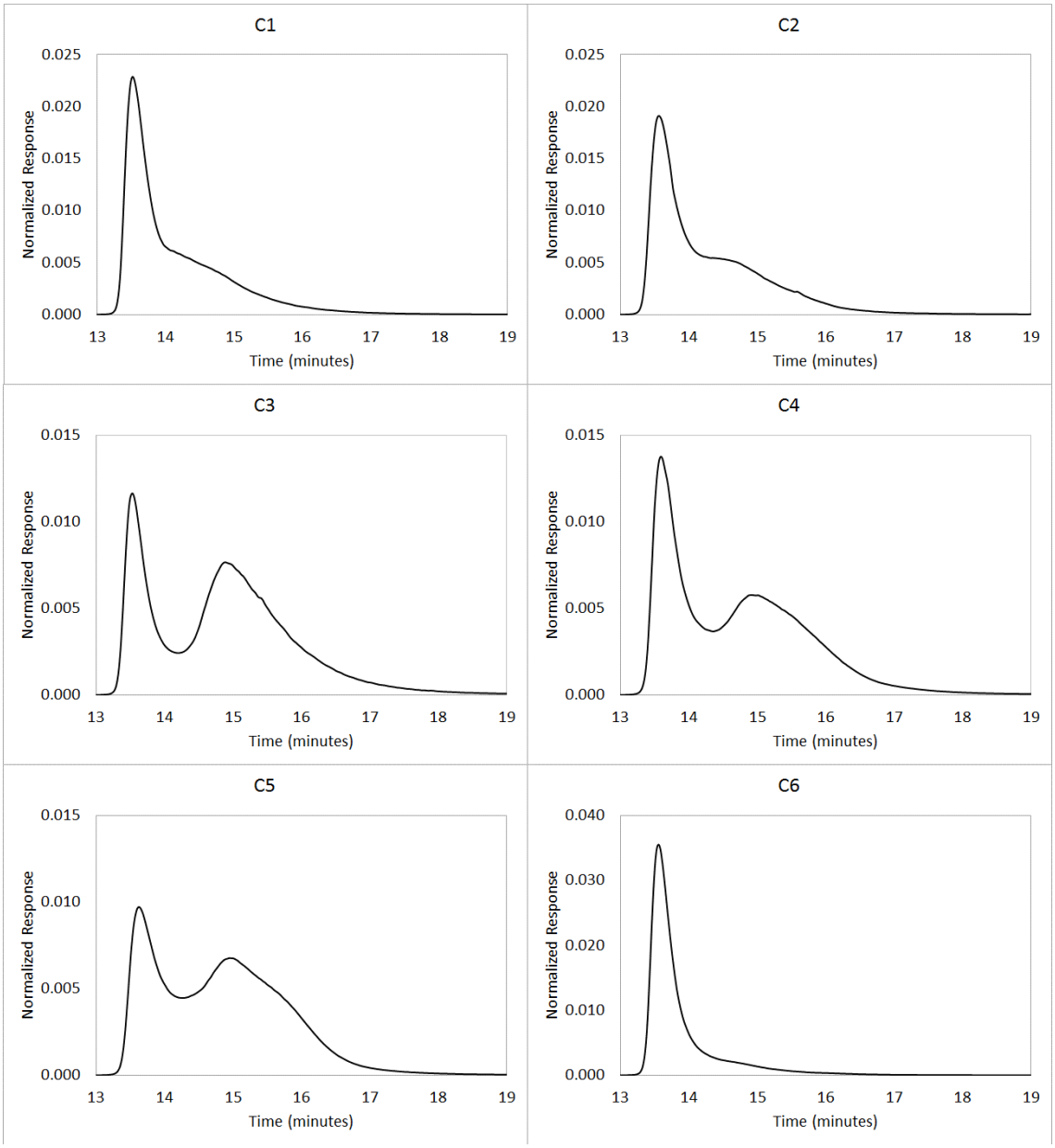

Fig. 2.3 – Asphaltenes solubility profile of 11 crude oil samples.

Figure reprinted with permission from "Determination of Stability of Asphaltenes through Physicochemical Characterization of Asphaltenes" by Andreas Prakoso, Abhishek Punase, Kristina Klock et al., 2016. SPE Publications, Copyright [2016] by Society of Petroleum Engineers.

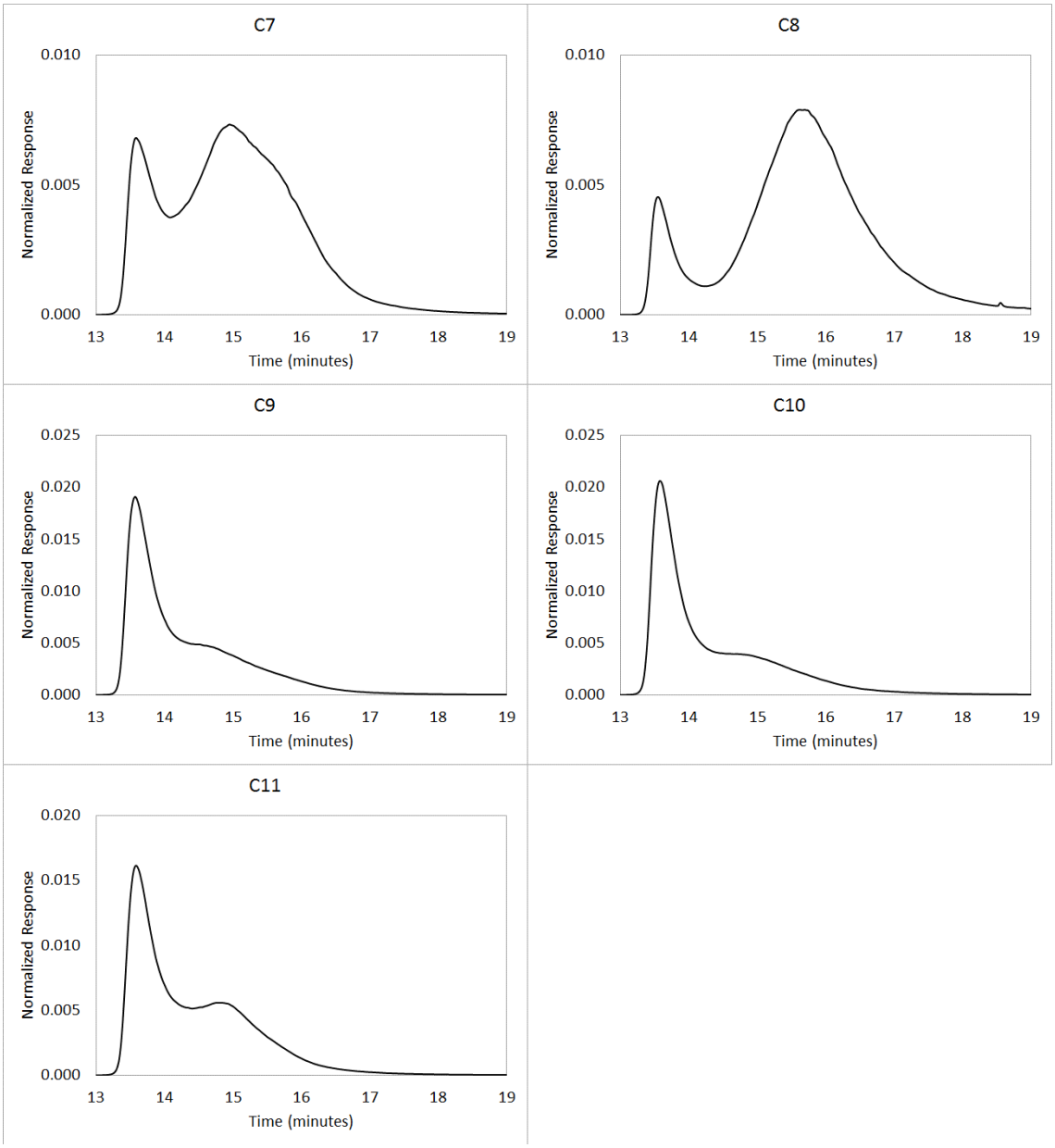

Fig. 2.3 cont. – Asphaltenes solubility profile of 11 crude oil samples.

Figure reprinted with permission from "Determination of Stability of Asphaltenes through Physicochemical Characterization of Asphaltenes" by Andreas Prakoso, Abhishek Punase, Kristina Klock et al., 2016. SPE Publications, Copyright [2016] by Society of Petroleum Engineers.

It should be noted that the ΔPS measurement is very accurate with a standard deviation of about 0.05 (approximately 4%). For clarity, sample calculation of ΔPS measurement is shown in the following section.

Sample Calculation for ΔPS

Solubility profile of crude oil C1 is shown below (Fig. 2.4) and the region corresponding to middle 50% area of distribution is shaded. As described previously, ΔPS represents the time taken to elute the material corresponding to the 50% middle area of the distribution. Mathematically, this concept is represented by Eq. 2.1.

$$\Delta PS = t(75\%) - t(25\%) \tag{2.1}$$

Where, t(75%) and t(25%) represent the time that it takes to elute the material corresponding to 75% and 25% area, respectively. The time corresponding to t(25%) and t(75%) in this case is around 14.5518 and 13.5118 minutes, respectively. Therefore, ΔPS for this sample equals 1.04 minutes.

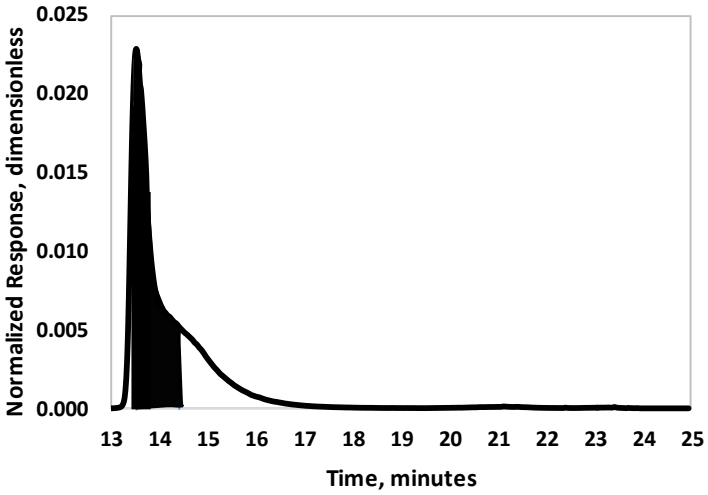

Fig. 2.4 – Solubility profile of sample C1. The black shaded region represent the middle 50% area distribution of the curve.

Experimental Results and Discussion

11 different crude oil and bitumen samples were first characterized in terms of their density, viscosity, SARA (Saturates, Aromatics, Resins, and Asphaltenes) fractions, and the ΔPS parameter. All the analyses were conducted on the original bulk oil sample (as shown in Fig. 2A-1) without any pre-treatment to maintain its natural state. As observed, API gravity and viscosity of the crude oil samples have great variation, ranging from 6.11 to 27.05 °API and from 500 to 19,000,000 cP, which enables us to visualize the behavior of asphaltenes (as shown in Fig. 2A-2) of different crude oils having different properties (Table 2.1).

Table 2.1 – Physical properties of crude oil.

API gravity was measured under standard conditions (60 °F) while viscosity was obtained at room temperature (22.3 °C). The weight of SARA fractions was measured by following ASTM D2007-11.

Sample	Gravity, °API	Viscosity, cP	SARA Fractions of Crude Oil Samples, wt.%				ΔPS, dimensionless
			Saturates	Aromatics	Resins	Asphaltenes	
C1	18.84	884	22.63	37.57	16.03	23.76	1.04
C2	6.11	12,100,000[a]	10.68	29.10	20.14	40.08	1.17
C3	27.05	676	24.28	25.00	5.43	45.30	1.99
C4	7.97	251,000[a]	12.70	42.11	22.93	22.26	1.79
C5	11.56	209,000[a]	10.14	38.01	13.09	38.76	1.83
C6	17.12	496	30.03	41.84	15.56	12.57	0.40
C7	12.56	263,000[a]	32.02	21.95	7.95	38.08	2.02
C8	10.01	19,200,000[a]	11.05	30.47	16.06	42.41	2.80
C9	8.19	53,200	23.60	20.20	21.90	34.30	1.24
C10	12.19	168,000[a]	11.01	44.89	20.75	23.35	1.25
C11	12.09	10,100	16.51	37.81	17.10	28.58	1.36

[a] Viscosity values were obtained through viscosity-temperature correlations due to limitations of the equipment. Similarly all API gravity values were also estimated using density-temperature correlations to obtain value at standard conditions.

SARA fractionation is based on the solubility of the crude oil components in different solvents and provides information on the weight percent distribution of each fraction within an oil sample (Speight 2014). However, the amount of each fraction does not produce sufficient direct information to characterize the crude oil samples

(Evdokinmov 2004; Redelius and Soenen 2015). Hence, to assess the contribution of SARA fractions on the physical properties of crude oil, the weight ratio of heavy (resins + asphaltenes) to light (saturates + aromatics) fractions is compared with the viscosity and density results (Fig. 2.5). It can be observed that both viscosity and density have direct linear relationship with the heavy to light weight ratio of the SARA fractions, thus indicating that an increase in concentration of heavier fractions (resins + asphaltenes) will make the crude oil denser and more viscous. Oil samples C3, C4, and C9 showed deviation from the linear trend and were treated as outlier in these correlations. It should be noted that the density of crude oil in Fig. 2.5-B is estimated from the measured API gravity values given in Table 2.1.

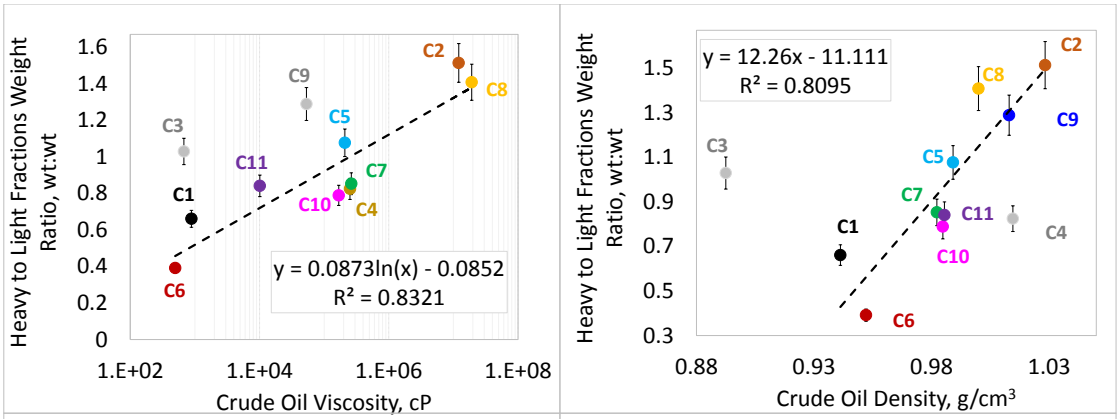

Fig. 2.5 – The relation between SARA fractions and physical properties of crude oils.
Outliers for the correlation between heavy to light fraction weight ratio with crude oil viscosity (C3 and C9) and with crude oil density (C3 and C4) are given in grey and were excluded from the correlations given on each graph.

In addition to highlighting the basic correlation between the physical properties and the SARA fractions of crude oil, Fig. 2.5 also indicate that the density and viscosity

of oil samples do not follow the same incremental order from sample C6 (lowest heavy to light ratio of 0.39) to sample C2 (highest heavy to light ratio of 1.51). To better understand the mechanism behind the variations in the order of the viscosity and density, we analyzed the elemental composition of the crude oil with carbon, hydrogen, and trace metal contents (Table 2.2). Similar elemental analysis is also carried out for n-pentane insoluble asphaltenes fraction of crude oils and the results are tabulated in Table 2.3.

Table 2.2 – Elemental composition of crude oil.

Elements	C1	C2	C3	C4	C5	C6	C7	C8	C9	C10	C11
C, wt.%	81.0	81.2	84.4	83.5	80.6	81.3	72.9	80.8	80.3	80.9	80.9
H, wt.%	11.0	10.4	13.4	10.6	10.5	11.5	10.5	10.3	10.3	11.0	10.8
H/C, ratio	0.136	0.128	0.159	0.127	0.130	0.141	0.144	0.127	0.128	0.136	0.133
Al, ppm	ND	ND	ND	ND	ND	1.2	ND	ND	ND	2.35	ND
B, ppm	4.0	18.1	ND	1.9	1.6	9.4	20.5	3.3	22.8	14.6	2.7
Ca, ppm	7.1	10.2	ND	2.5	ND†	7.0	1.5	291.0	84.1	14.4	ND
Cu, ppm	ND	ND	ND	ND	ND	1.8	ND	ND	ND	ND	ND
Fe, ppm	6.8	31.9	ND	3.7	224.0	6.4	147.0	5.0	14.6	80.3	2.5
K, ppm	5.0	13.0	5.1	5.7	5.2	5.1	6.0	42.0	23.0	5.1	5.8
Mg, ppm	2.1	ND	ND	ND	ND	12.4	1.2	20.3	5.1	2.7	ND
Mo, ppm	ND	14.6	ND	1.4	475.0	ND	ND	11.4	7.8	2.4	8.9
Na, ppm	74.5	504.0	14.8	58.1	8.5	21.5	17.0	209.0	235.0	67.0	23.3
Ni, ppm	20.0	9.8	7.5	95.3	88.4	4.3	20.9	100.0	80.3	78.4	68.1
P, ppm	2.0	2.1	2.1	2.3	2.1	2.1	2.4	2.2	2.0	2.1	2.4
Pb, ppm	ND	ND	ND	ND	ND	ND	ND	ND	ND	2.0	ND
S, ppm	14300	58200	1190	36000	52400	32000	8100	62200	68700	23500	44100
Si, ppm	ND	131.0	ND	ND	45.1	3.5	112.0	2.7	7.5	11.4	ND
Sn, ppm	ND	ND	ND	ND	1.4	ND	1.2	ND	1.5	1.4	1.2
Ti, ppm	ND	3.9	ND	2.7	ND	ND	ND	ND	3.2	4.2	2.9
V, ppm	38.8	258.0	ND	402	469	10.4	77.3	512.0	218.0	110.0	172.0
Zn, ppm	ND	ND	ND	4.1	ND	ND	1.2	ND†	5.0	1.1	ND
Metals, ppm *	**154**	**845**	**27**	**575**	**1,271**	**70**	**273**	**1,191**	**678**	**371**	**285**

†ND: non-detectable - Signifies that the metal concentration is lower than the detection limit (0.01-0.1 µg/L)
*Metals (in ppm) is the sum of all metallic elements (i.e. Al, Ca, Cu, Fe, K, Mg, Mo, Na, Ni, Pb, Sn, Ti, V, and Zn)
Relative error range for the CHN analyzer and trace metal composition are ±1% and between ± 1.4 to 2.7%, respectively.

Table 2.3 - Elemental composition of n-pentane insoluble asphaltenes of crude oil.

Elements	C1	C2	C3	C4	C5	C6	C7	C8	C9	C10	C11
C, wt.%	83.9	78.6	80.5	81.8	80.4	78.8	79.3	78.4	66.4	79.0	80.3
H, wt.%	8.4	8.4	11.9	8.0	8.2	7.4	7.0	7.6	8.0	7.8	8.2
H/C, ratio	0.100	0.106	0.148	0.098	0.102	0.094	0.088	0.097	0.120	0.099	0.102
Al, ppm	ND	ND	ND	ND	ND	60.5	ND	ND	6.3	14.3	ND
B, ppm	58.8	7.2	ND	11.2	ND	8.3	149.0	8.7	100.0	13.8	6.4
Ca, ppm	27.7	8.0	ND	ND	ND	535.0	195.0	805.0	270.0	70.0	35.6
Cu, ppm	ND	ND	ND	ND	ND	40.1	ND	ND	ND	ND	ND
Fe, ppm	107.0	15.5	ND	12.8	761.0	154.0	1,340	12.0	46.4	427.0	46.1
K, ppm	53.8	25.0	26.0	28.0	ND	141.0	6.5	91.6	60.0	24.0	26.0
Mg, ppm	ND	ND	ND	ND	ND	332.0	13.2	57.9	22.1	18.3	23.8
Mo, ppm	52.7	5.5	ND	54.9	1,460	ND	ND	29.7	38.1	13.7	ND
Na, ppm	1,690	262.0	43.8	147.0	34.1	764.0	2,450	65.0	1,750	325.0	1,100
Ni, ppm	279.0	346.0	44.3	309.0	251.0	59.5	201.0	260.0	277.0	293.0	172.0
P, ppm	10.0	10.0	11.0	9.9	ND	17.0	12.0	11.0	11.0	9.6	11.0
Pb, ppm	ND	ND	ND	ND	ND	ND	ND	ND	ND	8.4	ND
S, ppm	86600	50900	2600	83400	78400	88300	26100	85100	106000	35500	33800
Si, ppm	301.0	11.0	ND	ND	16.2	157.0	913.0	6.4	41.0	66.6	ND
Sn, ppm	ND	ND	ND	6.0	ND	ND	24.1	ND	12.0	17.0	ND
Ti, ppm	13.8	11.1	ND	17.1	ND	ND	ND	ND	14.3	22.1	ND
V, ppm	753.0	1,490	ND	792.0	1,290	145.0	793.0	1,310	775.0	489.0	358.0
Zn, ppm	ND	5.2	ND	ND	ND	16.9	9.1	ND	9.0	5.2	ND
Metals, ppm *	**2977**	**2168**	**114**	**1367**	**3796**	**2248**	**5032**	**2631**	**3280**	**1727**	**1762**

†ND: non-detectable - Signifies that the metal concentration is lower than the detection limit (0.01-0.1 µg/L)
*Metals (in ppm) is the sum of all metallic elements (i.e. Al, Ca, Cu, Fe, K, Mg, Mo, Na, Ni, Pb, Sn, Ti, V, and Zn)
Relative error range for the CHN analyzer and trace metal composition are ±1% and between ± 1.4 to 2.7%, respectively.

Crude oil comprises of distinct molecules that are physically or chemically bonded to each other (Mullins and Sheu 1998). The polar asphaltenes fraction of the crude oil generally consists of the non-hydrocarbon and unsaturated hydrocarbon compounds, thus an increase in its concentration will lower the hydrogen content and hydrogen to carbon ratio. Conversely, the non-hydrocarbon content of the crude oil will tend to increase with the increase in the asphaltenes content. Fig. 2.6 depicts that most of the oil samples analyzed in this study follow a linear trend for hydrogen content, hydrogen to carbon weight ratio, and non-hydrocarbon content with the asphaltenes content of the crude oils, as described in the literature (Prakoso et al. 2015; Evdokinmov 2004). However, four samples namely C3, C4, C7, and C9 behave as outliers and are

excluded from the trend analysis. It is important to understand more about the behavior of the outliers rather than the samples following regular trends to develop a better analysis of the precipitation tendency of asphaltenes derived from different characteristic crude oils.

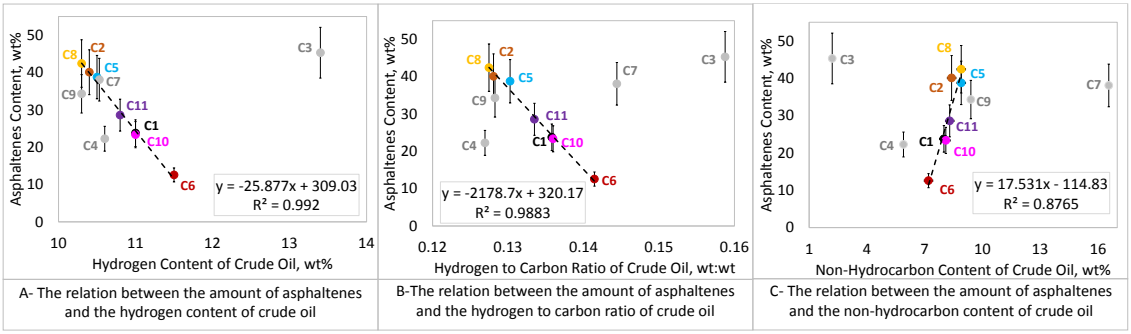

Fig. 2.6 – The relation between asphaltenes content and the hydrogen, carbon, and non-hydrocarbon content of crude oils.
Outliers given in grey dots (C3, C4, C7, and C9) were excluded from the correlations given on each graph.

For sample C3, the hydrogen content and hydrogen to carbon weight ratio are measured very high (H = 13.4 wt% - Fig. 2.6-A and H/C = 0.159 - Fig. 2.6-B). Consequently, the non-hydrocarbon content of sample C3 can be observed to be extremely low (2.2 wt% - Fig 2.6-C). Since wax fraction mostly comprises of paraffinic hydrocarbon compounds (Prakoso et al. 2015), we believe that the n-pentane insoluble asphaltenes content for C3 does not reflect the real asphaltenes content due to high wax content of C3 which precipitates out along with asphaltenes. Crude oils were reported having water content in the range of 0.5 to 4 wt%. However, C7 was reported as having the greatest water content among all 11 samples. Using thermal analysis, the bulk oil sample has been measured to contain 28 wt% water, which exists as water-in-oil

emulsion. C7 asphaltenes also has high hydrogen content and non-hydrocarbon contents. Hence, the high hydrogen and non-hydrocarbon (mainly oxygen) contents of C7 should be associated to water (H_2O). As dewatering of the crude oil sample prior to analysis might be important, thus mechanical, thermal, and chemical methods were tested to remove water. However, while the mechanical methods were not sufficient to remove the entire water content of C7, the thermal and chemical water removal methods caused alteration in the chemical composition of crude oil. Therefore, C7 was subjected to the analyses directly without dewatering which might be the reason behind the deviations in correlations. It should be also noted that since both water and asphaltenes are polar, their interaction results in higher amount of emulsion formation with water attached to asphaltenes (Kar and Hascakir 2015).

Still, the elemental analysis results are not sufficient to explain the anomalous behavior of samples C4 and C9. Therefore, we carried out detailed analysis on the solubility profiles of the crude oil to evaluate asphaltenes stability. The ΔPS parameters of crude oils were calculated by using solubility profiles given in Fig. 2.3 to understand the stability of asphaltenes within bulk crude oil based on their solubility in different solvents (given in the last column of Table 2.1). As described in the previous studies conducted by Rogel et al. (2010), the value of ΔPS is inversely related to the asphaltenes stability, therefore, a higher ΔPS results in the lower asphaltenes stability and higher precipitation tendency. Accordingly, the asphaltenes of the sample C8 is found to be the most unstable with a ΔPS value of 2.80 and C6 is the most stable with a ΔPS value of 0.40. To analyze the effect of mutual interactions between different crude oil

components on the overall asphaltenes stability, we compared the ΔPS parameter with asphaltenes content and resins to asphaltenes weight ratio (Fig. 2.7).

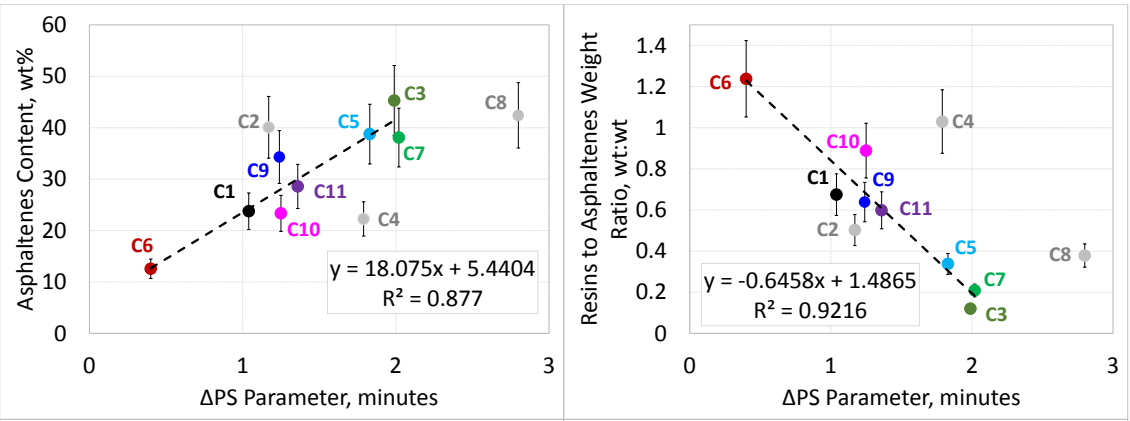

A-Contribution of the asphaltenes content towards overall asphaltenes stability

B- Contribution of resins to asphaltenes weight ratio on overall asphaltenes stability

Fig. 2.7 – The relation between asphaltenes content and resins to asphaltenes ratio with ΔPS parameter.
Outliers given in grey dots (C2, C4, and C8) were excluded from the correlations given on each graph.

It can be observed that the ΔPS parameter increases with the increase in asphaltenes content (Fig. 2.7-A). In other words, as the amount of asphaltenes increases in the bulk oil, their precipitation tendency increases. The stability of asphaltenes at constant pressure and temperature is controlled by the mutual interaction of asphaltenes with the other fractions of the crude oil (Lian et al. 1994; Wang and Buckley 2003). Fig. 2.7-B suggests that as the resins to asphaltenes ratio increases, the asphaltenes stability increases, highlighting the role of resins in maintaining the stability of asphaltenes. From the comparative correlations given in Fig. 2.7, samples C2, C4, and C8 can be observed to not follow the trends and behave as outliers. To further investigate the possible reasons for the anomalous behavior of the outliers, an integrated analysis of the SARA

fractions and elemental composition with ΔPS parameter was conducted and the results are given in Fig. 2.8.

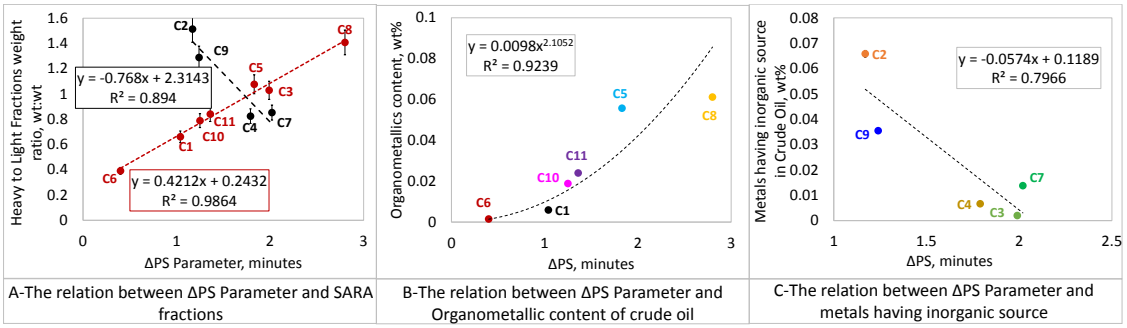

Fig. 2.8 – The relation of SARA fractions, organometallic content, and metals having inorganic source with ΔPS parameter.
Samples following regular and expected trend are given with red dots, while the outliers are highlighted using black dots.

Fig. 2.8-A correlates the heavy to light fraction ratio of crude oils with its ΔPS parameter. Samples C1, C3, C5, C6, C8, C10, and C11 show an expected trend of linear increase (red dashed line in Fig. 2.8-A) in asphaltenes destability with higher heavy fraction (resins + asphaltenes) concentration. Contrarily, an inverse relationship is observed for the crude oil samples C2, C4, C7, and C9. The linear decreasing trend (black dashed line in Fig. 2.8-A) indicates that the stability of asphaltenes increases with the decrease in heavy to light fraction ratio. The ΔPS values given with red dots in Fig. 2.8-A also yield exponential correlation with organometallic content of crude oil (Fig. 2.8-B). This exponential dependence between the organometallics content and ΔPS indicates that there exists a threshold value in ΔPS above which an increase in the metallic content does not affect the stability of asphaltenes. Presence of organometallic elements beyond the saturation limit will consequently result in exposure of highly

electronegative ions towards each other. Thus, further attraction and formation of heavier unstable clusters will not continue. We counted as only the vanadium and nickel contents of crude oils as the organometallic content of crude oils for this study (Speight 2001). The other metals are assumed to be in the inorganic content of crude oil; due to reservoir rock migration into crude oil, such as sand, clay, salts, etc (Table 2.2). Because there is a possibility of the origin of the monovalent (i.e. Na and K), divalent (i.e.; Ca and Mg), and trivalent (i.e.; Al and Fe) ions in crude oils being inorganic. Hence, these elements might be in crude oil as mineral forms (i.e.; carbonates, clays, salts). Due to small amounts of these elements present in crude oil when compare to bulk oil carbon and hydrogen contents, the contribution of the inorganic elements in bulk crude oil may be ignored. However, it should be noted that the impact of the mineral content of crude oils on asphaltenes stability might be important even at small quantities (Patton and Jessen 1964; Carbognani 2000; Ibrahim and Idem 2004). Thus, the y-axis in Fig. 2.8-C is named as metals having inorganic sources in crude oil. These elements mainly include aluminum, potassium, calcium, magnesium, sodium, and silicon. It has been observed that while the data points given in black dots in Fig. 2.8-A do not correlate with the vanadium and nickel content of crude oils (Fig. 2.8-B), they do correlate with the inorganic content of crude oils (Fig. 2.8-C). These impurities or reservoir fines in the form of metals with inorganic source affect the solubility of asphaltenes in different solvents and result in misleading ΔPS values (Coelho et al. 2016). High concentration of sodium and potassium in sample C2 may be the reason for its anomalous behavior. C9 can also be seen to contain high amounts of sodium and sulfur (Table 2.2). Possible

presence of sodium sulfate salt originating from reservoir minerals can affect the overall asphaltenes stability (Rodriguez-Navarro et al. 2000). To validate the presence of reservoir fines within the asphaltenes, we analyzed the n-pentane insoluble portion of crude oil C9 using scanning electron microscopy (SEM) technique and the images at two different resolutions are given in Fig.2.9. The dendritic or branched structure of an inorganic mineral shown clearly at 9,500x magnification confirms the migration of reservoir fines along with the crude oil and its interaction with asphaltenes. Furthermore, it should be recollected that the main focus of this study is to evaluate the effect of impurities on asphaltenes solubility and stability. Therefore, it is not important for the outlying samples to constitute a very strong correlation as they can deviate from the linear trend due to different reasons (presence of water, clays, organometallic or inorganic elements).

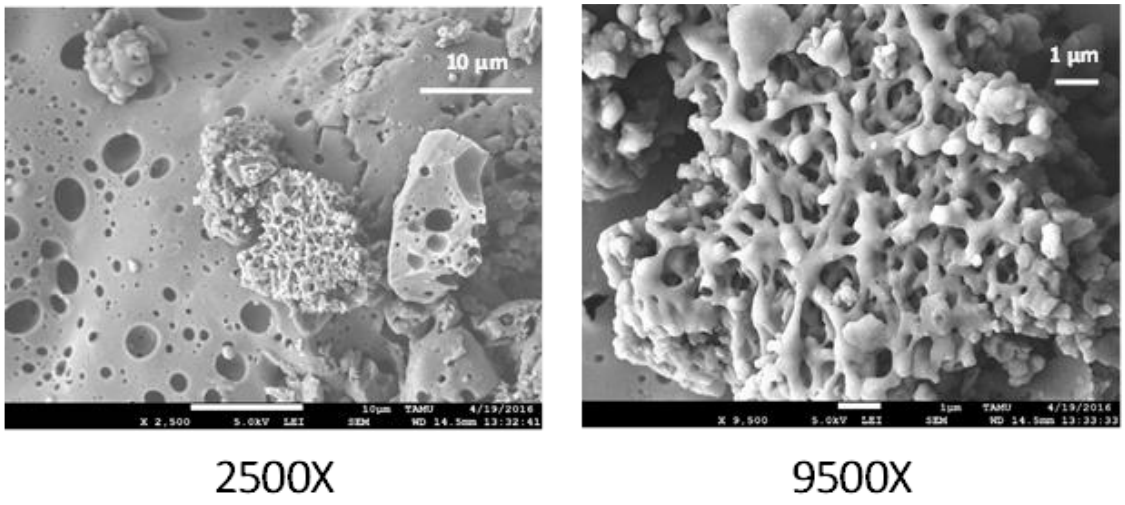

Fig. 2.9 – SEM images of the n-pentane insoluble asphaltenes fraction of crude oil C9 at 2,500x and 9,500x magnifications.

Conclusions

Part 1 of the dissertation determines the factors affecting the asphaltenes stability within the crude oil based on its solubility. Understanding the overall asphaltenes stability behavior is complex and depends not only on the interaction of asphaltenes molecules among themselves but also on their interaction with other crude oil components and reservoir components. Presence of paraffinic wax and water within the crude oil samples along with impurities in the form of reservoir fines can greatly affect the stability of asphaltenes. Among the trace metal content of crude oil, composition of organometallics elements such as vanadium and nickel can destabilize asphaltenes. Conversely, the metal content of crude oil having inorganic source like sodium, potassium, and sulfur are seen to impact the asphaltenes solubility. Novel correlations were developed to quantitatively describe the effect of impurities on the overall asphaltenes stability. Additionally, due to lack of real data representing asphaltenes behavior within reservoir, it is difficult to accurately model the asphaltenes stability. Thus, the data set presented in this study can be used to develop better understanding through equation of state calculations of asphaltenes phase behavior. Therefore, results obtained in the current study can serve as an input data for simulations studies for the potential readers who are seeking for the experimental data to model asphaltenes phase behavior.

3. PART 2: EFFECT OF ELECTRICAL CHARGES ON ASPHALTENES STABILITY

Abstract

Stability of asphaltenes is affected mainly by the change in pressure and temperature within the reservoir or in production lines. Destabilized asphaltenes results in several flow assurance problems due to their higher precipitation tendency. While there are numerous studies investigating the role of pressure and temperature on asphaltenes stability, the role of reservoir components on asphaltenes stability still remains unknown.

Hence, part 2 investigates the effect of reservoir rock-asphaltenes interaction on asphaltenes stability. 11 different crude oil samples from all around the world and their asphaltenes were analyzed. Both n-pentane and n-heptane asphaltenes surfaces were visualized under scanning electron microscope (SEM) and their surface morphology were analyzed through Electron Dispersive Spectroscopy (EDS) technique. Inorganic (mainly salts and clays) presence was observed on asphaltenes surfaces, which might be the consequence of the reservoir rock-oil interaction. Thus, the inorganic content of separated asphaltenes were investigated by mixing asphaltenes and deionized water vigorously by a centrifuge to separate the inorganic content of asphaltenes from asphaltenes' surfaces. The supernatant of these mixtures was subjected to total dissolved solids (TDS), pH, and conductivity measurements.

The TDS level was observed high which proves the physical interaction of asphaltenes with reservoir rock and this interaction is also found to generate high conductivity mainly due to sodium salts. The electrostatic charges created in water due

to inorganic content of asphaltenes were determined by zeta potential. Precipitation tendency of the colloids were found low for most of the asphaltenes samples and they are mainly because of the presence of excessive amount of negatively charged particles.

Part 2 of the dissertation proves the presence of electrical charges on asphaltenes surface and highlights its importance on asphaltenes stability.

Introduction

Asphaltenes, which represents the heaviest and the most polar fraction of the crude oil, can cause various operational problems in both upstream as well as downstream processes of oil production (Carahan et al. 1999; Akbarzadeh et al. 2007). Challenges related to addressing these problems arise due to the non-unique chemical composition and molecular structure of asphaltenes (Speight 2006; Leontaritis 1989). Several studies highlight that an asphaltene molecule can contain different aromatic and napthanic compounds that can combine to form either one ("island") or multiple ("archipelago") polycyclic aromatic hydrocarbon (PAH) structure(s) (Sabbah et al. 2011; Schuler et al. 2015). In addition to carbon and hydrogen, the PAH structures can also contain heteratoms such as oxygen, nitrogen, sulfur, and heavy metals (Speight 1991; Mullins and Sheu 1998). Presence of these elements and their spatial orientation within the PAH structure can create electrical charges and impart polarity to asphaltene molecules (Exner 1975; Nalwaya 1999). The electrostatic (induced by superficial charges) and van der Waals (dipole-dipole interactions) forces exhibited by asphaltene molecules can bring them together to form more complex and heterogeneous asphaltenes clusters (Alshareef et al. 2011; McKenna et al. 2013). These asphaltenes clusters can

interact with other reservoir components and exist as dissolved/dispersed particles/molecules/colloids within the crude oil (Pfeiffer and Saal 1940; Yen 1992; Goual and Firoozabadi 2002; Gawrys and Kilpatrick 2005; Mullins 2009; Eyssautier et al. 2011; Mullins et al. 2013).

During oil production, changes in thermodynamic conditions (Hirchberg et al., 1984), oil compostion, presence of clays (Mukhametshina et al. 2015; Kar et al. 2015a; Kar et al., 2016; Prakoso et al. 2016a; Prakoso et al. 2016b), and ions in reservoir brine (Demir et al. 2016a) can impact the stability of asphaltenes clusters. Understanding the effect of all these phenomena on overall asphaltenes stability is complicated, as it involves the contribution of solvent power, polarity, and electrical charges existing within crude oil, its solubility fractions, and other reservoir components. The effect of solubility of asphaltenes within crude oil can be assessed through onset asphaltene precipitation test and solubility profile analysis (Hammami et al. 2000; Rogel et al. 2010; Prakoso et al. 2015; Prakoso et al. 2017; Punase and Hascakir 2016; Prakoso et al. 2016a; Kar et al. 2015b). Likewise, impact of polarity can be studied by measuring dielectric constant and estimating dipole moment of crude oil and its solubility fractions (Goual and Firoozabadi 2002; Punase et al. 2016; Punase and Hascakir 2017). However, limited studies have been conducted to evaluate the contribution of electrical charges on asphaltenes stability (Tang and Morrow 1997; Gonzalez et al. 2016; Demir et al. 2016b). In this study, we aim to investigate the source of electrical charges on asphatlenes surface and evaluate the impact of electrical charges on asphaltenes stability.

Impurities within the reservoir environment like salts, rock and clay minerals, aquifer water, etc. are known to carry electrical charges. Reservoir rocks like carbonates and sandstones have been reported to carry positive and negative charges, respectively (Duba et al. 1978; Knight and Dvorkin 1992; Brovelli et al. 2011; Gomaa et al. 2015). Similarly, clay minerals such as kaolinite, illite, smectite, and bentonite are known to carry overall negative charge (Sill and Klein 1981). Moreover, based on the composition, the reservoir brine may also contain an overall positive or negative charge. These impurities, in the form of inorganic minerals, can interact with crude oil components and impart an overall electrical charge on asphaltenes surface. The force of attraction or repulsion between the charged surfaces can significantly impact the stability of asphaltenes. Therefore, we analyzed asphaltenes surface under electron microscope to visualize the presence of inorganic content and subsequently test the behavior of asphaltenes fraction within deionized water solution.

Experimental Procedure

The asphaltenes fractions (both n-pentane and n-heptane) of 11 crude oil analyzed in part 1 of this dissertation (Table 2.1) were visualized under the ultra-high resolution JEOL JSM-7500F field emission scanning electron microscope (FE-SEM) to confirm the presence of impurities on asphaltenes' surface. Also, surface chemistry of the samples was analyzed through Energy Dispersive X-ray Spectroscopy (EDS) technique. It should be noted that the depth of resolution for EDS is around 1-5 μm (Lee 2002, Klein and Hercules 1983), giving it the ability to capture elements transmitted

from materials located beneath the surface. After analyzing the surface morphology of asphaltenes, the electrical characterization of the colloidal interface between dispersed asphaltenes clusters and a continuous liquid phase was investigated, as it can provide important insights toward asphaltenes precipitation tendency. Thus, the extracted n-pentane and n-heptane insoluble asphaltenes fractions of 11 crude oil samples, were allowed to interact with deionized water. 300 mg of asphaltenes samples were mixed with 30 ml deionized water and the mixtures were centrifuged for 20 minute at 1500 rpm before measuring the total dissolved solids (TDS) in the supernatant of the solution. TDS measurements for each of the 11 asphaltenes-water samples were measured on daily basis till the stabilized values (no change for three consecutive days) were observed. The stabilized TDS levels for the test samples were observed after 6 to 8 days. The variation in achieving stabilized TDS values occur primarily due to the differences in asphaltenes.

Once the stabilized TDS readings were obtained, the supernatant samples were used to measure various electrical properties such as conductivity, pH, particle size, and zeta potential values. Oakton CON 11 series conductivity and Oakton pH 5+ meters were used to measure the conductivity and pH of the samples, respectively. To comprehend the degree of electrostatic repulsion between asphaltenes clusters dispersed in water, zeta potential measurements were carried out using Brookhaven Instruments Corporation ZetaPALS Analyzer. Additionally, the particle size measurements were also conducted using the same apparatus. For each measurement, approximately 2 ml of the supernatant sample was taken in a transparent polystyrene four sided cuvettes and

analyzed under light beams to quantitatively assess the particle size and zeta potential values. It should be noted that these measurements were repeated at least 5 times and the reported results represents the average values of parameters.

Experimental Results and Discussion

11 different crude oil and bitumen samples analyzed in this study were firstly characterized in terms of their physical properties such as density and viscosity, and their solubility fractions (Saturates, Aromatics, Resins, and Asphaltenes - both n-pentane and n-heptane insoluble). All these measurements were carried out by following procedures described in chapter 2 and the results are tabulated in Table 2.1.

Presence of impurities (or inorganic minerals) on the surface of extracted n-pentane and n-heptane insoluble asphaltenes fraction of three distinct crude oil samples C1, C6, and C8 are visualized under the SEM, as shown in Fig. 3.1 and Fig. 3.2.

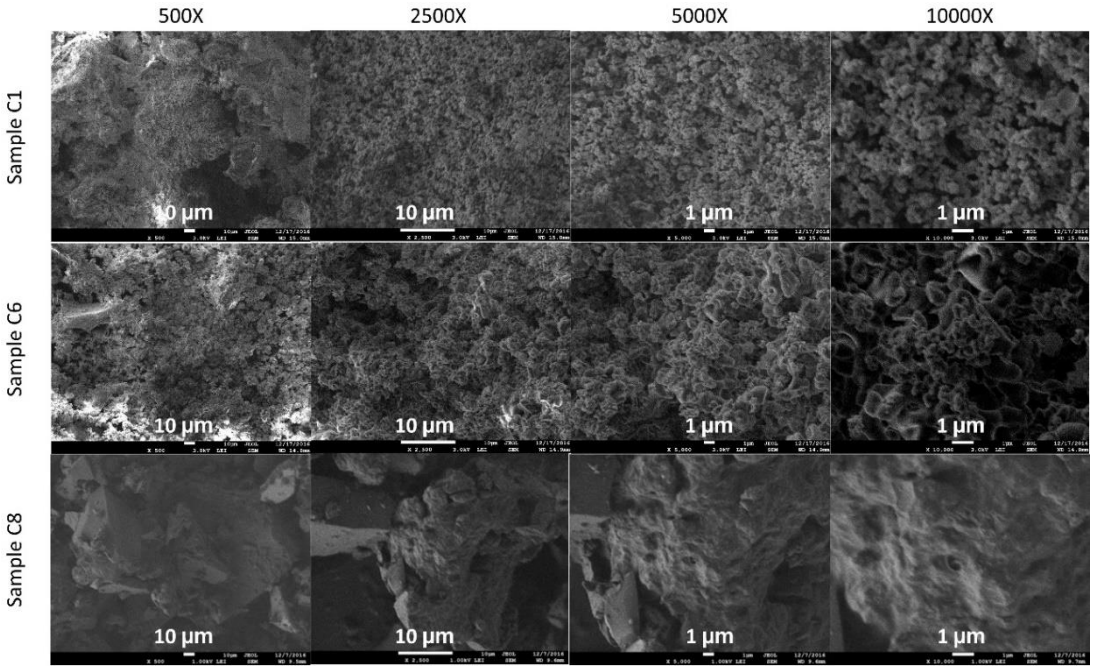

Fig. 3.1 – SEM images of n-pentane asphaltenes of C1, C6, and C8 oil samples at different magnifications.

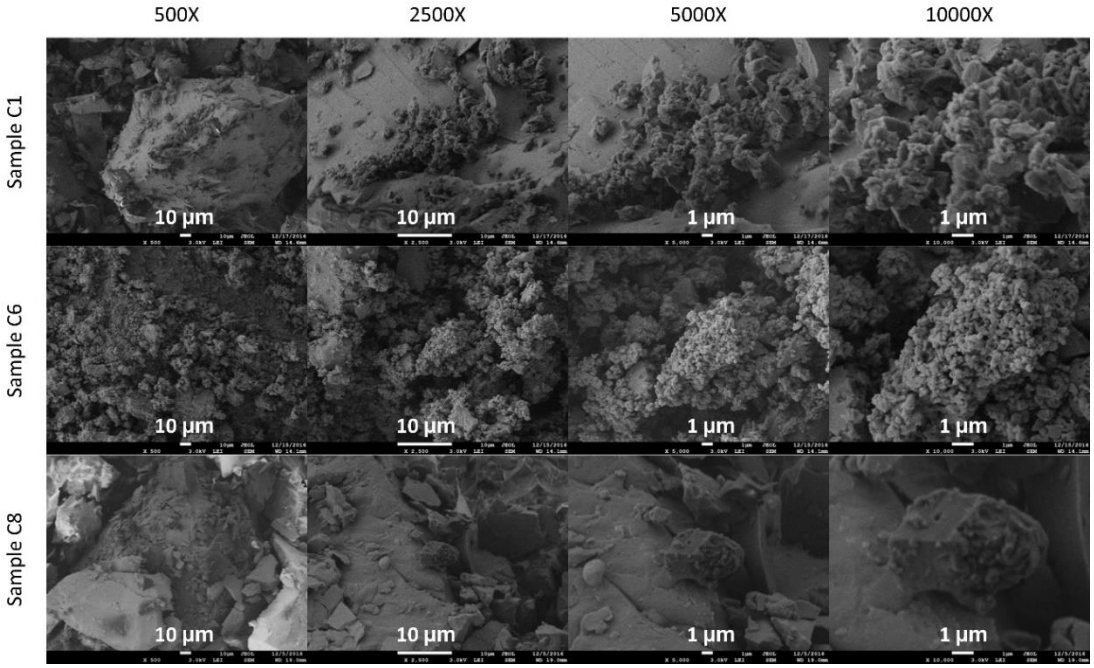

Fig. 3.2 – SEM images of n-heptane asphaltenes of C1, C6, and C8 oil samples at different magnifications.

Moreover, surface morphology of the examined asphaltenes surface, obtained through EDS technique, is also presented in Table 3.1. The EDS results indicate that in addition to the organic hydrocarbons, asphaltenes clusters also consist of inorganic minerals constituted mainly by sodium, chlorine, and calcium. Interaction of asphaltenes with reservoir components are believed to be the source of these inorganic minerals.

Table 3.1 – EDS results highlighting the surface morphology of n-pentane (nC5) and n-heptane (nC7) insoluble asphaltenes fractions of sample C1, C6, and C8.

Elements	Carbon, wt%		Oxygen, wt%		Sulfur, wt%		Sodium, wt%		Chlorine, wt%		Calcium, wt%	
	nC5	nC7	nC5	nC7	nC5	nC7	nC5	nC7	nC5	nC7	nC5	nC7
C1	91.04	90.02	7.49	8.08	1.33	1.45	0.08	0.24	0.07	0.21	0.00	0.00
C6	89.99	84.98	5.58	12.12	4.20	2.63	0.09	0.07	0.09	0.10	0.05	0.10
C8	91.36	91.31	4.89	2.79	3.45	5.33	0.11	0.17	0.15	0.32	0.04	0.08

Simple visual assessment of these asphaltenes samples highlight that inorganic minerals are attached on to the surface of both n-pentane as well as n-heptane asphaltenes. Moreover, from the EDS results of the three crude oil samples analyzed, it can be observed that the carbon concentration is lower and concentration of inorganic elements (summation of sodium, chlorine, and calcium content) is higher for n-heptane asphaltenes. Thus, suggesting greater interaction affinity of n-heptane asphaltenes with more clays or other reservoir components. Although, similar trend is observed for most of the other asphaltenes samples, there are still some inconsistencies as shown by the SEM-EDS results included in the appendix section (Fig. 3A-1 and 3A-2). Such variations in the interaction affinity between asphaltenes and the reservoir components can affect the charge distribution on the asphaltenes cluster and consequently impact the overall stability of asphaltenes. Therefore, in addition to the SEM-EDS results which

provide evidence about the existence of inorganic content at the superficial level of asphaltenes clusters, it is important to assess the electrical properties generated on the asphaltenes surface.

Electrical properties of the extracted asphaltenes samples were measured by preparing its solution in deionized water. Stabilized total dissolved solids (TDS) of the supernatant of the asphaltenes-water solutions were measured to evaluate the interaction behavior of the inorganic constituents with polar water compound and the results are provided in Table 3.2. It should be noted that all the electrical properties were measured 4-5 times and the values enlisted in Table 3.2 are averaged values. For detailed analysis, all the measurement values as well as the statistical significance of these measurements are included in appendix 3-C and 3-D, respectively.

Table 3.2 – Electrical properties of n-pentane (nC5) and n-heptane (nC7) insoluble asphaltenes.

Sample	Total Dissolved Solids (ppm)		pH		Conductivity (µS)		Particle Size (nm)		Zeta Potential (mV)	
	nC5	nC7	nC5	nC7	nC5	nC7	nC5	nC7	nC5	nC7
C1	8.17	68.20	3.12	6.28	16.37	136.70	4879.2	1496.8	-29.60	-13.60
C2	55.90	82.20	6.95	3.62	112.10	164.90	5626.9	10236.0	-23.01	-39.20
C3	1.27	2.80	4.74	2.31	2.54	5.58	1895.4	5782.4	-6.17	-14.00
C4	21.00	15.50	5.72	5.99	41.80	31.50	14088.0	2197.2	-24.84	-6.80
C5	16.90	2.68	4.56	1.91	33.70	5.33	12847.8	5764.9	-17.60	-12.20
C6	39.10	131.00	2.76	3.21	78.30	259.00	3829.1	21754.0	-26.10	-7.90
C7	4.79	8.35	5.46	2.41	9.63	16.71	1258.7	13994.0	-17.13	-9.80
C8	46.80	68.30	5.83	3.36	94.40	137.70	1880.0	5165.8	-23.13	-5.70
C9	45.20	73.70	4.97	3.37	90.50	147.40	188.1	183.6	-37.70	-53.30
C10	8.48	13.90	4.31	2.76	16.90	27.80	2042.2	14155.0	-25.05	-23.90
C11	5.50	3.66	4.81	2.25	11.10	7.14	12822.2	24157.0	-16.77	-12.20

The TDS value ranges from 1.27 to 55.9 ppm for n-pentane asphaltenes and from 2.8 to 131 ppm for n-heptane asphaltenes. Such high values are indicative of the physical interaction of inorganic constituents present within the reservoir with asphaltenes

fractions. Since inorganic components may carry electrical charge, the presence of these constituents can impart an overall charge to the supernatant water and consequently generate electrical conductivity. Hence, the electrical conductivity of the supernatant samples were tested and the results, as shown in Table 3.2, shows a large variation from 2.54 to 112.1 µS for n-pentane and from 5.58 to 259 µS for n-heptane asphaltenes, respectively. It is important to note that the TDS and electrical conductivity results follow a direct linear relationship, thus indicating the impact of inorganic constituents on electrical conductivity.

Furthermore, to quantitatively evaluate the impact of electrical charges on the stability of asphaltenes, zeta potential and particle size of solids in the supernatant solutions were measured. Zeta potential indicates the degree of electrostatic repulsion between similarly charges dispersed colloidal clusters immersed in a continuous dispersing medium (Jada and Salou 2002). Hence, higher absolute values of zeta potential represent a stable solution with lower aggregation tendency, whereas an inverse behavior is observed for samples having smaller absolute zeta potential values (Riddick 1968). It can be observed that the zeta potential of both n-pentane and n-heptane asphaltenes all the 11 samples are negative. Thus, suggesting the presence of excessive amount of negatively charged particles, mainly associated to sandstones and clay minerals on asphaltenes surface (Duba et al. 1978; Knight and Dvorkin 1992; Brovelli et al. 2011; Gomaa et al. 2015; Sill and Klein 1981). Since the interaction between these charge particles can affect the overall stability of asphaltenes, it is important to comparatively assess zeta potential with particle size and other asphaltenes stability

parameters. The zeta potential and particle size values of the asphaltenes can be observed to follow an inverse linear relationship, indicating that samples with higher zeta potential values are more stable and have less tendency to form large clusters. Another important observation from Table 3.2 is that sample C3 has the lowest absolute zeta potential value and is least stable compared to all the analyzed samples. It should be noted that sample C3, as described in chapter 2, contains high amount of wax in its n-pentane insoluble asphaltenes fraction and exist in solid state at room temperature and atmospheric pressure. Hence, a comparative evaluation of zeta potential with content of n-pentane insoluble fraction of the crude oil samples were carried out and the result is highlighted in Fig. 3.3.

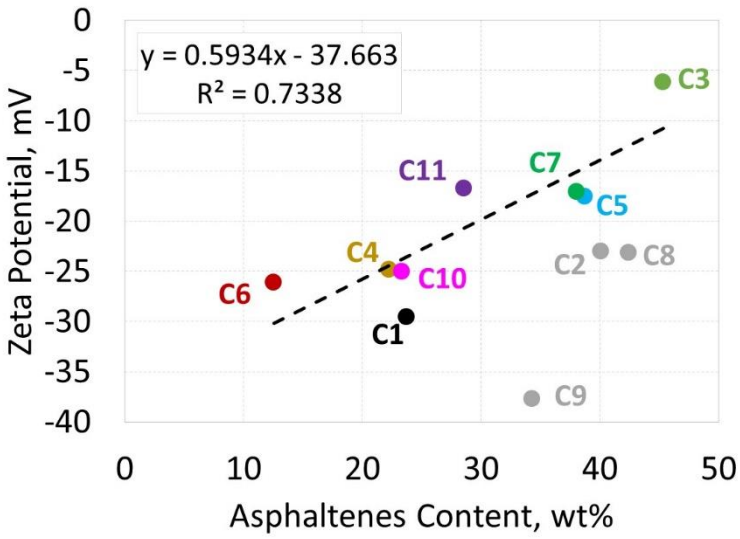

Fig. 3.3 – Comparative assessment of zeta potential and content of n-pentane insoluble asphaltenes fraction of crude oil.

Fig. 3.3 indicates that with exception of samples C2, C8, and C9, all the other samples exhibit a direct linear relationship between zeta potential and asphaltenes content of crude oil. This behavior suggests that the electrical charges arising due to the presence of inorganic impurities may stabilize the asphaltenes clusters and result in lower precipitation tendency.

Furthermore, from the data presented in Table 3.2, it can be seen that the TDS and zeta potential values of the analyzed samples do not correlate linearly. For example, samples C2 and C8 have higher TDS content as compared to sample C9 (indicative of higher amount of suspensions present in the supernatant), however the zeta potential values of these samples is lower than sample C9. Also, comparison between n-pentane and n-heptane asphaltenes fractions of crude oil indicate non-linear relationship between TDS and zeta potential values. For example, an increase in the TDS value for n-heptane asphaltenes as compared to n-pentane asphaltenes of sample C1 or C6 results in reduction of their absolute zeta potential. Contrarily, for sample C2 or C9, an inverse behavior is observed wherein lower TDS yields lower absolute zeta potential for the n-heptane asphaltenes. This non-linear trend suggests that in addition to the amount, the type of inorganic minerals present on the asphaltenes surface also affects the zeta potential and consequently the stability of asphaltenes. Within the reservoir environment, the source of inorganic minerals interacting with asphaltenes can be either positively charged (carbonate rock minerals) or negatively charged (sandstone rock minerals; clays – kaolinite, illite, smectite, chlorite; or reservoir brine). If the inorganic mineral attached to the asphaltenes surface originates from carbonate rocks, then it will

lower the net negative charge and lower the absolute zeta potential value of the supernatant sample. Similarly, an inorganic mineral carrying negative charge will result in higher absolute zeta potential values. Fig. 3.4-A highlights the influence of positively charged inorganic minerals (obtained through EDS analyses) on the zeta potential values. A direct linear relationship between the carbon plus oxygen content and the zeta potential of the asphaltenes indicates that an increase in the carbon and oxygen content (either organic or inorganic source) causes a reduction in the absolute zeta potential values and destabilizes the asphaltenes clusters. Due to the depth limitations associated with EDS results and since the zeta potential measurements were conducted by vigorously centrifuging the asphaltenes with deionized water, it is important to analyze the composition of asphaltenes through elemental analyses as well. The elemental composition of the n-pentane insoluble asphaltenes given in Table 2.3 is used and elements are grouped together into negatively charged (aluminum, iron, potassium, sodium, sulfur, and silicon) and positively charged (calcium and magnesium). As described earlier, an increase in the negatively charged minerals will increase the absolute zeta potential values of the asphaltenes and provide higher stability. Thus the correlation between zeta potential and negatively minus positively charged minerals, as observed in Fig. 3.4-B, follows a linear relationship.

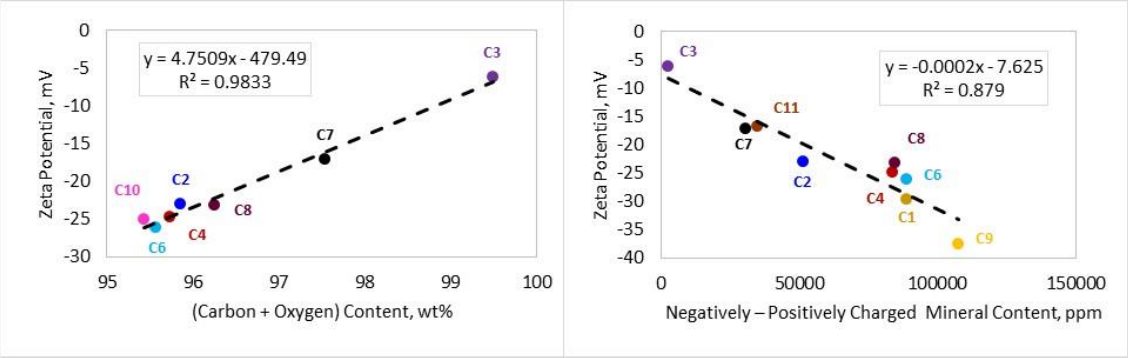

A – Contribution of positively charged carbonate minerals on zeta potential values

B – Combined contribution of negatively and positively charged minerals on zeta potential values

Fig. 3.4 – Influence of different charged minerals on zeta potential of n-pentane asphaltenes.

To better visualize the electrostatic interaction of asphaltenes surfaces, strong electrolyte solution having 8,000 ppm NaCl was prepared using deionized water. The n-pentane and n-heptane insoluble asphaltenes were exposed to this electrolyte solution. After letting the water to evaporate overnight, the optical microscopic images of asphaltenes were acquired by Meiji Techno Japan-Microscope and ProgRes CT5-Camera at 100x magnification. The behavior of the n-pentane asphaltenes samples within electrolyte solution is shown in Fig. 3.5.

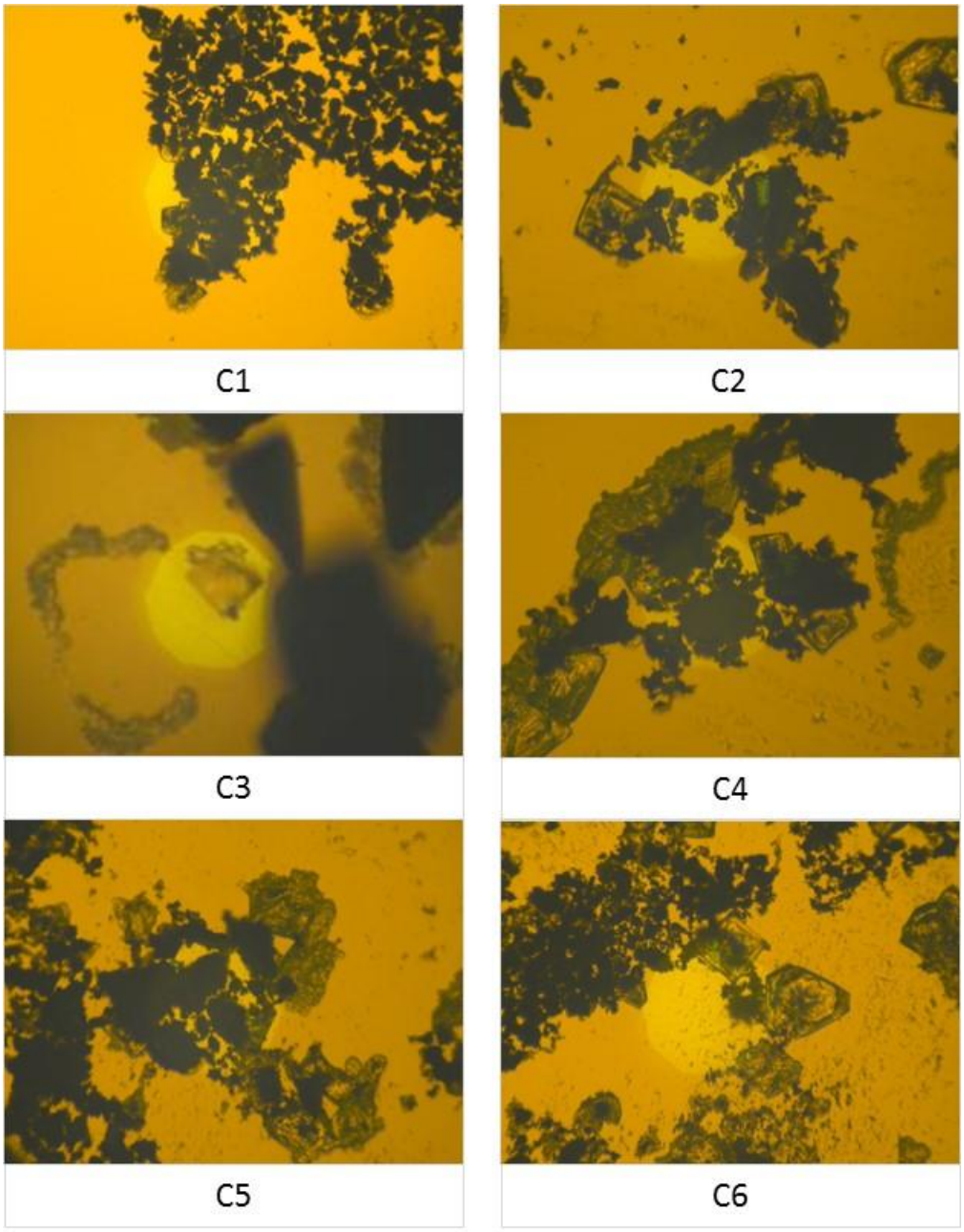

Fig. 3.5 – Visualization of the electrostatic interactions of n-pentane insoluble asphaltenes with NaCl solution under optical microscopy (100X magnification).

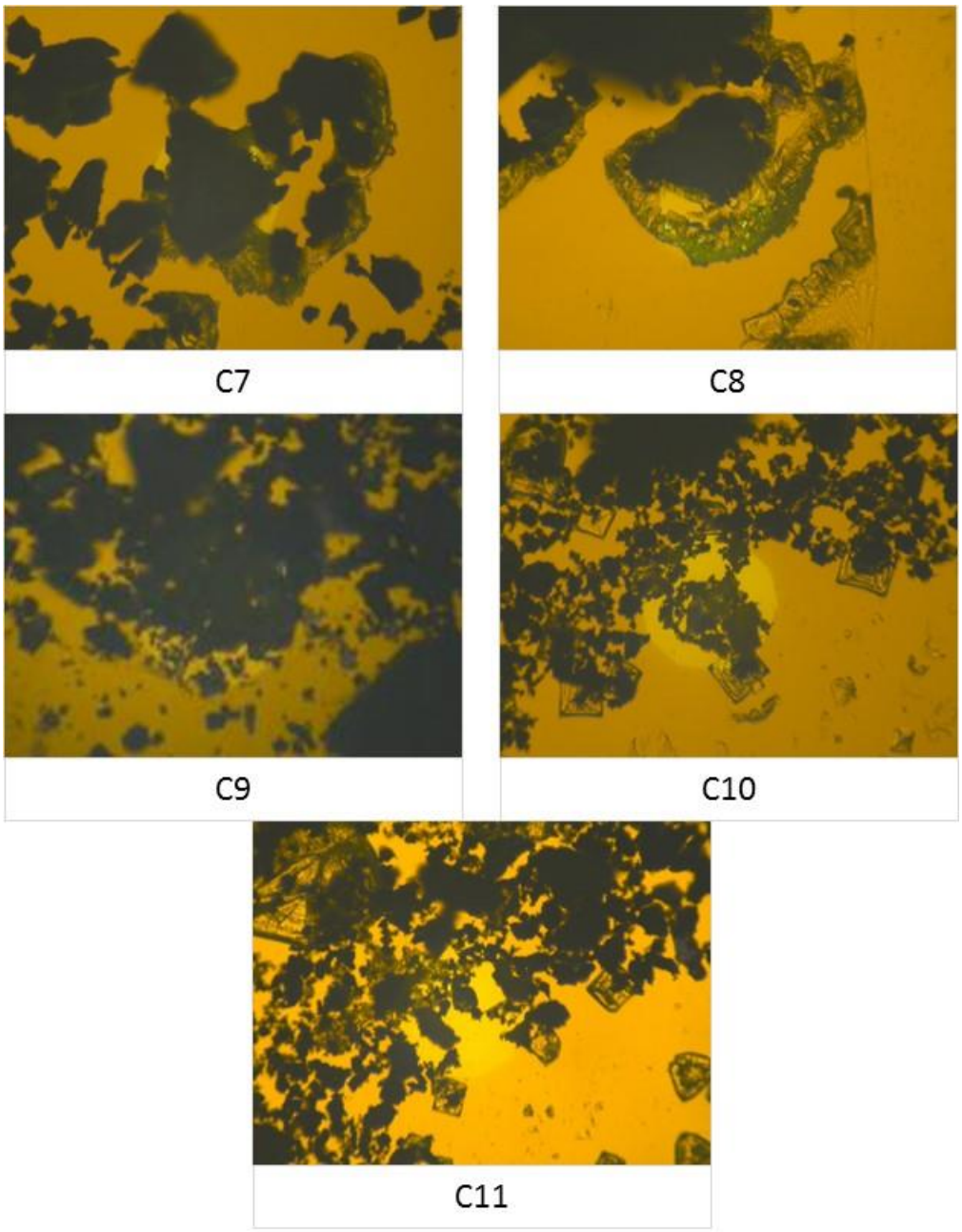

Fig. 3.5 cont. – Visualization of the electrostatic interactions of n-pentane insoluble asphaltenes with NaCl solution under optical microscopy (100X magnification).

Optical microscopy images given in Fig. 3.5 shows the interaction of NaCl solutions with n-pentane asphaltenes on overnight waited samples. Hence, the water in NaCl solution was evaporated completely and enabled us to visualize the accumulation of asphaltenes clusters around the salt crystals. Asphaltenes clusters of sample C3, having the lowest zeta potential value is observed to have a higher interaction affinity towards each other as compared to the salt molecule. Thus, the salt molecule has minimum interaction and cannot stabilize the C3 asphaltenes sample. Contrarily, sample C9 having the highest absolute zeta potential value experiences greatest electrostatic repulsion between the asphaltenes cluster and therefore is observed to interact vigorously with the salt molecule. Hence, through this analysis the impact of electrostatic charges on asphaltenes stability that was determined through zeta potential measurements were also validated through asphaltenes interaction with NaCl solution. Similar interaction tendency can be observed between the n-heptane insoluble asphaltenes and the electrolyte solution (as shown through the microscopic analysis given in Fig. 3.6).

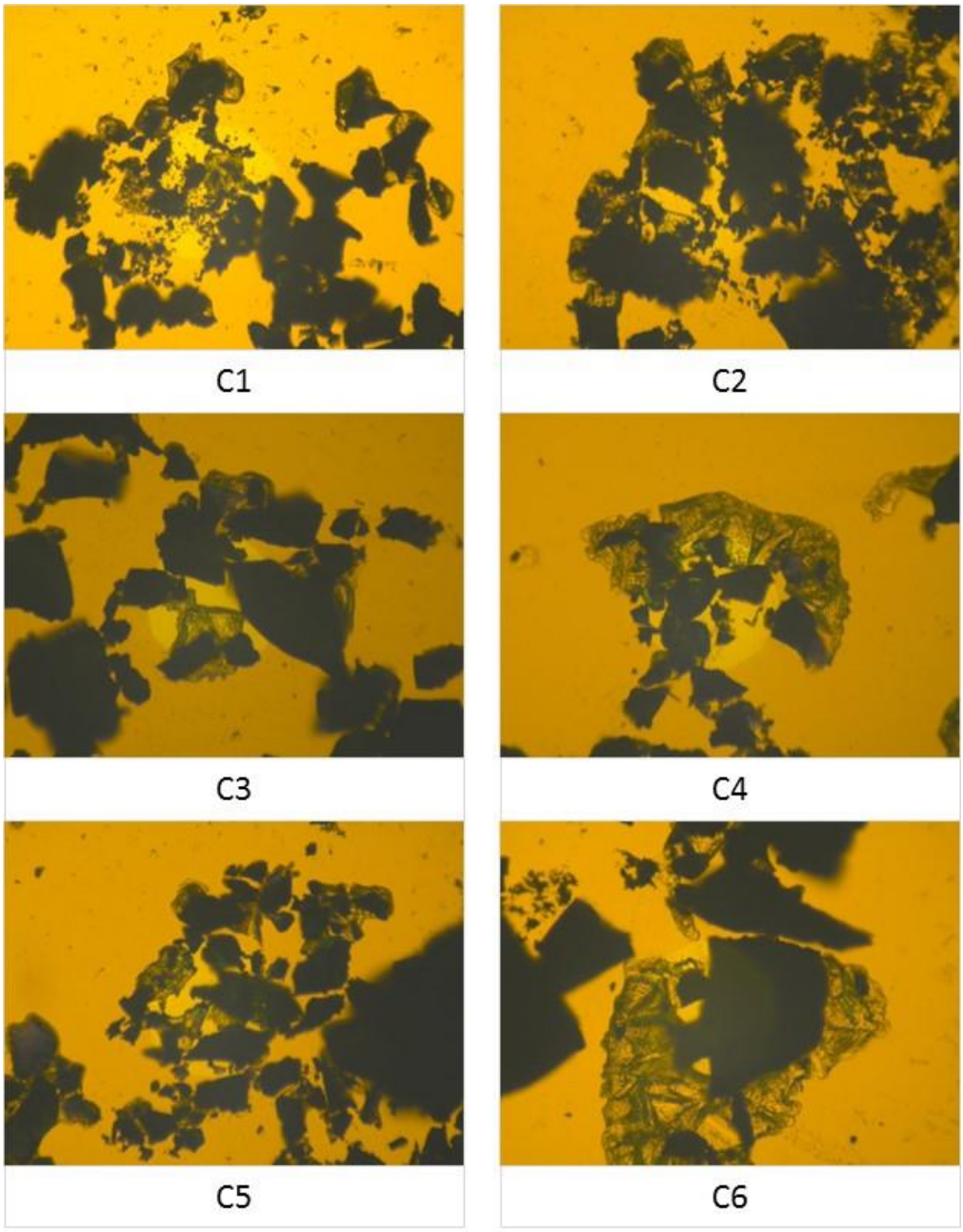

Fig. 3.6 – Visualization of the electrostatic interactions of n-heptane insoluble asphaltenes with NaCl solution under optical microscopy (100X magnification).

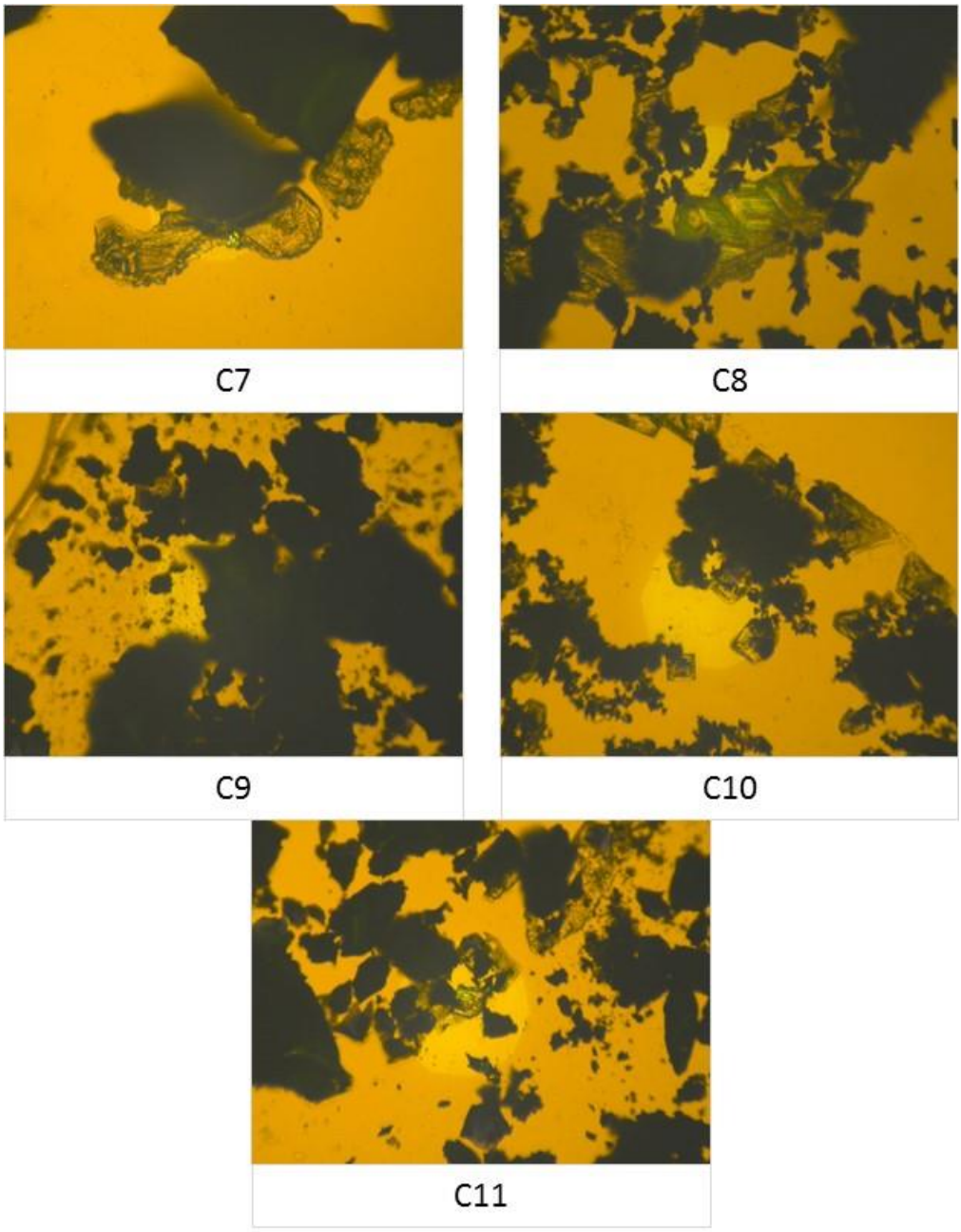

Fig. 3.6 cont. – Visualization of the electrostatic interactions of n-heptane insoluble asphaltenes with NaCl solution under optical microscopy (100X magnification).

In addition to the aforementioned trends, another observation that can be inferred by comparing the TDS and zeta potential values of n-pentane insoluble asphaltenes is that for most of the samples (excluding C6, C7, C8, and C10) TDS and absolute zeta potential values are directly related to each other. This direct correlation suggests that an increase in the inorganic minerals within asphaltenes surface will increase the zeta potential and stabilize the asphaltenes. However, for the anomalous samples, it is observed that an increase in the TDS values reduces the absolute zeta potential of sample and destabilizes asphaltenes clusters. From the EDS results provided in appendix 3-B, it can be seen that n-heptane asphaltenes of samples C3, C6, C7, C10, and C11 have greater positive (calcium) minus negative (sodium, chlorine, sulfur, silicon, and aluminum) elemental content compared to n-pentane asphaltenes. Out of these samples, the TDS content of C3 and C11 is very small, thus its influence on the zeta potential values may not be very significant. Contrarily, higher TDS of more positively charged n-heptane asphaltenes of samples C6, C7, and C10 can reduce the net zeta potential and destabilize the clusters more.

It should be noted that salinity can significantly affect the asphaltenes stability by attracting two negatively charged asphaltenes clusters and canceling out their electrical repulsions. However, while reservoir salinity may not have a noteworthy impact on stable asphaltenes, since, asphaltenes impurity content might be originated from the reservoir salinity, the external salinities added to the reservoir might have detrimental effect on asphaltenes stability and resulted in asphaltenes precipitation. Hence, prior to injection of water to the reservoir to displace oil, it is recommended that the analyses of

the interaction between injected water and asphaltenes should be conducted (Ali and Hascakir, 2017). Especially, the impact of low salinity water flooding and injection of sea water to displace oil in the reservoir might be considerable on asphaltenes stability and results in asphaltenes precipitation.

Conclusions

This study presents a novel perspective of investigating the overall stability of asphaltenes by considering the presence of inorganic impurities within the asphaltenes clusters. The surface morphology of n-pentane and n-heptane insoluble asphaltenes fractions of 11 different crude oil and bitumen samples were analyzed under SEM. Presence of inorganic impurities on asphaltenes surface were visualized through SEM images and validated using EDS analysis. The charge distribution of these impurities over asphaltenes clusters were studied through various electrical properties measurement. Comparative assessment of the electrical properties with asphaltenes stability parameter suggest that an increase in electrostatic repulsion between these clusters enhances the overall asphaltenes stability and reduces its precipitation tendency. However, while engineering an Enhanced Oil Recovery (EOR) fluid, the electrostatic charges of that fluid should be determined properly to not disturb the asphaltenes stability.

4. PART 3: EFFECT OF POLARITY OF ASPHALTENES ON ASPHALTENES STABILITY*

Abstract

Asphaltenes represent the heaviest and the most polar fraction of crude oil. The interaction of asphaltenes with other fractions of crude oil can affect its overall polarity and stability. Due to the complex nature of the molecules constituting asphaltenes, determining asphaltenes polarity and thereby predicting its stability is, however, difficult. A more practical way to estimate asphaltenes instability would have important implications in predicting oil production performance. In this study, we present a method combining dielectric constant measurements of crude oil fractions with a modified effective medium approximation to estimate instability of asphaltenes. Furthermore, we show that the dielectric constant of resins fractions comprising mainly organic constituents with minimum impurities provide the best representation of crude oils with regards to physical properties such as density and viscosity. Two new analytical correlations relating the overall dielectric constant of crude oil mixtures and their constituents are suggested. These correlations provide insight towards asphaltenes stability with crude oil and can be directly used to estimate the overall precipitation tendency of asphaltenes.

Introduction

A physical property highlighting the stability of a molecule is known as polarity, which describes the electron sharing nature of atoms forming the molecules (Wulfberg 2000; Sorrell 2006). Asphaltenes are the most polar components of crude oils due to their complex molecular structure with several polar functional groups (Speight 1991; Bestougeff and Byramjee 1994). Once the asphaltenes stability is disturbed, the polar sides of the molecules interact with each other, leading to the agglomeration and precipitation of asphaltenes. Asphaltenes precipitation has several detrimental consequences which may reduce oil production significantly and make the transportation and processing of crude oil difficult (Leontaritis et al. 1988; Gaspar and Travalloni-Louvisse 1993; Kokal and Sayegh 1995; Yen and Chiliangarian 1994; Amin et al. 2005; Akbarzadeh et al. 2007). Onset Asphaltenes Precipitation (OAP) test is the simplest method used to determine the asphaltenes precipitation tendency when they are exposed to a normal alkane, thus, OAP provides indirect assessment of asphaltenes' stability (Buenrostro-Gonzalez et al. 2004). Since there is still not a direct method which can quantitatively determine the asphaltenes stability, it is vital to understand the factors disturbing asphaltenes stability.

The presence of elements having different electronegativity or asymmetrical bonding structure within asphaltenes can create an unequal distribution of electrons, thus, generating dipoles with partial negative (δ^-) and partial positive (δ^+) charges (Smyth 1929; Pauling 1931; Sidgwick 1936; Nelson et al. 1967). The product of charge density and distance between the centers of positive and negative charges within the

molecule is defined as the dipole moment (Feynman et al. 1964). Since the determination of charge density and charge separation for a mixture of complex molecules like asphaltenes is difficult, direct measurement of polarity or dipole moment is not practical. Therefore, indirect assessment of polarity through measurement of physical properties such as dielectric constant, refractive index, and density is commonly used (Goual and Firoozabadi 2002; Wattana et al. 2005). Several models are used to correlate the dipole moment and dielectric constant values and are widely applied to estimate the polarity (Debye 1929; Onsager 1936; Böttcher 1952). Dielectric constant measurement is typically carried out using parallel plate capacitors, with the polar molecules placed in the space between the capacitor plates (Fotland and Anfindsen 1998). The electrical charge stored in the capacitor, when placed in external electric field generates an internal electric field in the opposite direction to reduce the net or effective voltage across the capacitor plates. Higher polarity substances will generate greater internal electric field opposing the external field and reduce the capacitance to a larger extent, thereby establishing a direct relationship with the dipole moment (Clark 1929).

Estimation of asphaltenes dielectric constant is achievable, however, stability of asphaltenes in bulk crude oil is affected by not only the asphaltenes molecules but also the mutual interaction of asphaltenes with the of other crude oil components (Murzakov et al. 1980; Wattana et al. 2005; Birdi 2008). Crude oils are complex hydrocarbon mixtures, hence, the crude oil components are simplified by grouping them under four main fractions; Saturates, Aromatics, Resins, and Asphaltenes (SARA). Resins and asphaltenes fractions have been found to have high polarity due to their complex

molecular structure comprising of different polar functional groups (Speight 1991; Exner 1975; Nalwaya et al. 1999). Contrarily, saturates and aromatics fractions are known to be non-polar because of their uniform and symmetrical molecular structure. However, a recent study has highlighted that the presence of highly electronegative elements within these non-polar fractions in the form of functional groups can impart partial polarity to these molecules (Prakoso et al. 2015). Interaction between these polar and partially polar fractions can alter the overall polarity of the crude oil and can affect the stability of asphaltenes molecules (Goual and Firoozabadi 2004; Akbarzadeh et al, 2007; Mullins 2009; Mullins et al. 2013; Kar and Hascakir 2015).

Due to the limitations associated with dielectric spectroscopic techniques, most of the works related to asphaltenes polarity measurement have been conducted on its dispersed solution in solvents like benzene, xylene, and toluene (Swanson 1942; Maruska and Rao 1987; Halvorson 1997; Ese et al. 1998; Guoal and Firoozabadi 2002). These studies measured the dielectric constant values at different weight concentrations of asphaltenes in the solution and then extrapolated the data to estimate the dielectric of pure state asphaltenes. Large variation in the reported dielectric constant necessitates a more accurate determination of dielectric properties of solid asphaltenes. To the best of the authors' knowledge, the study conducted by Evdokimov and Losev (2010) is the only work related to the measurement of dielectric constant of solid phase asphaltenes. In this study, a novel cylindrical capacitor design is developed to directly measure the dielectric constant of crude oils and their SARA fractions. The associative nature of the dielectric constant of polar and partially polar constituents present within heterogeneous

crude oil mixtures were analyzed using both experimentally obtained and analytically estimated dielectric constant data. The novel method presented here combining a practical dielectric measurement setup with a modified effective medium approximation estimates to first order asphaltenes stability. It has the potential to provide a practical platform to predict oil production performance where asphaltenes precipitation has important implications on the rate of success.

Experimental Procedure

In the scope of this experimental study, the stability of asphaltenes from nine crude oil samples was aimed to be determined through dielectric constant measurements. The behavior of asphaltenes alone and within the bulk crude oil samples was investigated. First, crude oil samples were characterized in terms of their density, viscosity, and Saturates, Aromatics, Resins, and Asphaltenes (SARA) contents. An Anton Paar DMA 4100 density meter was used to measure API gravity at standard conditions. A Brookfield DV-III Ultra rheometer was used to measure viscosity at ambient condition (22.3°C). ASTM 2007-11 (n-pentane) method was used to separate the SARA fractions of the crude oils (ASTM D2007-11).

SARA fractionation method classifies the crude oil components based on their solubility and polarity (Jewell et al. 1972). According to solubility of crude oil components in different solvents, crude oil samples are grouped under saturates, aromatics, resins, and asphaltenes; saturates and aromatics represent the non-polar fractions of crude oil, and resins and asphaltenes are known as polar fractions. Prior to dielectric constant measurements, SARA fractions were characterized by Fourier

Transform Infrared (FTIR) spectroscopy to verify that the SARA fractions were free from the chemicals used during SARA separation (Prakoso et al. 2015).

We estimated the polarity of bulk crude oil samples as well as their individual SARA fractions through dielectric constant measurements. For this purpose, an in-house cylindrical capacitor was fabricated (Fig. 4.1). The two co-axial cylinders of the capacitor made of aluminum are attached on a nonconductive Teflon base using RTV 102 white adhesive. All the capacitance measurements were carried out by using the Newport true RMS multimeter, having measurement range from 0.1 pF to 430 μF and an accuracy of ± 5% (rdg+10 dgts). Capacitance values were measured with an alternating voltage at a test frequency of 1 kHz, which minimizes changes in the dielectric properties during the measurement or migration of charged or highly polar particles within the fractions. The dimensional correlation between the radii and lengths of the cylinders was determined by following Gauss's flux theorem for a cylindrical charged surface. The overall capacitance for this specific geometry is given by Eq. 4.1 (Sears 1982; Nalwa 1999).

$$C = \frac{2\pi\varepsilon_o \varepsilon L}{\ln(b/a)} \tag{4.1}$$

Where C denotes the capacitance (F), ε_o is the permittivity of vacuum (8.85×10^{-12} F/m), ε represents the dielectric constant of the medium, L is the length of the cylinders (m), a is the radius of the solid inner cylinder (m), and b is the radius of the outer co-axial cylinder (m). The dimensions of the capacitor were optimized as per the expected

amount of SARA fractions from the ASTM D2007-11 method (Fig. 4.1). Detailed description about the capacitor design is given in appendix 4-A.

To determine the dielectric constant of the test sample, the capacitance measurements were conducted in two steps. Step 1 corresponds to a calibration step consisting of measuring the capacitance of air by keeping the annulus of the capacitor empty (C_{Air}). During step 2, the annulus is completely filled by the test sample and the capacitance is re-measured (C_{Sample}). Since all the dimensional parameters of the capacitor and the permittivity of vacuum remains unchanged between the two steps, the ratio of the measured capacitances (C_{Sample}/C_{Air}) gives the dielectric constant of the sample.

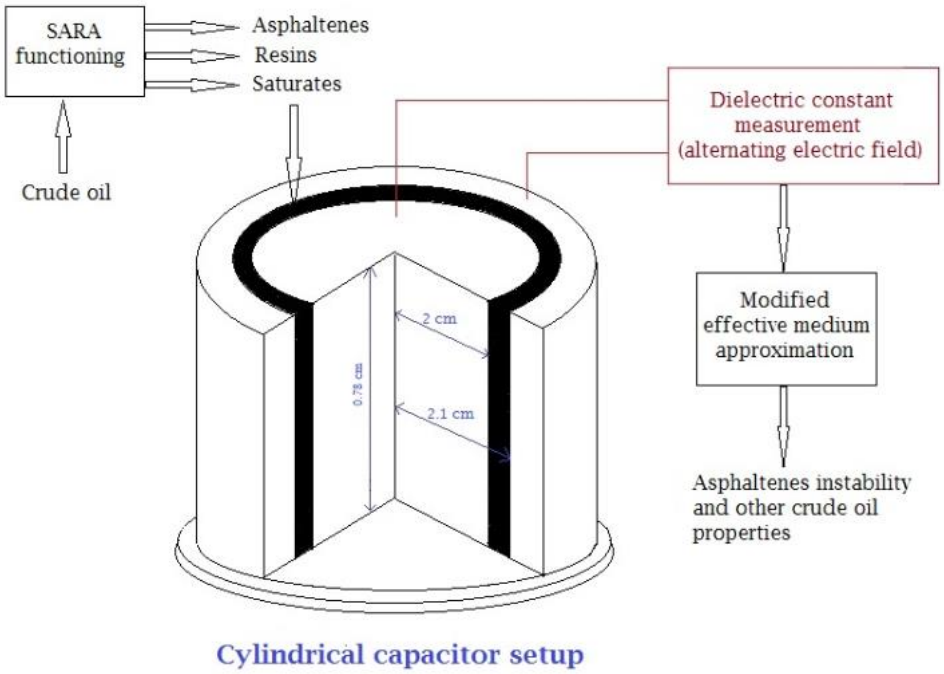

Fig. 4.1 –Description of experimental setup and method.

Figure reprinted with permission from "Stability Determination of Asphaltenes through Dielectric Constant Measurements of Polar Oil Fractions" by Abhishek Punase and Berna Hascakir, 2017. Energy and Fuels, 31 (1), 65-77, Copyright [2017] by American Chemical Society.

The capacitor was cleaned thoroughly before each measurement with water, mineral oil, and toluene, and was dried under ambient environment. To verify the absence of before each measurement, C_{Air} was re-measured.

Experimental Results and Discussion

Testing the Accuracy of the In-house Built Capacitor

Before measuring the dielectric constant of crude oils and their fractions, it is important to test the accuracy of in-house built capacitor. Hence, the dielectric constants of several known liquid and solid materials were measured and compared with the data compiled from the literature (Table 4.1).

Table 4.1 – Comparison of the measured dielectric constants with data compiled from literature.

(Young and Frederikse 1973; Li et al. 2011)

Material	Dielectric Constants	
	Measured Value	Value from literature
n-pentane	1.76	1.84
n-hexane	1.80	1.88
n-heptane	1.82	1.90
n-decane	1.86	2.00
Toluene	2.38	2.40
Water	82.00	80.00
Sodium Chloride*	5.41	5.50
Potassium Chloride*	4.30	4.50
Stearic acid*	2.17	1.7-4.2
Powdered Swiss Glass*	5.99	5.0-10.0

*The dielectric constants of solid samples were corrected by excluding the contribution of air in the pores of the solid materials.

The small variation in measured and reported values of dielectric constants given in Table 4.1 may be due to the difference in the purity and/or brand of the tested

samples. All the solvents used in this study were CHROMA SOLV® grade with high purity (higher than 99%), except for n-hexane and n-decane (95% purity). Reference salts also had 99% purity. The dielectric constant of solid materials includes the error generated by the air in the pore space of the solid materials. Therefore, a correction was applied to the measured data by using density correlation. First, the true density of the two salts was compiled from the literature (Sirdeshmukh et al. 2001). Then, density of the salts was measured in the laboratory by including the contribution of air in the pores (with an assumed dielectric constant of 1). This measurement was achieved by simply dividing the mass of the salt with the occupied volume. The results were then used to calculate the corrected dielectric constants provided in Eq. 4.2.

$$\varepsilon_{corrected} = (\varepsilon_{measured} - 1)\left(\frac{\rho_{solid}}{\rho_{measured}}\right) + 1 \tag{4.2}$$

Where, ε and ρ denotes the dielectric constant and density, respectively. The subscript "measured" signifies the measured parameter value in the laboratory which includes the contribution of air in the pore space of the samples, and the subscript "solid" represents the compiled parameter value of the solid material from literature. The measured and literature-provided values of the chemicals listed in Table 4.1 show good matches for liquids and solid samples.

The Dielectric Constant Measurements of Crude Oils and Their Fractions

Polarity and stability of asphaltenes from nine different heavy oil and bitumen samples were investigated. First, crude oils were characterized physically in terms of

their API gravity, viscosity, and SARA contents (Table 4.2). The viscosity, API gravity, and the amount of SARA fractions show a wide range of variation which enables a study of different asphaltenes behaviors. It is believed that polarity and destabilization of asphaltenes are mainly due to the impurity content of the bulk oil and its asphaltenes (Prakoso et al. 2016; Punase et al, 2016). The density and molecular weight of the components may provide information on the impurity content of crude oils. Hence, the density of asphaltenes is estimated by measuring the mass and density of bulk crude oil and its deasphalted oil fraction and applying simple mass balance correlation. The density values of each of the nine tested asphaltenes samples are tabulated in Table 4.2. Asphaltenes fraction of oil C3 has been previously reported to contain high amount of paraffinic wax (Nalwaya et al. 1999). Hence, a lower value of C3 asphaltenes density is observed in comparison to all the other crude oil asphaltenes fractions.

Table 4.2 – Characterization of crude oil samples and asphaltenes density.

Sample	Gravity, °API	Viscosity, cP*	Crude Oil Components based on ASTM D2007-11, wt.%				Asphaltenes Density[1], g/cm³	
			Saturates	Aromatics	Resins	Asphaltenes	Bulk	Solid
C1	18.84	884	22.63	37.57	16.03	23.76	0.59	1.82
C2	6.11	12,100,000[a]	10.68	29.10	20.14	40.08	0.80	1.07
C3	27.05	676	24.28	25.00	5.43	45.30	0.50	1.16
C4	7.97	251,000[a]	12.70	42.11	22.93	22.26	0.70	1.42
C5	11.56	209,000[a]	10.14	38.01	13.09	38.76	0.72	1.26
C6	17.12	496	30.03	41.84	15.56	12.57	0.56	1.71
C7	12.56	263,000[a]	32.02	21.95	7.95	38.08	0.58	1.34
C8	10.01	19,200,000[a]	11.05	30.47	16.06	42.41	0.70	1.23
C9	8.19	53,200	23.60	20.20	21.90	34.30	0.57	1.64
C10	12.19	168,000[a]	11.01	44.89	20.75	23.35	0.71	1.30
C11	12.09	10,100	16.51	37.81	17.10	28.58	0.59	1.93

* Viscosity values are given at ambient conditions and were obtained through viscosity-temperature correlations due to limitations of the equipment. Similarly all API gravity values were also estimated using density-temperature correlations to obtain value at standard conditions.

[1] Bulk density of asphaltenes measured by dividing asphaltenes mass to the volume occupied by the asphaltenes cluster, hence, this density includes the contribution of air presence in the void spaces created by asphaltenes' clusters. The bulk density of asphaltenes contain 25 to 70 volume percent of air Solid density of asphaltenes are measured by following mixing rule with deasphalted oil (DAO) and toluene, since, both DAO and toluene are miscible with asphaltenes, true asphaltenes volume is corrected (Ryan 1990; Gaikwad et al. 2015).

Dielectric constant provides an indirect measure on the polarity of each component in the crude oil, thus, we measured the dielectric constant of bulk crude oil samples and deasphalted oil, saturates, resins, and asphaltenes fractions of crude oils (Table 4.3). The dielectric constants of aromatics fraction could not be determined due to the typically low quantities of aromatics fractions extracted through SARA fractionation.

Table 4.3 – Measured dielectric constants of bulk crude oil samples and deasphalted oil, saturates, resins, and asphaltenes fractions of crude oils.

Sample	Dielectric Constants*				
	Crude Oil	Deasphalted Oil (DAO)	Saturates	Resins	Asphaltenes[l]
C1	2.47	2.69	1.90	1.80	4.20
C2	2.27	2.45	1.91	2.61	3.30
C3	1.80	2.00	1.58	1.36	4.60
C4	2.23	2.53	1.79	2.45	3.80
C5	2.23	2.71	1.84	2.23	3.40
C6	2.59	2.62	1.91	1.94	5.00
C7	3.33	3.48	1.95	1.90	3.86
C8	1.92	3.77	1.59	2.41	4.00
C9	2.31	2.52	1.97	2.23	2.81
C10	2.12	2.49	1.91	2.18	3.80
C11	2.12	2.64	1.83	2.06	4.90

*The dielectric constant measurement values are corrected by considering the artifact due to the additional electrical field created due to the small dimensions of the set-up. This electrical field results in shift in the true capacitance value for air (Scott and Curtis 1939).

[l]Measured dielectric constant of asphaltenes is corrected by using Equation 2. The true density of asphaltenes are given in Table 4.2.

It can be observed that the asphaltenes fraction of crude oils exhibits the greatest dielectric constant values (in the range of 3.30 to 5.00). The dielectric constant of resins fraction were obtained within the range of 1.80-2.61 and saturates fraction dielectric constant were measured in the range of 1.58-1.91. The dielectric constant of Deasphalted Oil (DAO), which is the mixture of saturates, aromatics, and resins fractions and

obtained after asphaltenes separation, was measured in the range of 2.00-3.77. Finally, the crude oil dielectric constants were given in the range of 1.72-2.34.

Since polarity is indicative of the intermolecular force of attraction, the physical properties of the samples can reflect this attraction. For aliphatic hydrocarbons, the dielectric constant has been observed to correlate linearly with molecular weight, boiling point, and freezing point (Carey 1998; Wypych 2001). As DAO and crude oil represent a complex heterogeneous system of liquid-liquid and solid-liquid particles (Pfeiffer and Saal 1940; Yen 1992; Gawrys and Kilpatrick 2005; Eyssautier et al 2011), accurate determination of the aforementioned properties is difficult. On the other hand, density and viscosity of crude oil can be measured easily. Thus, we carried out a comparative analysis of the dielectric constants of saturates, resins, and asphaltenes fractions (Table 4.3) with density and viscosity of crude oil (Table 4.2) to evaluate the effect of crude oil physical characteristic on the dielectric constant of individual fractions. Our results suggest that the dielectric constant of resins exhibit strong correlation with the density as well as the viscosity of the crude oil (Fig. 4.2). Previously, dielectric constant and physical properties like density and refractive index were found to be correlated (Debye 1929; Onsager 1936). In our study, instead of dielectric constant of crude oil, only dielectric constant of resins correlates with crude oil density (Fig. 4.2-A).

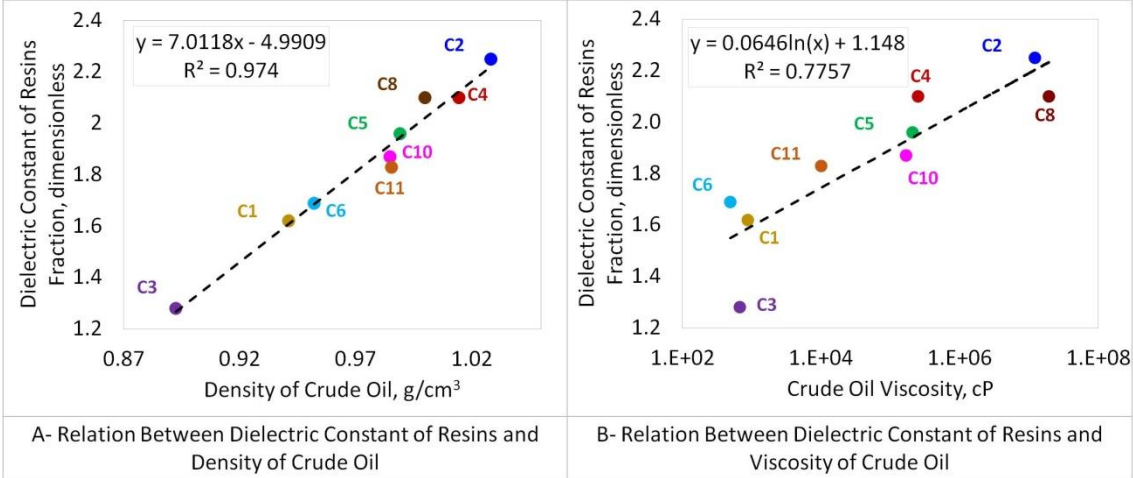

Fig. 4.2 – The relation between dielectric constant of resins and physical properties of crude oil.

Figure reprinted with permission from "Stability Determination of Asphaltenes through Dielectric Constant Measurements of Polar Oil Fractions" by Abhishek Punase and Berna Hascakir, 2017. Energy and Fuels, 31 (1), 65-77, Copyright [2017] by American Chemical Society.

The authors believe that the higher degree of coherence between the physical properties of crude oil and the dielectric constant of resins fraction as compared to asphaltenes fraction may arise due to the impurities present within or along-with the asphaltenes molecules. Within the reservoir environment, the most polar asphaltenes fraction of the crude oil can physically and chemically interact with different minerals present in reservoir rocks, clays, and brines (Kar and Hascakir 2015). These physical or chemical interactions can increase the presence of polar molecules like calcium carbonate, magnesium carbonate, sodium chloride, sodium sulfate, etc. and consequently result in higher dielectric constant values for the asphaltenes fractions. Therefore, resins fraction comprising of mainly organic constituents, provides a better representation of the organic origin of the crude oil, as a result, physical properties of crude oils dominated by the organic constituents.

The overall dielectric constants of crude oil samples are also provided in Table 4.3. While all crude oil components contribute to the overall polarity, the dielectric constant calculation for a complex mixture is difficult. Nonetheless, various effective medium approximations relating the dielectric constant of mixtures with the dielectric constants of corresponding constituents exist in literature (Lowry 1929; Bruggeman 1935; Böttcher 1952; Looyenga 1965; Bohren and Huffman 1983; Wu et al. 2004). Lowry (1929) proposed a basic summation rule of constituent dielectric constants to obtain the dielectric constant of the mixture. Wu et al. (2004) suggested a model which includes the contribution of dielectric constant of the constituents towards the mixture dielectric constant in logarithmic scale. In the current study, we used six different correlations to estimate bulk oil dielectric constant using the measured values of volumetric fractions and dielectric constants of DAO and asphaltenes fractions. Details pertaining to the analytical models can be found in the appendix section (Appendix 4-B). Volume fraction of asphaltenes within crude oil can be estimated by using its weight fraction obtained through SARA fractionation (as given in Table 2.1) and the measured density values given in Appendix 4-C. Since crude oil is considered to be a binary mixture of asphaltenes and DAO, the volume fraction of DAO is equal to unity minus the volume fraction of asphaltenes. Analytically estimated and experimentally determined dielectric constant values of crude oil samples are compared in Table 4.4.

Table 4.4 – Dielectric constant of crude oil obtained through different analytical models and comparison with experimentally determined values.

Sample	Lowry (1929)	Bruggeman (1935)	Böttcher (1952)	Looyenga (1965)	Bohren and Huffman (1983)	Wu et al. (2004)	Experimental Data
C1	3.02	2.98	4.19	2.98	2.98	2.96	2.47
C2	2.75	2.73	4.67	2.73	2.73	2.72	2.27
C3	3.39	3.19	5.78	3.21	3.16	3.12	1.80
C4	2.77	2.74	3.70	2.74	2.74	2.73	2.23
C5	2.94	2.93	5.02	2.93	2.93	2.93	2.23
C6	2.88	2.83	3.33	2.83	2.82	2.81	2.59
C7	3.61	3.53	4.88	3.58	3.56	3.59	3.33
C8	3.85	3.85	7.13	3.85	3.85	3.85	1.92
C9	2.62	2.60	3.96	2.57	2.59	2.59	2.31
C10	2.76	2.73	3.77	2.73	2.72	2.71	2.12
C11	3.15	3.06	4.27	3.07	3.06	3.04	2.12

Comparison of the bulk oil dielectric constants highlights that the experimental values do not match the analytical results. Also, each of the analytical correlations can be seen to overestimate the overall dielectric constant values of the bulk oil mixture. This deviation in the result arises due to the drawbacks associated with these models to incorporate the effect of self-association or mutual interaction between the constituents of the mixtures (polar and non-polar). Most of these correlations assume that the mixture dielectric constant follows an additive mixing rule related to the volumetric contribution of all components dielectric constant. While these correlations may provide important information on how the dielectric constant of each material contributes to the overall mixture dielectric constant value, they do not represent the complex system which includes both polar and non-polar functional groups like crude oils.

The interaction of the numerous polar and non-polar components of crude oils will impact the overall dielectric constant of crude oil. While the hydrocarbon

compounds induce less polarity, the polar functional groups associated with these compounds can lead to higher molecular polarity (Prakoso et al. 2016). Conversely, studies conducted by Kumler (1942) and Sazanovich et al. (2001) have highlighted that the presence of stable and symmetrically bonded large porphyrin molecules containing highly electronegative elements such as nickel, vanadium, and iron may generate very low polarity. These mutual interactions make the crude oil mixture deviate from the standard mixing rule and generate lower dielectric constant values as compared to the analytical results. Moreover, the existing models do not provide information on how the overall stability of asphaltenes is affected by the mutual interaction of asphaltenes with deasphalted oil. Hence, we modified Lowry (1929) and Wu (2004) correlations to estimate effective medium properties to first order. These two correlations were chosen due to their linear nature relationship, other correlations (as shown in Appendix 4-B) present square or cubic order relationships between mixture and component dielectric constants values. Moreover, through statistical analyses explained in Appendix 4-D section, it was observed that the variation between experimentally measured crude oil dielectric constant and the analytically computed results by these two approaches shows statistical significance and good correlation. Before discussing the modified correlations, it is important to recollect that the DAO mixture comprises also of saturates fraction that can destabilize asphaltenes, along with the aromatics and resins fractions that works towards increasing the stability of asphaltenes. Thus, instead of summing the product of volume fraction and dielectric constant of asphaltenes and DAO, we subtracted them.

Eqs. 4.3 and 4.4 depict the modified version of Lowry (1929) and Wu (2004) correlations, respectively.

$$Modified\ Lowry\ Parameter = v_{Asphaltenes}\varepsilon_{Asphaltenes} - v_{DAO}\varepsilon_{DAO} \quad (4.3)$$

$$Modified\ Wu\ Parameter = 10^{\{\log_{10}(v_{Asphaltenes}\varepsilon_{Asphaltenes}) - \log_{10}(v_{DAO}\varepsilon_{DAO})\}} \quad (4.4)$$

Where v and ε denotes the volume fraction and dielectric constant of asphaltenes and DAO in crude oil mixture. To understand the effect of the modified parameters obtained from Eqs. 4.3 and 4.4 on asphaltenes stability, the Colloidal Instability Index (CII) was also calculated based on the data given in Table 4.2. CII considers the crude oil mixture as a colloidal solution made up of asphaltenes, asphaltenes flocculants (saturates), and asphaltenes peptizers (aromatics and resins) (Asomaning 2003). Eq. 4.5 provides the mathematical definition of CII, where the terms represent weight percentages of each fraction within the crude oil (Table 4.2).

$$CII = \frac{(Asphaltenes + Saturates)}{(Aromatics + Resins)} \quad (4.5)$$

An increase in CII indicates lower stability and higher propensity of asphaltenes precipitation within the crude oil mixture. A comparative assessment of CII with the modified correlation parameters is shown in Fig. 4.3. All these parameters were calculated using the weight percent, density, and dielectric constant data presented in Table 4.2 and Table 4.3.

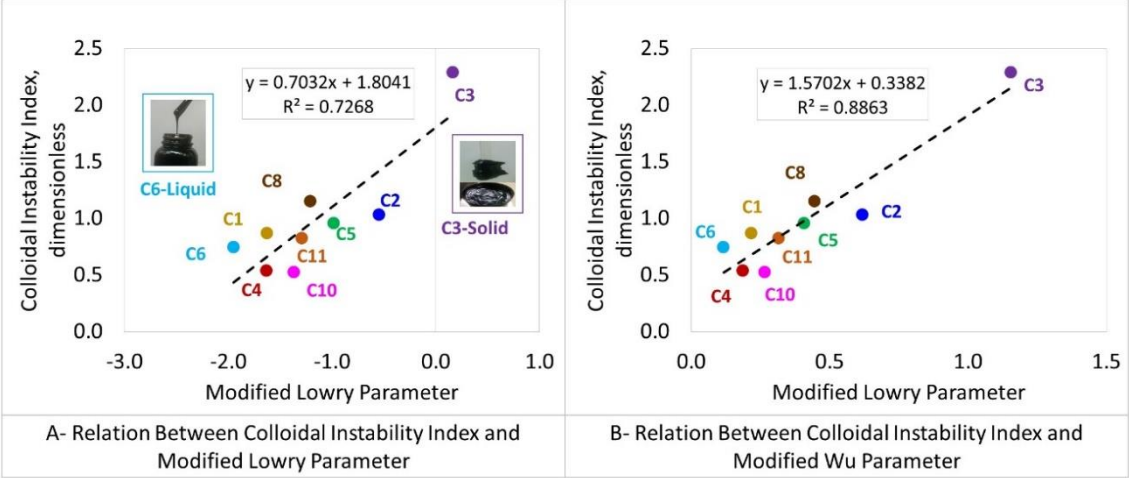

Fig. 4.3 – Stability determination of crude oils through dielectric constant and Colloidal Instability Index (CII) measurements.
Samples C7 and C9 were excluded from the above comparative assessment.

Figure reprinted with permission from "Stability Determination of Asphaltenes through Dielectric Constant Measurements of Polar Oil Fractions" by Abhishek Punase and Berna Hascakir, 2017. Energy and Fuels, 31 (1), 65-77, Copyright [2017] by American Chemical Society.

Direct linear correlation can be observed between the CII and the modified Lowry and Wu parameters, highlighting that the asphaltenes become more unstable at higher modified parameter values. Crude oil samples exhibit a similar trend for both of the modified parameters, with the modified Wu parameter showing higher degree of coherence with CII (Fig. 4.3-B) as compared to the modified Lowry parameter (Fig. 4.3-A). Another important observation from Fig. 4.3 is that C3 has the highest value for both the modified parameters and it is the only sample with positive value of modified Lowry parameter. High instability of C3 can lead to severe asphaltenes precipitation challenges. Visual inspection of the crude oil samples also indicate that at room temperature and atmospheric pressure condition, C3 (inset purple framed picture) exists as solid wax that does not flow. The fluidity of other crude oil samples were observed to decreases with

increase in the modified parameter values; C6 (inset blue framed picture) is provided as an example to highlight the differences in C3 and C6 mobility.

In summary, to first order the modified Lowry parameter greater than zero and the colloidal instability index greater than 1.5 determine instable asphaltenes. Similarly, the modified Wu parameter greater than unity represents the precipitation region for asphaltenes.

Conclusions

Assessment of asphaltenes stability within crude oil was studied through the polarity estimation of bulk crude oil and its solubility fractions. A novel technique of measuring the dielectric constant through an in-house-built cylindrical capacitor was described. Dielectric constant measurement of 11 crude oil samples, along with their saturates, resins, asphaltenes, and deasphalted oil fractions was conducted. As stated in the literature, our results validates that asphaltenes represents the most polar fraction of crude oil. The dielectric constant of resins was observed to correlate highly with the physical properties of crude oil samples. Impurities present in the asphaltenes fraction in the form of inorganic minerals is believed to greatly influence its dielectric constant values. Six different analytical models were analyzed to validate the mixing rules related to the dielectric constant of DAO and asphaltenes within crude oil mixture. All the analytical models overestimate the crude oil dielectric constant due to non-incorporation of mutual interaction between asphaltenes and DAO fractions. Two modified correlations based on Lowry (1929) and Wu et al. (2004) studies were developed. These

modified correlations can be directly used to estimate the overall stability and precipitation tendency of asphaltenes within crude oil.

5. CONCLUSIONS

Through this dissertation, a comprehensive understanding of asphaltenes stability within crude oil, in its natural state was evaluated. Assessment of various factors influencing the overall stability and precipitation tendency of asphaltenes were analyzed. It was observed that in addition to the thermodynamic changes, the compositional variation of the crude oil also affects the mutual interactions and solubility of asphaltenes. In addition to the interaction of asphaltenes clusters among itself, the presence of paraffinic wax and water within the crude oil samples along with impurities in the form of reservoir fines is shown to greatly affect the stability of asphaltenes. From the compositional perspective, the organometallics content (vanadium and nickel) of the crude oil destabilizes asphaltenes. Conversely, the metal content of crude oil having inorganic source like sodium, potassium, and sulfur are seen to increase asphaltenes solubility and stability.

Moreover, presence of inorganic minerals originating from the reservoir components like clays, rock minerals, and salts were observed to create electric charges on the surface of asphaltenes. The electrostatic forces between the charged clusters is also shown to influence the stability of asphatlenes. For the 11 samples analyzed, the surface charge distribution is analyzed through TDS, electrical conductivity, and zeta potential measurement carried out on the supernatant of asphaltenes-deionized water. Most of the samples showed a positive linear relationship between TDS and the absolute zeta potential values, indicating the stabilizing nature of the inorganic minerals present on the asphaltenes surface and complimenting the stability behavior observed through

solubility perspective. However, some samples exhibit lower absolute zeta potential values with an increase in the inorganic mineral content, thus increasing the instability of asphaltenes clusters and causing higher precipitation tendency. Therefore, by this study, a quantitative measure of the impact of amount as well as the type of inorganic minerals present within the reservoir environment on the overall asphaltenes stability is assessed for the first time.

Furthermore, since crude oil is a mixture of polar and non-polar fractions, the effect of polarity on asphaltenes stability was also analyzed. An indirect estimation of dipole moment with dielectric constant measurement through an in-house-built cylindrical capacitor was carried out. By means of the capacitor, dielectric constant of crude oils, deasphalted oils, saturates, resins, and asphaltenes fractions were measured in its natural state. The results validates that asphaltenes is the most fraction of the crude oil. Additionally, using the measured dielectric constant data of asphaltenes and deasphalted oil fractions, the associative nature of dielectric constant for heterogeneous crude oil mixtures was tested. Six analytical models were used and all of them overestimated the crude oil dielectric constant. The mutual interaction between asphaltenes and DAO fractions are considered as the primary reason for the overestimation. Two modified parameters based on Lowry (1929) and Wu et al. (2004) studies were developed and the combined assessment of these polarity based parameters with a solubility based parameter (Colloidal Instability Index), provides a novel, quick, and dynamic tool to predict asphaltenes stability.

Among the samples analyzed in this study, sample C3 is observed to be least stable from both solubility (highest ΔPS parameter) and polarity (highest modified Lowry and Wu parameter) perspective. Also, small amount of inorganic minerals attached to the asphaltenes fractions of sample C3 leads to lower degree of electrostatic repulsion between the asphaltenes clusters and increases asphaltenes destability.

An integrated and novel approach incorporating the combined effects of solubility and polarity phenomena towards determination of asphaltenes stability is developed. High degree of coherence between the stability parameters representative of solubility (Colloidal Instability Index) and polarity (modified Lowry or modified Wu parameters) provides an alternative to the oil field operator of using an effective, efficient, and time saving procedure of measuring asphaltenes precipitation propensity. Furthermore, this study also highlights for the first time, the contribution of electrostatic forces on the overall asphaltenes stability. Presence of inorganic minerals attached to the asphaltenes surface were observed to carry electrical charge and these charges create electrostatic interactions in addition to the polar interactions, thus affecting the overall stability of asphaltenes.

REFERENCES

Akbarzadeh, K., Hammami, A., Kharrat, A., Zhang, D., Allenson, S., Creek, J., Shah, K., Jamaluddin, A., Marshall, A.G., Rodgers, R.P., Mullins, O.C., Solbakken, T. 2007. Asphaltenes – Problematic but Rich in Potential. *Oilfield Review* **19** (02): 22-43.

Ali, M., Hascakir, B. 2017. Water-Rock Interaction for Eagle Ford, Marcellus, Green River, and Barnett Shale Samples and Implications for Hydraulic Fracturing Fluid Engineering. SPE Journal 22 (01): 162-171. SPE-177304-PA.

Alshareef, A.H., Scherer, A., Tan, X., Azyat, K., Stryker, J.M., Tykwinski, R.R., Gray, M.R. 2011. Formation of Archipelago Structures during Thermal Cracking Implicates a Chemical Mechanism for the Formation of Petroleum Asphaltenes. *Energy Fuels* **25** (05): 2130-2136.

Amin, A., Riding, M., Sheplar, R., Smedstad, E., Ratulowski, J. 2005. Subsea Development from Pore to Process. *Oilfield Review* **17** (01): 4-17.

Asomaning, S. 2003. Test Methods for Determining Asphaltenes Stability in Crude Oils. *Petroleum Science and Technology* **21** (3-4): 581-590.

ASTM. D2007-11: Standard Test Method for Characteristic Groups in Rubber Extender and Processing Oils and Other Petroleum-Derived Oils by the Clay-Gel Absorption Chromatographic Method. 2011. West Conshohocken, PA: ASTM International.

Barrera, D.M., Ortiz, D.P., Yarranton, H.W. 2013. Molecular Weight and Density Distributions of Asphaltenes from Crude Oils. *Energy Fuels* **27** (05): 2474-2487.

Becker, H.L. 2000. Asphaltenes: To Treat or Not. Presented at SPE Permian Basin Oil and Gas Recovery Conference, Midland, Texas. SPE-59703-MS. http://dx.doi.org/10.2118/59703-MS.

Bestougeff, M.A., Byramjee, R.J. 1994. Chemical Constituents of Asphaltenes. *Dev. Pet. Sci.* **49** (01): 67-94.

Bohren, C.F.; Huffman, D.R. 1983. *Absorption and Scattering of Light by Small Particles*. John Wiley and Sons Inc., Toronto. ISBN: 0-471293-40-7.

Borton, D., Pinkston, D.S., Hurt, M.R., Tan, X., Azyat, K., Scherer, A., Tykwinski, R., Gray, M., Qian, K., Kenttämaa, H.I. 2010. Molecular Structure of Asphaltenes Based on Dissociation Reactions of their Ions in Mass Spectroscopy. *Energy Fuels* **24** (10): 5548-5559.

Böttcher, C.J.F. 1952. *Theory of Electric Polarization*. Elsevier, Amsterdam. ISBN: 0-444-41019-8.

Brovelli, A., Cassiani, G. 2011. Combined Estimation of Effective Electrical Conductivity and Permittivity of Soil Monitoring. *Water Resources Research* **47** (08): 1-14.

Buckley, J.S. 1999. Predicting the Onset of Asphaltenes Precipitation from Refractive Index Measurements. *Energy Fuels* **13** (02): 328-332.

Buenrostro-Gonzalez, E., Lira-Galeana, C., Gil-Villegas, A., Wu, J. 2004. Asphaltenes Precipitation in Crude Oils: Theory and Experiments. *AIChE Journal* **50** (10): 2552-2570.

Carbognani, L. 2000. Effects of Iron Compounds on the Retention of Oil Polar Hydrocarbons Over Solid Sorbents. *Petroleum Science and Technology* **18** (3-4): 335-360.

Carey, A.A. 1998**.** *The Dielectric Constant of Lubrication Oils*. Computational Systems Inc., Knoxville.

Cenegy, L.M. 2001. Survey of Successful World-wide Asphaltenes Inhibitor Treatments in Oil Production Fields. Presented at SPE Annual Technical Conference and Exhibition, New Orleans, Lousiana. SPE-71542-MS. http://dx.doi.org/10.2118/71542-MS.

Clark, F.M. 1929. The Properties of Dielectrics. II. The Dielectric Constant. *Journal of the Franklin Institute* **208** (01): 17-44.

Coelho, R.S.C., Ovalles, C., Benson, I.P., Hascakir, B. 2016. Clay-Asphaltenes Interaction During Hybrid Solvent-Steam Injection into Bitumen Reservoirs. Presented at SPE Canada Heavy Oil Technical Conference, 7-9 June, Calgary, Alberta, Canada. SPE-180723-MS.

Debye, P. 1929. *Polar Molecules*. Dover, New York City. ISBN: 1-258453-91-6.

Demir, A.B., Bilgesu, H.I., Hascakir, B. 2016a. The Effect of Clay and Salinity on Asphaltene Stability. Presented at SPE Western Regional Meeting, 23-26 May, Anchorage, Alaska, USA. SPE-180425-MS.

Demir, A.B., Bilgesu, H.I., Hascakir, B. 2016b. The Effect of Brine Concentration on Asphaltene Stability. Presented at SPE Annual Technical Conference and Exhibition, 26-28 September, Dubai, UAE. SPE-181706-MS.

Duba, A., Piwinskii, A.J., Santor, M., Weed, H.C. 1978. The Electrical Conductivity of Sandstone, Limestone, and Granite. *Geophysical Journal International* **53** (03): 583-597.

Ese, M.H., Yang, X., Sjoblom, J. 1998. Film Forming Properties of Asphaltenes and Resins. A Comparative Langmuir-Blodgett Study of Crude Oils from North Sea, European Continent, and Venezuela. *Colloid and* Polymer Science 276 (09): 800-809.

Evdokinmov, I.N. 2004. Bifurcated Correlations of Properties of Crude Oils with their Asphaltenes Content. *Fuel* **84** (01):13-28.

Evdokimov, I.N., Losev, A.P. 2010. Electrical Conductivity and Dielectric Properties of Solid Asphaltenes. *Energy Fuels* **24** (07): 3959-3969.

Exner, O. 1975. *Dipole Moments in Organic Chemistry*. Georg Thieme Publishers, Stuttger, Germany. ISBN: 3-135235-01-7.

Eyssautier, J., Levitz, P., Espinat, D., Jestin, J., Gummel, J., Grillo, I., Barrè, L. 2011. Insight into Asphaltenes Nanoaggregate Structure Inferred by Small Angle Neutron and X-Ray Scattering. *J. Phys. Chem.* **115** (21): 6827–6837.

Fan, T., Buckley, J.S. 2002. Rapid and Accurate SARA Analysis of Medium Gravity Crude Oils. *Energy Fuels* **16** (06): 1571-1575.

Feynman, R.P., Leighton, R.B., Sands, M. 1964. *The Feynman Lectures on Physics*. Vol. 2, Addison-Wesley, Redwood City, CA. ISBN: 0-465023-82-7.

Fotland, P.; Anfindsen, H. 1998**.** *Conductivity of Asphaltenes*. In Structure and Dynamics of Asphaltenes; Mullins O.C., Sheu, E.Y., Eds.; Plenunm Press, New York, 247-266.

Gaikwad, R., Hande, A., Das, S., Mitra, S.K., Thundat, T. 2015. Determination of Charge on Asphaltenes Nanoaggregates in Air Using Electrostatic Force Microscopy. *Langmuir* **31** (02): 679-684.

Gaspar, G., Travalloni-Louvisse, A.M. 1993. Adsorption of Asphaltenes and its Effect on Oil Production. *SPE Production and Facilities* **8** (02): 91-96. SPE 21039-PA. https://doi.org/10.2118/21039-PA.

Gaspar, A., Zellermann, E., Labbidi, S., Reece, J., Schrader, W. 2012. Characterization of Saturates, Aromatics, Resins, and Asphaltenes Heavy Crude Oil Fractions by Atmospheric Pressure Laser Ionization Fourier Transform Ion Cyclotron Resonance Mass Spectrometry. *Energy Fuels* **26** (06): 3481-3487.

Gawrys, K.L., Kilpatrick, P.K. 2005. Asphaltenic Aggregates are Polydisperse Oblate Cylinders. *Journal of Colloid and Interface Science* **288** (02): 325-334.

Gomaa, M.M., Kassab, M.A., El-Sayed, N.A. 2015. Study of Petrographical and Electrical Properties of some Jurrasic Carbonate Rocks, North Sinai, Egypt. *Egyptian Journal of Petroleum* **24** (03): 343-352.

Goual, L. and Firoozabadi, A. 2002. Measuring Asphaltenes and Resins, and Dipole Moment in Petroleum Fluids. *AIChE Journal* **48** (11): 2646-2663.

Goual, L., Firoozabadi, A. 2004. Effect of Resins and DBSA on Asphaltenes Precipitation from Petroleum Fluids. *AIChE Journal* **50** (02): 470-479.

Halvorson, K. 1997. Dipole Moment and Molecular Weights of Alkane Precipitated Solid Fractions for some North-Sea Oils. MSc Thesis, Univ. of Bergen, Institute of Chemistry, Bergen, Norway.

Hammami, A., Phelps, C.H., Monger-McClure, T., Little, T.M. 2000. Asphaltenes Precipitation from Live Oils: An Experimental Investigation of Onset Conditions and Reversibility. *Energy Fuels* **14** (01): 14-18.

Hirchberg, A.dejong, L.N.J., Schipper, B.A., Meijer, J.G. 1984. Influence of Temperature and Pressure on Asphaltene Flocculation. *SPE J.* **24** (03): 283-293.

Hoepfner, M.P., Limsakoune, V., Chuenmeechao, V., Maqbool, T., Fogler, H.S. 2013, A Fundamental Study of Asphaltenes Deposition. *Energy Fuels* **27** (02), 725-735. http://dx.doi.org/10.1021/ef3017392.

Ibrahim, H.H., Idem, R.O. 2004. Correlations of Characteristics of Saskatchewan Crude Oils/Asphaltenes with their Asphaltenes Precipitation Behavior and Inhibition Mechanisms: Differences between CO_2- and n-Heptane-Induced Asphaltenes Precipitation. *Energy Fuels* **18** (05): 1354-1369.

Jada, A., Salou, M. 2002. Effects of the Asphaltene and Resin Contents of the Bitumens on the Water-Bitumen Interface Properties. *Journal of Petroleum Science and Engineering* **33** (1-3): 185-193.

Jamaluddin, A.K.M., Nazarko, T.W., Sills, S., Fuhr, B.J. 1996. Deasphalted Oil - A Natural Asphaltenes Solvent. *SPE Production & Facilities* **11** (03): 161-165. 10.2118/28994-PA.

Jewell, D.M., Weber, J.H., Bunger, J.W., Plancher, H., Latham, D.R. 1972. Ion-Exchange, Coordination, and Adsorption Chromatographic Separation of Heavy-End Petroleum Distillates. *Anal. Chem.* **44** (08): 1391-1395.

Kar T, Hascakir B. 2015. The role of resins, asphaltenes, and water in water–oil emulsion breaking with microwave heating. Energy Fuels **29** (06): 3684-90.

Kar, T., Mukhametshina, A., Unal, Y., Hascakir, B. 2015a. The Effect of Clay Type on Steam-Assisted-Gravity-Drainage Performance. *Journal of Canadian Petroleum Technology* **54** (06): 412-423. SPE-173795-PA. https://doi.org/10.2118/173795-PA.

Kar, T., Yeoh, J.J., Ovalles, C., Rogel, E., Benson, I., Hascakir, B. 2015b. The Impact of Asphaltene Precipitation and Clay Migration on Wettability Alteration for Steam Assisted Gravity Drainage (SAGD) and Expanding Solvent-SAGD (ES-SAGD). Presented at SPE Canada Heavy Oil Technical Conference, Calgary, Alberta, Canada.

Kar, T., Ovalles, C., Rogel, E., Vien, J., Hascakir, B. 2016. The Residual Oil Saturation Determination for Steam Assisted Gravity Drainage (SAGD) and Solvent-SAGD. *Fuel* **172** (01): 187-95.

Khalifeh, M., Kharrat, R., Bagherzadeh, H., Izadi, M. 2013. An Experimental and Simulation Study of Asphaltenes-Induced Permeability Impairment under Natural Depletion Condition. Presented at SPE European Formation Damage Conference and Exhibition, Noordwijk, The Netherlands, 5-7 June 2013. SPE-165196-MS. http://dx.doi.org/10.2118/165196-MS.

Kharrat, A.M., Zacharia, J., Cherian, V.J., Anyatonwu, A. 2007. Issues with Comparing SARA Methodologies. *Energy Fuels* **21** (06): 3618-3621.

Khayan, M. 1984. *Proposed Classification and Definitions of Heavy Crude Oils and Tar Sands*. New York: The Future of Heavy Crude and Tar Sands, McGraw-Hill.

Klein, J.C., Hercules, D.M. 1983. Surface Characterization of Model Urushibara Catalysts. *Journal of Catalysis* **82** (02): 424-441. http://dx.doi.org/10.1016/0021-9517(83)90209-9.

Knight, R.J., Dvorkin, J. 1992. The Seismic and Electrical Properties of Sandstones at Low Saturations. *Journal of Geophysical Research* **97** (B12): 17425-17432.

Kokal, S.L., Sayegh, S.G. 1995. Asphaltenes: The Cholesterol of Petroleum. Presented at SPE Middle East Oil Show, Bahrain, 11-14 March. SPE-29787-MS. http://dx.doi.org/10.2118/29787-MS.

Kumler, W.D. 1942. The Dipole Moment of ms-Tetraphenylporphirine. *J. Amer. Chem. Soc.* **64** (12): 2993-2994.

Lee, T.W. 2002. *Microelectronic Failure Analysis: Desk Reference 2002 Supplement*, 4th ed. edition, 5. Materials Park, Ohio, USA, ASM International (Reprint).

Leontaritis, K.J., Mansoori, G.A., Jiang, T.S. 1988. Asphaltenes Deposition in Oil Recovery: A Survey of Field Experiences and Research Approaches. *J. Pet. Sci. Eng.* **1** (03): 229-239.

Leontaritis, K.J. 1989. Asphaltenes Deposition: A Comprehensive Description of Problem Manifestations and Modeling Approaches. Presented at SPE Production Operations Symposium, Oklahoma City, Oklahoma. SPE-18892-MS. http://dx.doi.org/10.2118/18892-MS.

Leontaritis, K.J., Amaefule, J.O., Charles, R.E. 1994. A Systematic Approach for the Prevention and Treatment of Formation Damage Caused by Asphaltenes Deposition. *SPE Production & Facilities* **9** (03): 157-164. SPE-23810-PA. http://dx.doi.org/10.2118/23810-PA.

Li, Z., Firoozabadi, A. 2010. Modeling Asphaltenes Precipitation by n-Alkanes from Heavy Oils and Bitumens Using Cubic-Plus-Association Equation of State. *Energy Fuels* **24** (02): 1106-1113. 10.1021/ef9009857.

Li, A., Wang, H., Ouyang, Z., Cooks, R.G. 2011. Paper Spray Ionization using Non-polar Solvents. Supplementary Material for *Chem. Commun.* **47** (10): 2811-2813.

Lian, H., Lin, J., Yen, T.F. 1994. Peptization Studies of Asphaltenes and Solubility Parameter Spectra. *Fuel* **73** (03): 423-428.

Liu, P., Shi, Q., Chung, K.H., Zhang, Y., Pan, N., Zhao, S., Xu, C. 2010. Molecular Characterization of Sulfur Compounds in Venezuela Crude Oil and Its SARA Fractions by Electrospray Ionization Fourier Transform Ion Cyclotron Resonance Mass Spectrometry. *Energy Fuels* **24** (09): 5089-5096.

Loeber, L., Muller, G., Morel, J., Sutton, O. 1998. Bitumen in Colloid Science: A Chemical, Structural and Rheological Approach. *Fuel* **77** (13): 1443-1450.

Looyenga, H. 1965. Dielectric Constants of Heterogeneous Mixtures. *Physica* **31** (03): 401-406.

Lowry, H.H. 1929. The Significance of the Dielectric Constant of a Mixture. *Journal of Franklin Institute* **203** (03): 433-439.

Maruska, H.P., Rao, B.M.L. 1987. The Role of Polar Species in the Aggregation of Asphaltenes. *Fuel Science and Technology International* **5** (02): 119-168.

McKenna, A.M., Donald, L.J., Fitzsimmons, J.E., Juyal, P., Spicer, V., Standing, K.G., Marshall, A.G., Rodgers, R.P. 2013. Heavy Oil Composition. 3. Asphaltene Aggregation. *Energy Fuels* **27** (03): 1246-1256.

Meyer, R.F., de Witt, W. Jr. 1990. Definition and World Resources of Natural Bitumens. Denver, CO: U.S. Geological Survey Bulletin 1944, Department of the Interior, U.S. Geological Survey.

Mukhametshina, A., Kar, T., Hascakir, B. 2015. Asphaltenes Precipitation During Bitumen Extraction with Expanding Solvent Steam Assisted Gravity Drainage (ES-SAGD): Effects on Pore-Scale Displacement. *SPE Journal* **21** (02): 380-392. SPE-170013-PA. https://doi.org/10.2118/170013-PA

Mullins, O.C., Sheu, E.Y. 1998. *Structure and Dynamics of Asphaltenes*. Second Eds. New York, Plenunm Press.

Mullins, O.C., Sheu, E.Y., Hammami, A., Marshall, A.G. 2007. *Asphaltenes, Heavy Oils, and Petroleomics*. New York, Springer Science and Publishing Media.

Mullins, O.C. 2009. The Modified Yen Model. *Energy Fuels* **24** (04): 2179-2207.

Mullins, O.C., Seifert, D.J., Zue, J.Y., Zeybek, M. 2013. Clusters of Asphaltenes Nanoaggregates Observed in Oilfield Reservoirs. *Energy Fuels* **27** (04): 1752-1761.

Murzakov, R.M., Sabanenkov, S.A., Syunyaev, Z.I. 1980. Influence of Petroleum Resins on Colloidal Stability of Asphaltenes-Containing Disperse Systems. *Chemistry and Technology of Fuels and Oils* **16** (10): 674-677.

Nalwa, H.S. 1999. *Handbook of Low and High Dielectric Constant Materials and Their Applications*. Vol. 2, Academic Press, New York. ISBN: 0-125139-05-5.

Nalwaya, V., Tangtayakom, V., Piumsomboon, P., Fogler, S. 1999. Studies on Asphaltenes through Analysis of Polar Fractions. *Ind. Eng. Chem. Res.* **38** (03): 964-972.

Nelson, R.D. Jr., Lide, D.R. Jr., Maryott, A.A. 1967. Selected Values of Electric Dipole Moments for Molecules in the Gas Phase. National Standard Reference Data System.

Onsager, L. 1936. Electric Moments of Molecules in Liquids. *J. Amer. Chem. Soc.* **58** (08): 1486-1493.

Patton, C.C., Jessen, F.W. 1964. The Adsorption of Petroleum Residuals on Iron and Steel Surfaces. *Society of Petroleum Engineers*, SPE 1088-MS.

Pauling, L. 1931. The Nature of the Chemical Bond. Application of Results Obtained from the Quantum Mechanics and from a Theory of Paramagnetic Susceptibility to the Structure of Molecules. *J. Am. Chem. Soc.* **53** (04): 1367-1400.

Peramanu, S., Singh, C., Agrawala, M., Yarranton, H.W. 2001, Investigation on the Reversibility of Asphaltenes Precipitation, *Energy Fuels* **15** (04): 910-917.

Pfeiffer, J.P.H., Saal, R.N.J. 1940. Asphaltic Bitumen as Colloid System. *Journal of Physical Chemistry* **44** (02): 139-149.

Prakoso, A.A., Punase, A.D., Hascakir, B. 2015. A Mechanistic Understanding of Asphaltenes Precipitation from Varying Saturate Concentration Perspective. Presented at SPE Latin American and Carribean Petroleum Engineering Conference, 18-20 November, Quito, Ecuador, SPE-177280-MS. https://doi.org/10.2118/177280-MS

Prakoso, A.A., Punase, A., Klock, K., Rogel, E., Ovalles, C., Hascakir, B. 2016a. Determination of the Stability of Asphaltenes through Physicochemical Characterization of Asphaltenes. Presented at SPE Western Regional Meeting, 23-26 May, Anchorage, Alaska, USA. SPE-180422-MS. DOI: 10.2118/180422-MS.

Prakoso, A.A., Punase, A., Hascakir, B. 2016b. Pore Scale Representation of Near Wellbore Damage due to Asphaltene Deposition: Effect of Sand Grain Size and the Amount of Clay in Reservoir Rock. Presented at SPE International Heavy Oil Conference & Exhibition, 6-8 December 2016, Mangaf, Kuwait, SPE-184099-MS.

Prakoso, A., Punase, A., Hascakir, B. 2017. A Mechanistic Understanding of Asphaltene Precipitation from Varying Saturate Concentration Perspective. *SPE Production & Operation* **32** (01): 86-98. SPE-177280-PA.

Punase, A.D., Prakoso, A.A., Hascakir, B. 2016. The Polarity of Crude Oil Fractions Affects the Asphaltenes Stability. Presented at SPE Western Regional Meeting, 23-26 May, Anchorage, Alaska, USA, SPE-180423-MS. https://doi.org/10.2118/180423-MS

Punase, A., Hascakir, B. 2016. The Role of Deasphalted Oil in the Stability of Asphaltenes. Presented at American institute of Chemical Engineers Spring Meeting & 12th Global Congress on Process Safety, 4th International Conference on Upstream Engineering and Flow Assurance, 10-14 April 2016. Houston, Texas, USA

Punase, A., Hascakir, B. 2017. Stability Determination of Asphaltenes through Dielectric Constant Measurements of Polar Oil Fractions. *Energy and Fuels* **31** (01): 65-72.

Punase, A., Demir, A.B., Bilgesu, H., Hascakir, B. 2017. Inorganic Content of Asphaltenes Impacts Asphaltenes Stability. Presented at SPE Latin American and Caribbean Petroleum Engineering Conference, 17-19 May, Buenos Aires, Argentina, SPE-185543-MS.

Redelius, P., Soenen, H. 2015. Relation Between Bitumen Chemistry and Performance. *Fuel* **140** (01): 34-43.

Rodriguez-Navarro, C., Doehne, E., Sebastian, E. 2000. How Does Sodium Sulfate Crytallize? Implications for the Decay and Testing of Building Materials. *Cement and Concrete Research* **30** (10): 1527-1534.

Rogel, E., Ovalles, C., Moir, M. 2010. Asphaltenes Stability in Crude Oils and Petroleum Materials by Solubility Profile Analysis. *Energy Fuels* **24** (08): 4369-4374.

Ryan, B. 1990. Density of Coals from the Telkwa Coal Property. Northwestern British Columbia, Geological Fieldwork, Paper 1191-1, British Columbia Geological Survey Branch, 399-406.

Sabbah, H., Morrow, A.L., Pomerantz, A.E., Zare, R.N. 2011. Evidence of Island Structures as the Dominant Architecture of Asphaltenes. *Energy Fuels* **25** (04): 1597-1604.

Sazanovich, I.V., Galievsky, V.A., van Hoek, A., Schaafsma, T.J., Malinovskii, V.L., Holten, D., Chirvony, V.S. 2001. Photophysical and Structural Properties of Saddle-shaped Free Base Porphyrins: Evidence for an "Orthogonal" Dipole Moment. *Journal of Physical Chemistry B* **105** (32): 7818-7829.

Schuler, B., Meyer, G., Peña, D., Mullins, O.C., Gross, L. 2015. Unraveling the Molecular Structure of Asphaltenes by Atomic Force Microscope. *J. Am. Chem. Soc.* **137** (31): 9870-9876.

Scott, A. H., Curtis, H. L. 1939. Edge Correction in the determination of Dielectric Constant. US Department of Commerce, National Bureau of Standards, Research Paper RP1217, 747-775.

Sears, F.W. 1982. *University Physics.* 6th ed., Addison Wesley, Boston. ISBN: 8-185015-63-5.

Seifried, C.M., Lawati, S.A., Crawshaw, J.P., Boek, E.B. 2013. Asphaltenes Deposition in Capillary Flow. Presented at SPE Annualt Technical Conference and Exhibition, New Orleans, Lousiana, USA, 30 September - 2 October. SPE-166289-MS. http://dx.doi.org/10.2118/166289-MS.

Sidgwick, N.V. 1936. Dipole Moment and Molecular Structure. *Chem. Rev.* **19** (03): 183-194.

Sill, W.R., Klein, J.D. 1981. *The Electrical Properties of Clay*. Geological Survey (U.S.), University of Utah. Department of Geology and Geophysics.

Sirdeshmukh, D.B., Sirdeshmukh, L., Subhadra, K.G. 2001. *Alkali Halides: A Handbook of Physical Properties*. Springer, Berlin-Heidelberg. ISBN: 3-540421-80-7.

Smyth, C.P. 1929. The Properties of Dielectrics. I. Electric Moment and Molecular Structure. *Journal of the Franklin Institute* **207** (06): 813-824.

Sorrell, T.N. 2006. *Organic Chemistry*. 2nd ed., University Science Book, Sausalito, CA. ISBN: 1-891389-38-6.

Speight, J.G. 1991. *The Chemistry and Technology of Petroleum*: Chemical industries: v. 44, New York : M. Dekker, 2nd ed., rev. & expanded. ISBN: 0-8247-8481-2.

Speight, J.G. 2001. *Handbook of Petroleum Analysis*. New York, John Wiley and Sons Inc.

Speight, J.G. 2006. *The Chemistry and Technology of Petroleum*. New York, USA, CRC Press (Reprint)

Speight, J.G. 2014. *Chemistry and Technology of Petroleum*. 5th Edition, Boca Raton, FL, USA, CRC Press.

Speight, J.G., Long, R.B. 1996. The Concept of Asphaltenes Revisited. *Fuel Science and Technology International* **14** (1-2): 1-12.

Swanson, J.M. 1942. A Contribution to the Physical Chemistry of the Asphalts. *J. Phys. Chem.* **46** (01): 141-150.

Tang, G.Q., Morrow, N.R. 1997. *Salinity, Temperature, Oil Composition, and Oil Recovery by Waterflooding*. Society of Petroleum Engineers. doi: 10.2118/36680-PA.

Uetani, T. 2014. Wettability Alteration by Asphaltenes Deposition: A Field Example. Presented at Abu Dhabi International Petroleum Exhibition and Conference, Abu Dhabi, UAE, 10-13 November. SPE-171788-MS. http://dx.doi.org/10.2118/171788-MS.

Waldo, G.S., Carlson, R.M.K., Moldowan, J.M., Peters, K.E., Penner-Hahn, J.E. 1991. Sulfur Speciation in Heavy Petroleums: Information from X-ray Absorption Near-Edge Structure. *Geochimica et Cosmochimica Acta* **55** (03): 801-814. http://dx.doi.org/10.1016/0016-7037(91)90343-4.

Wang, J., Buckley, J.S. 2003. Asphaltenes Stability in Crude Oil and Aromatic Solvents - The Influence of Oil Composition. *Energy Fuels* **17** (06): 1445-1451.

Wattana, P., Fogler, H.S., Yen, A., Garcia, M.D.C., Carbognani, L. 2005. Characterization of Polarity- Based Asphaltenes Subfractions. *Energy Fuels* **19** (01): 101-110.

Wiehe, I.A. 2012. Asphaltenes Solubility and Fluid Compatibility. *Energy Fuels* **26** (07): 4004-4016.

Wu, Y., Zhao, X., Li, F., Fan, Z. 2004. Evaluation of Mixing Rules for Dielectric Constants of Composite Dielectrics by MC-FEM Calculation on 3D Cubic Lattice. *Journal of Electroceramics* **11** (03): 227-239.

Wulfberg, G. 2000. *Inorganic Chemistry*. University Science Book, Sausalito, CA. ISBN: 1-891389-01-7.

Wypych, G. 2001. *Handbook of Solvents*. ChemTech Publishing, New York. ISBN: 1-895198-24-0.

Yen, T.F. 1992. The Colloidal Aspect of a Macrostructure of Petroleum Asphalt. *Fuel Sci. Technology Int.* **10** (04): 723-733.

Yen, T.F., Chilingarian, G.V. 1994. *Asphaltenes and Asphalts 1*. Elsevier Science, Amsterdam, Netherlands. ISBN: 0-444-88291-X.

Young, K.F., Frederikse, H.P.R. 1973. Compilation of the Static Dielectric Constant of Inorganic Solids. *J. Phys. Chem. Ref. Data* **2** (02): 313-409.

APPENDIX

Appendix 2-A

Images of Bulk Oil and Asphaltenes Samples

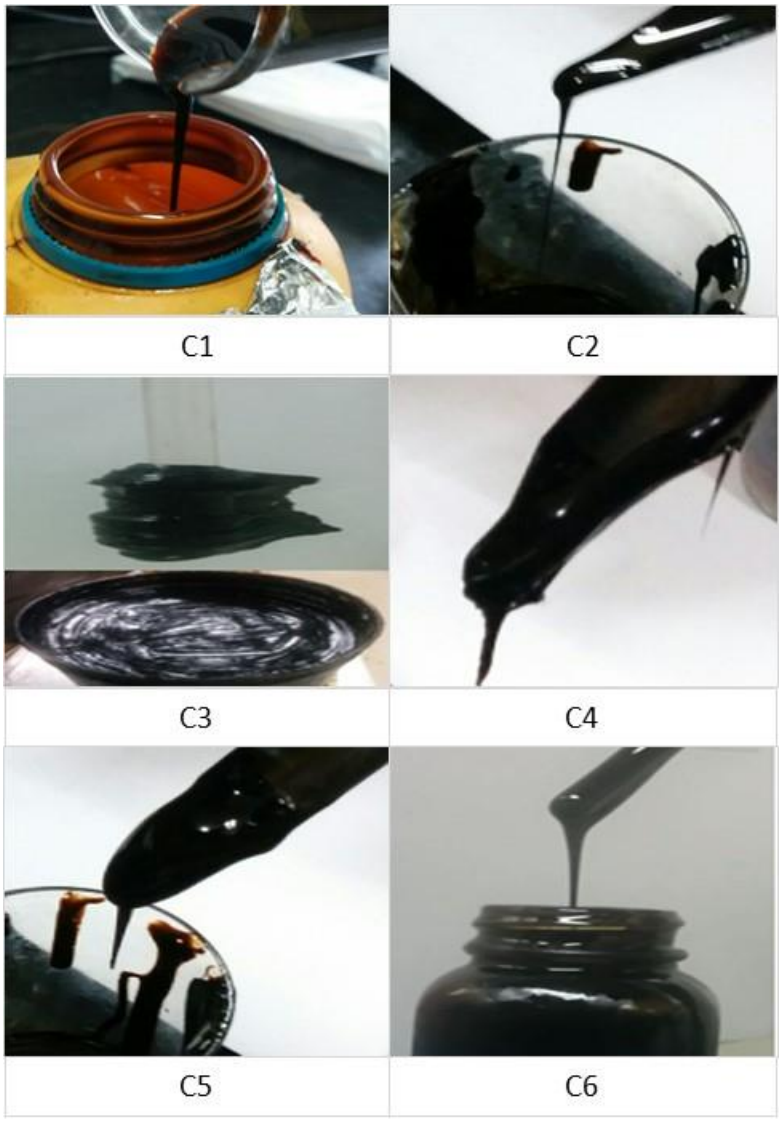

Fig. 2A-1 – Images of heavy oil and bitumen samples.

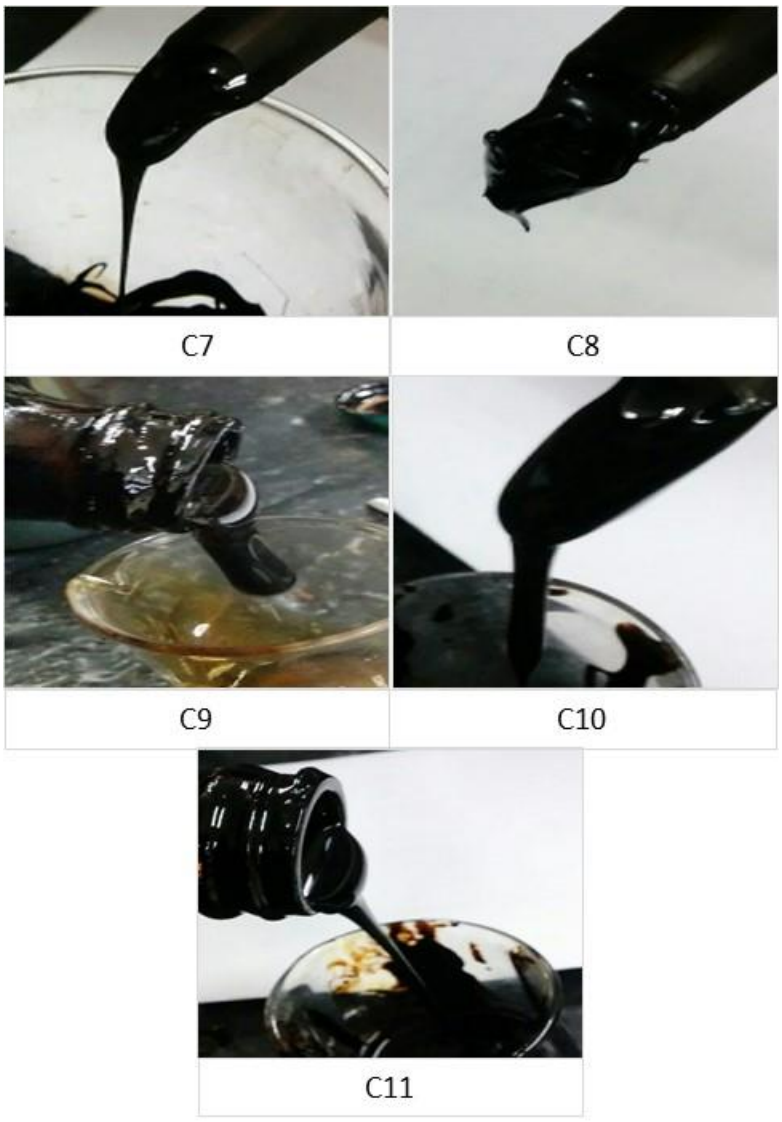

Fig. 2A-1 cont. – Images of heavy oil and bitumen samples.

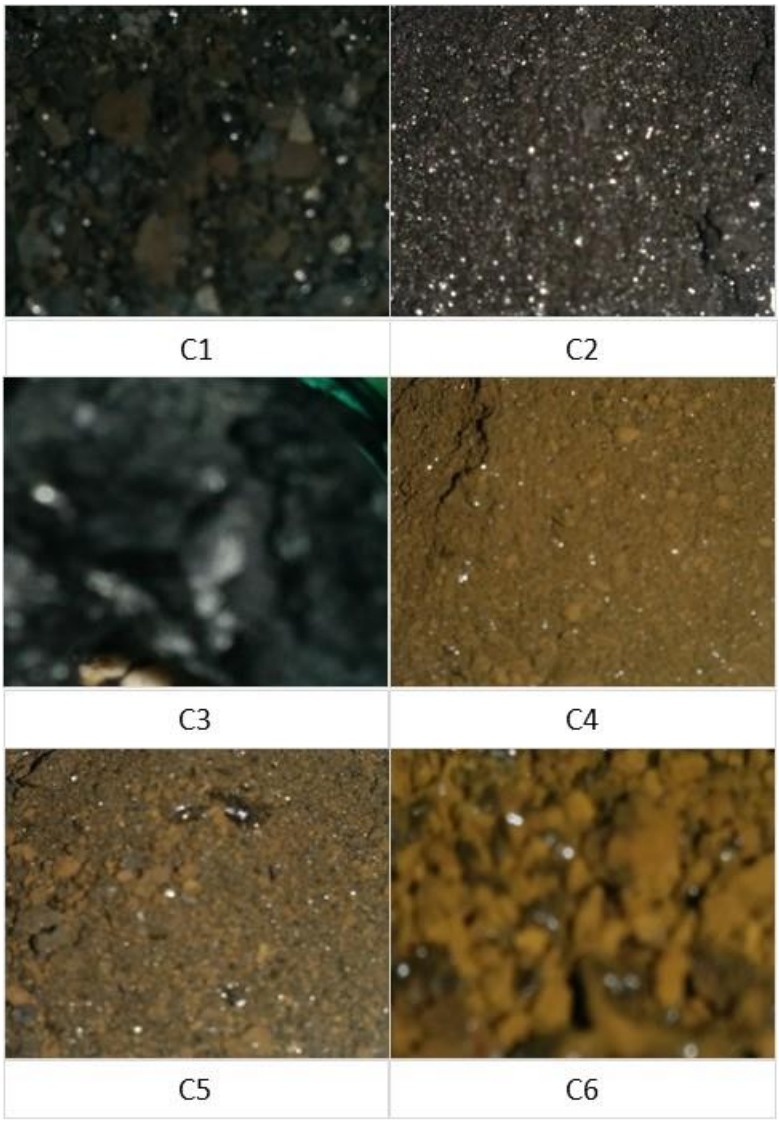

Fig. 2A-2 – Images of n-pentane insoluble asphaltenes fraction of heavy oil and bitumen samples.

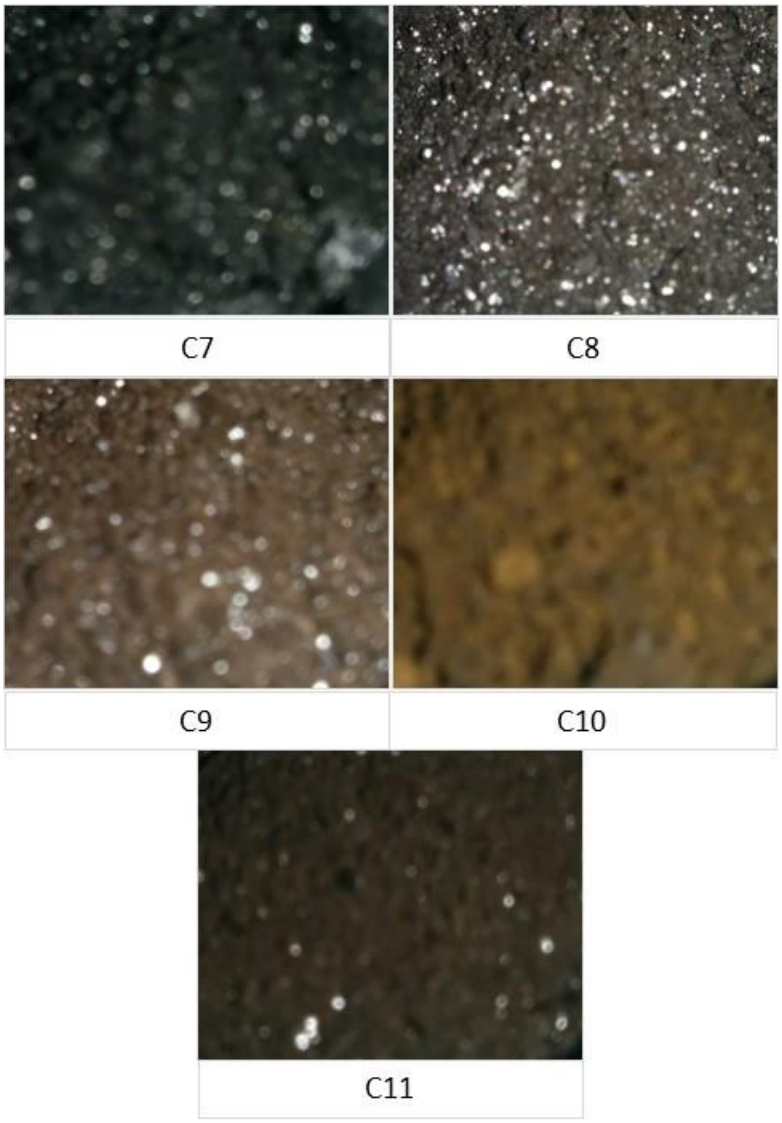

Fig. 2A-2 cont. – Images of n-pentane insoluble asphaltenes fraction of heavy oil and bitumen samples.

Appendix 3-A

Scanning Electron Microscopy (SEM) Images of Asphaltenes

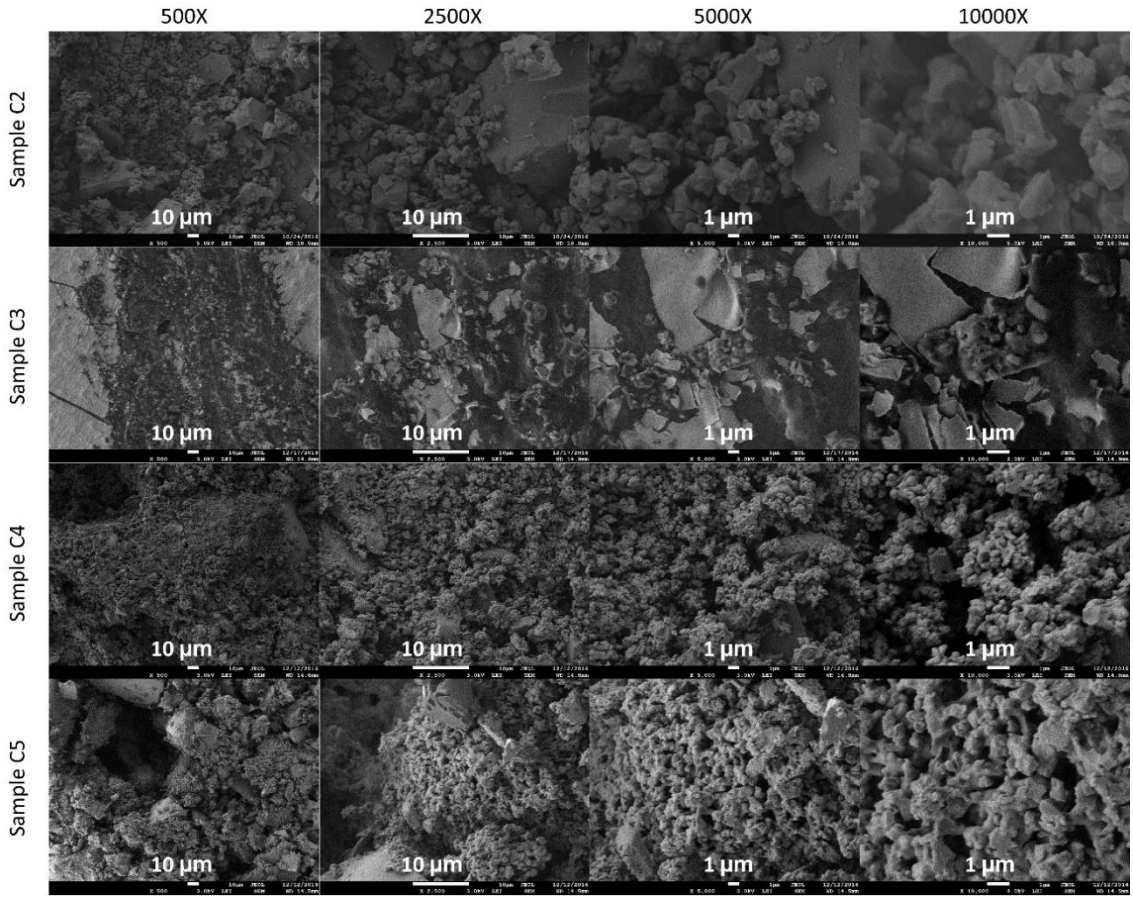

Fig. 3A-1 – SEM images of n-pentane asphaltenes of C2, C3, C4, and C5 oil samples at different magnifications.

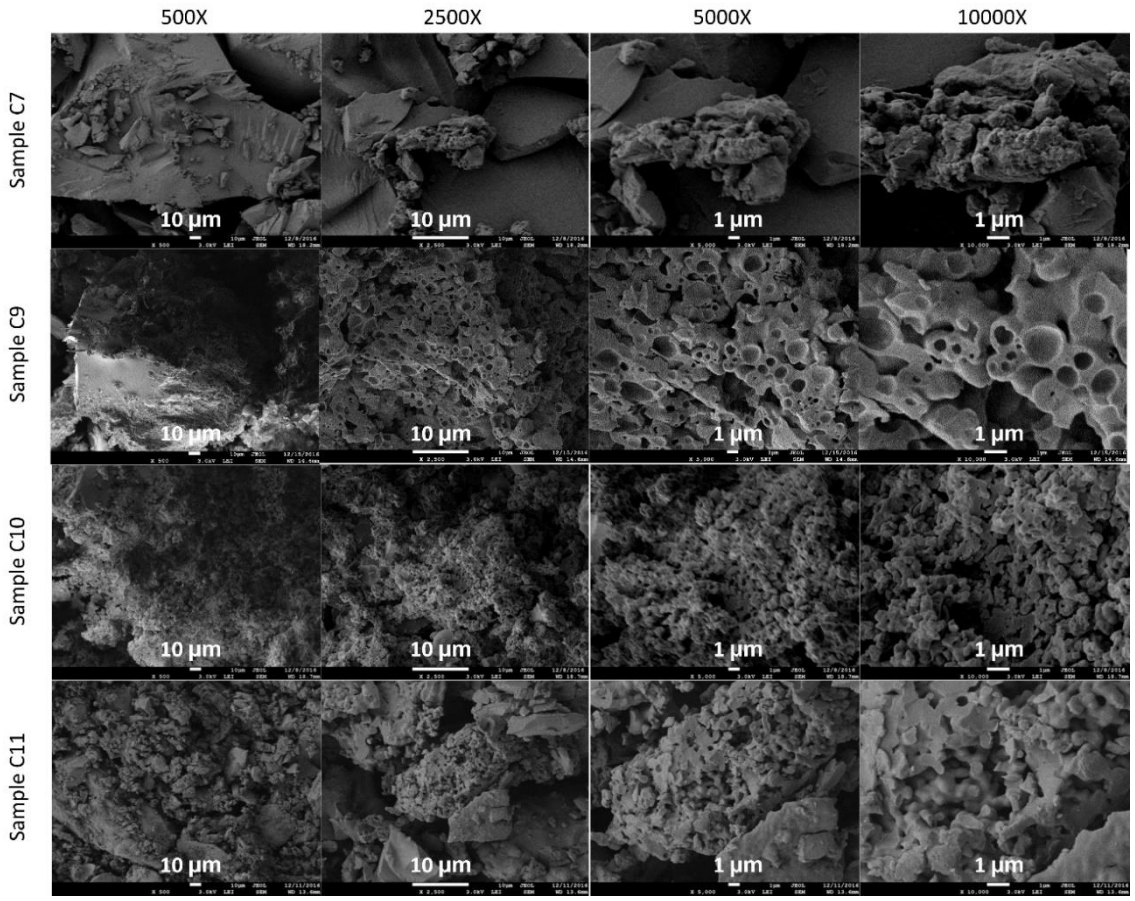

Fig. 3A-1 cont. – SEM images of n-pentane asphaltenes of C7, C8, C10, and C11 oil samples at different magnifications.

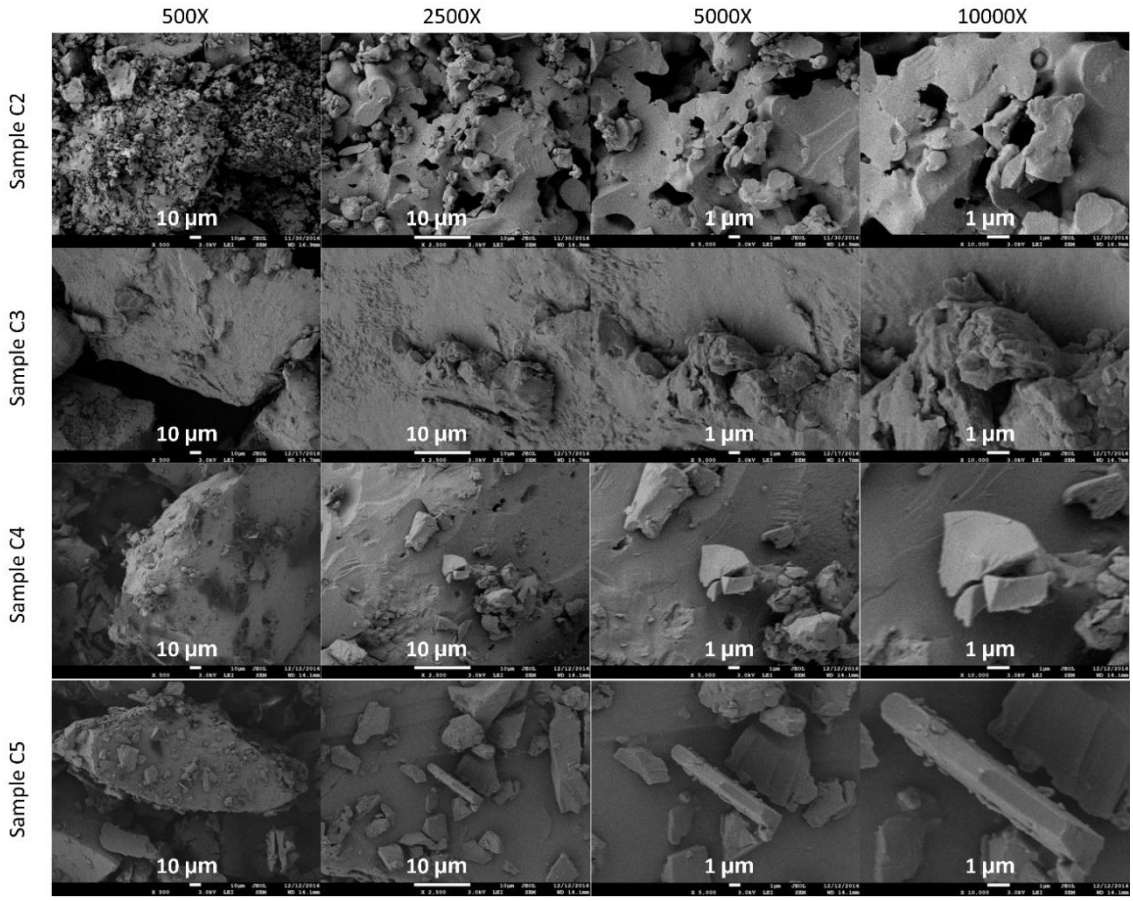

Fig. 3A-2 – SEM images of n-heptane asphaltenes of C2, C3, C4, and C5 oil samples at different magnifications.

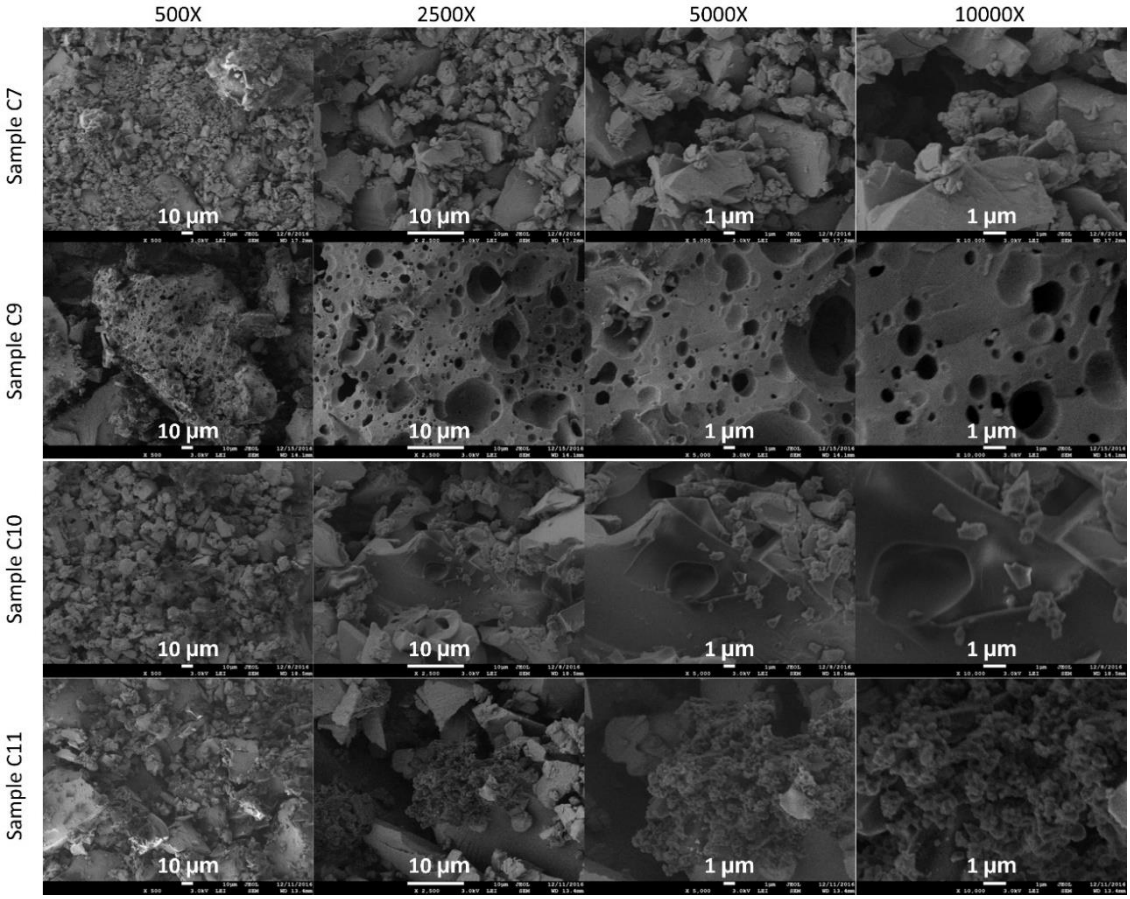

Fig. 3A-2 cont. – SEM images of n-heptane asphaltenes of C7, C9, C10, and C11 oil samples at different magnifications.

Appendix 3-B

Energy Dispersive Spectroscopy (EDS) Results

EDS analysis of the n-pentane insoluble asphaltenes fraction of C1 crude oil.

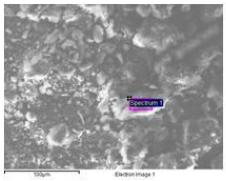
SITE 1

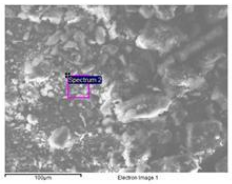
SITE 2

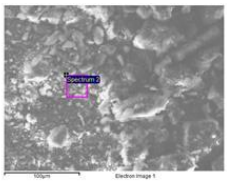
SITE 3

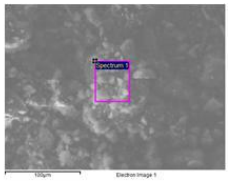
SITE 4

Location	C	O	S	Si	Na	Cl	V
Site 1	91.30	6.81	1.67	-	0.13	0.10	-
Site 2	90.78	6.62	2.41	-	0.08	0.11	-
Site 3	90.83	6.64	2.42	-	-	0.11	-
Site 4	91.04	7.49	1.33	-	0.08	0.07	-

EDS analysis of the n-heptane insoluble asphaltenes fraction of C1 crude oil.

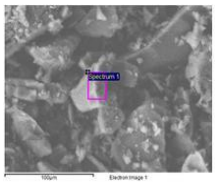
SITE 1

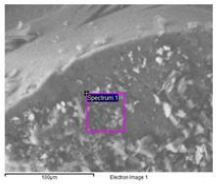
SITE 2

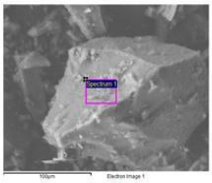
SITE 3

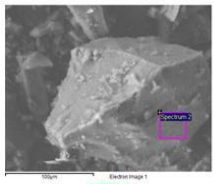
SITE 4

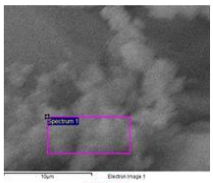
SITE 5

Location	C	O	S	Si	Na	Cl	V
Site 1	92.37	4.83	2.50	-	0.12	0.18	-
Site 2	91.36	3.99	3.46	-	0.37	0.82	-
Site 3	90.02	8.08	1.45	-	0.24	0.21	-
Site 4	90.60	4.30	4.02	-	0.14	0.64	-
Site 5	90.70	7.44	1.47	-	0.21	0.18	-

EDS analysis of the n-pentane insoluble asphaltenes fraction of C2 crude oil.

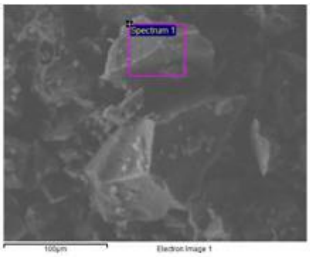
SITE 1

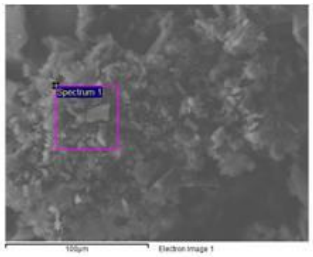
SITE 2

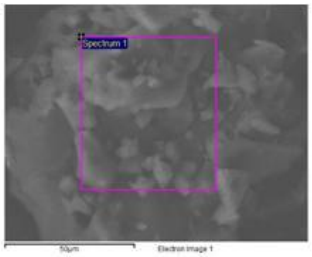
SITE 3

Location	C	O	S	Si	Na	Cl	V
Site 1	89.53	7.38	3.10	-	-	-	-
Site 2	88.68	7.18	2.60	1.55	-	-	-
Site 3	88.53	3.68	7.14	-	0.13	0.25	-

EDS analysis of the n-heptane insoluble asphaltenes fraction of C2 crude oil.

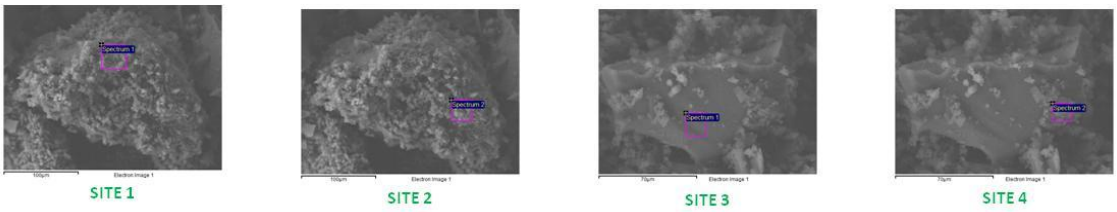

Location	C	O	S	Si	Na	Cl	V
Site 1	87.65	5.68	5.06	0.15	0.70	0.76	-
Site 2	88.07	3.05	2.86	0.15	0.29	0.49	-
Site 3	82.00	2.11	15.24	-	-	0.65	-
Site 4	85.55	2.11	10.98	0.24	0.22	0.91	-

EDS analysis of the n-pentane insoluble asphaltenes fraction of C3 crude oil.

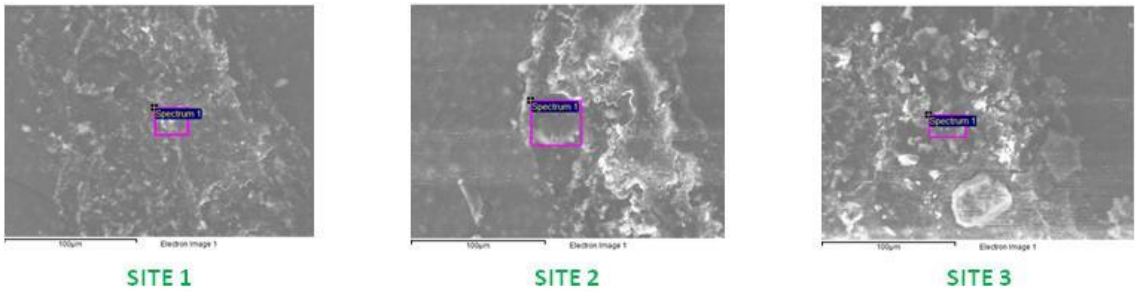

Location	C	O	S	Si	Na	Cl	V	Ca
Site 1	92.72	6.77	0.33	-	0.09	0.09	-	-
Site 2	94.56	3.81	1.53	-	-	0.07	-	0.03
Site 3	91.61	5.53	2.87	-	-	-	-	-

EDS analysis of the n-heptane insoluble asphaltenes fraction of C3 crude oil.

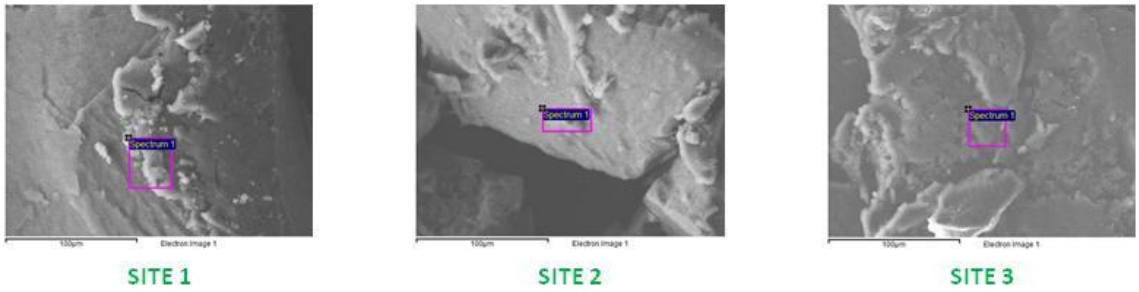

Location	C	O	S	Si	Na	Cl	V	Ca
Site 1	93.60	6.23	0.16	-	-	-	-	-
Site 2	92.33	7.46	0.21	-	-	-	-	-
Site 3	93.18	6.68	0.14	-	-	-	-	-

EDS analysis of the n-pentane insoluble asphaltenes fraction of C4 crude oil.

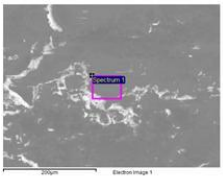

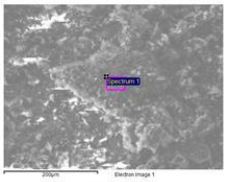

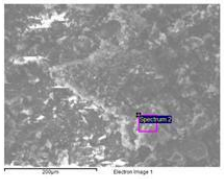

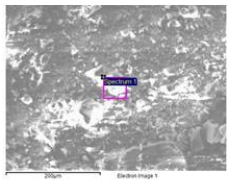

Location	C	O	S	Si	Na	Cl	V
Site 1	91.54	4.16	4.20	-	0.10	-	-
Site 2	91.60	4.13	4.27	-	-	-	-
Site 3	92.35	4.16	3.49	-	-	-	-
Site 4	91.35	4.27	4.38	-	-	-	-

EDS analysis of the n-heptane insoluble asphaltenes fraction of C4 crude oil.

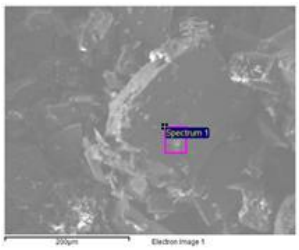

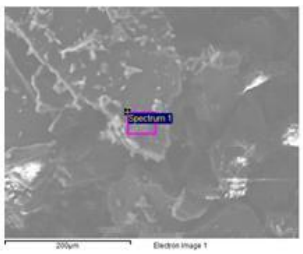

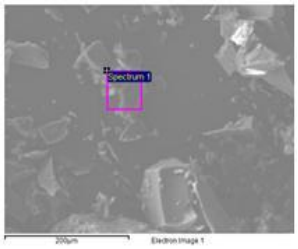

Location	C	O	S	Si	Na	Cl	V
Site 1	91.98	2.99	4.67	-	-	0.19	0.16
Site 2	92.17	3.14	4.12	-	0.13	-	0.11
Site 3	90.33	4.80	4.87	-	-	-	-

EDS analysis of the n-pentane insoluble asphaltenes fraction of C5 crude oil.

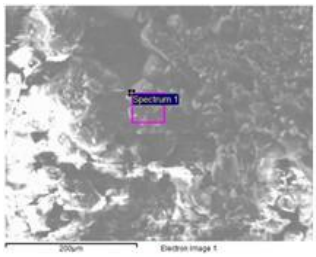

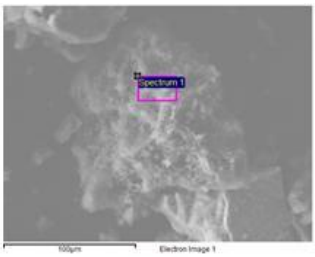

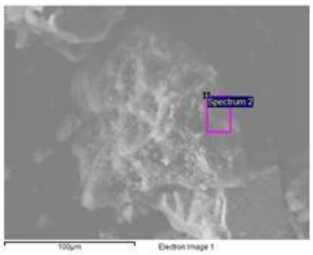

Location	C	O	S	Si	Na	Cl	V
Site 1	91.49	3.22	5.00	0.17	-	-	0.12
Site 2	91.64	4.08	4.28	-	-	-	-
Site 3	86.18	9.41	4.41	-	-	-	-

EDS analysis of the n-heptane insoluble asphaltenes fraction of C5 crude oil.

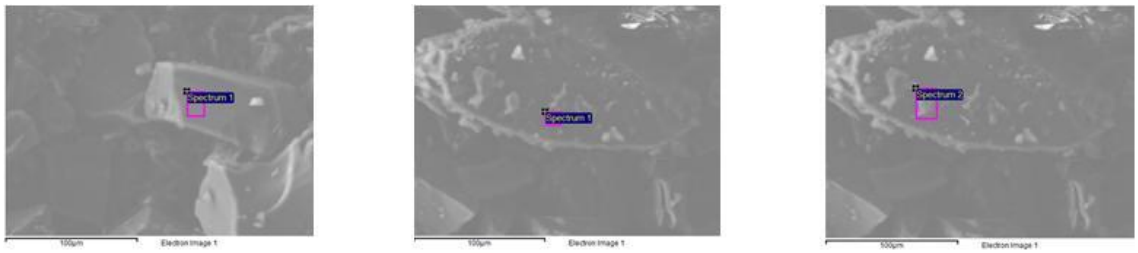

Location	C	O	S	Si	Na	Cl	V
Site 1	91.19	3.47	5.34	-	-	-	-
Site 2	89.71	2.08	8.06	-	-	-	0.14
Site 3	90.13	2.40	7.31	-	-	-	0.16

EDS analysis of the n-pentane insoluble asphaltenes fraction of C6 crude oil.

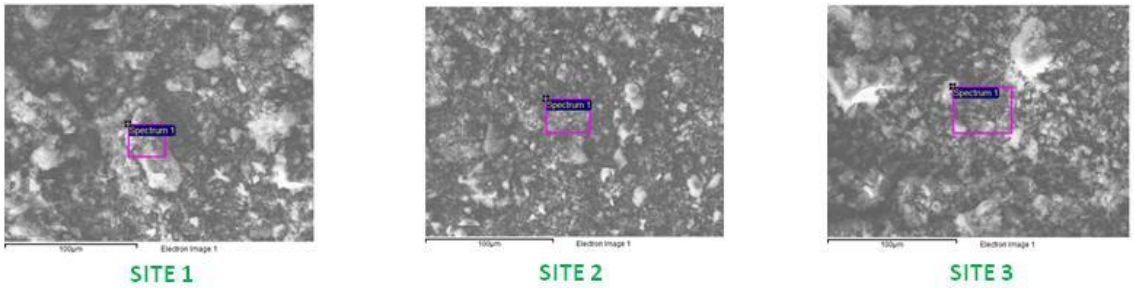

Location	C	O	S	Si	Na	Cl	V	Ca
Site 1	89.99	5.58	4.20	-	0.09	0.09	-	0.05
Site 2	89.98	4.99	4.72	-	0.10	0.12	-	0.09
Site 3	89.55	5.58	4.73	-	0.09	0.05	-	-

EDS analysis of the n-heptane insoluble asphaltenes fraction of C6 crude oil.

Location	C	O	S	Si	Na	Cl	V	Ca
Site 1	84.98	12.12	2.63	-	0.07	0.10	-	0.10
Site 2	88.15	6.11	4.88	-	0.23	0.46	-	0.16

EDS analysis of the n-pentane insoluble asphaltenes fraction of C7 crude oil.

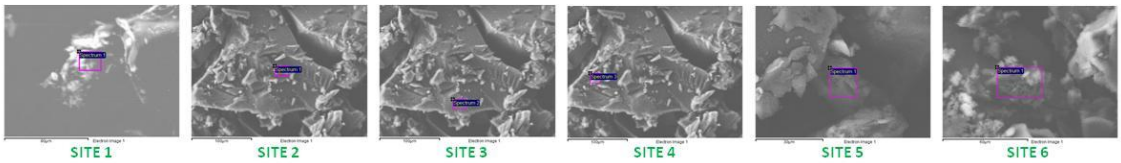

Location	C	O	S	Si	Na	Cl	V
Site 1	93.72	5.49	0.79	-	-	-	-
Site 2	90.81	6.73	2.47	-	-	-	-
Site 3	89.16	8.97	1.87	-	-	-	-
Site 4	90.32	7.68	2.00	-	-	-	-
Site 5	89.26	3.10	6.92	0.72	-	-	-
Site 6	90.14	8.20	1.66	-	-	-	-

EDS analysis of the n-heptane insoluble asphaltenes fraction of C7 crude oil.

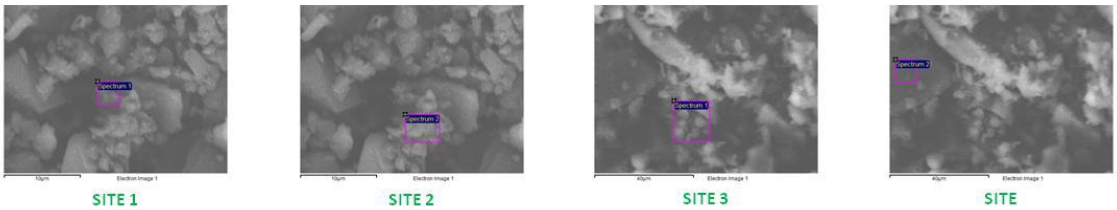

Location	C	O	S	Si	Na	Cl	V
Site 1	92.89	4.78	2.32	-	-	-	-
Site 2	92.76	5.41	1.83	-	-	-	-
Site 3	92.93	4.40	2.68	-	-	-	-
Site 4	90.08	5.02	4.90	-	-	-	-

EDS analysis of the n-pentane insoluble asphaltenes fraction of C8 crude oil.

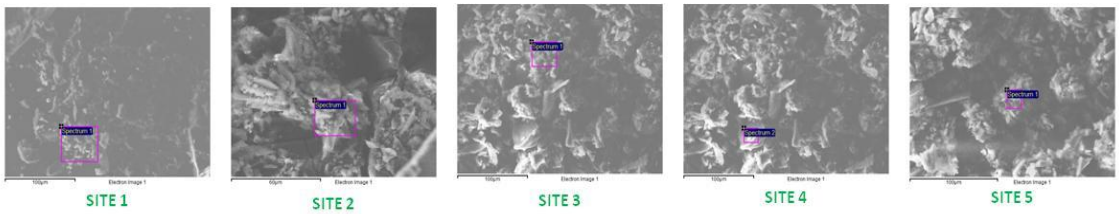

Location	C	O	S	Si	Na	Cl	V	Ca
Site 1	90.58	4.14	4.98	-	0.18	0.12	-	-
Site 2	90.32	3.82	5.44	-	0.20	0.22	-	-
Site 3	91.31	2.79	5.33	-	0.17	0.32	-	0.08
Site 4	91.36	4.89	3.45	-	0.11	0.15	-	0.04
Site 5	89.56	3.60	5.61	-	0.33	0.66	0.11	0.13

EDS analysis of the n-heptane insoluble asphaltenes fraction of C8 crude oil.

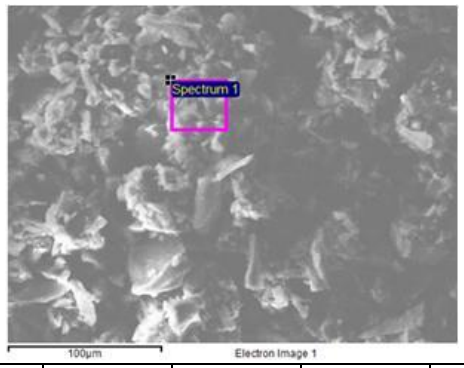

Location	C	O	S	Si	Na	Cl	V	Ca
Site 1	91.31	2.79	5.33	-	0.17	0.32	-	0.08

EDS analysis of the n-pentane insoluble asphaltenes fraction of C9 crude oil.

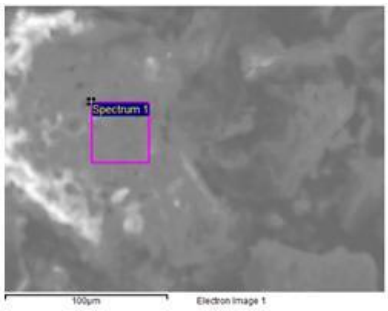

SITE 1

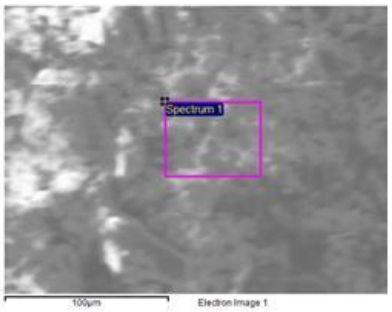

SITE 2

Location	C	O	S	Si	Na	Cl	V	Ca	Al
Site 1	88.27	4.18	6.02	-	0.80	0.66	0.06	-	-
Site 2	88.37	5.90	5.11	-	0.32	0.30	-	-	-

EDS analysis of the n-heptane insoluble asphaltenes fraction of C9 crude oil.

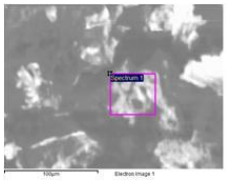

SITE 1

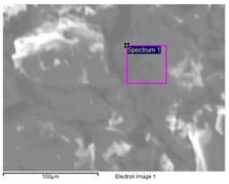

SITE 2

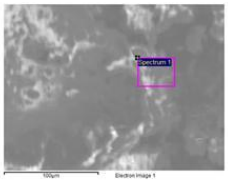

SITE 3

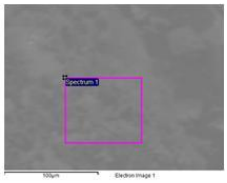

SITE 4

Location	C	O	S	Si	Na	Cl	V	Ca	Al
Site 1	69.90	21.65	7.11	0.09	0.11	0.22	-	0.83	0.10
Site 2	88.76	4.24	6.56	-	0.22	0.22	-	-	-
Site 3	87.17	4.80	8.02	-	-	-	-	-	-
Site 4	88.77	4.37	6.37	-	0.22	0.19	0.07	-	-

EDS analysis of the n-pentane insoluble asphaltenes fraction of C10 crude oil.

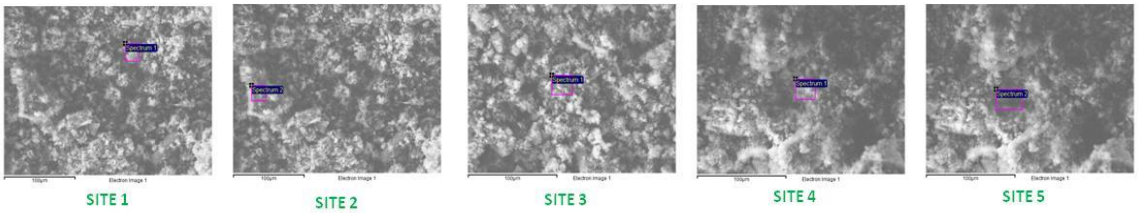

Location	C	O	S	Si	Na	Cl	V
Site 1	91.76	5.37	2.87	-	-	-	-
Site 2	91.25	4.18	4.57	-	-	-	-
Site 3	91.95	5.10	2.95	-	-	-	-
Site 4	90.86	4.57	4.57	-	-	-	-
Site 5	89.05	2.65	8.30	-	-	-	-

EDS analysis of the n-pentane insoluble asphaltenes fraction of C10 crude oil.

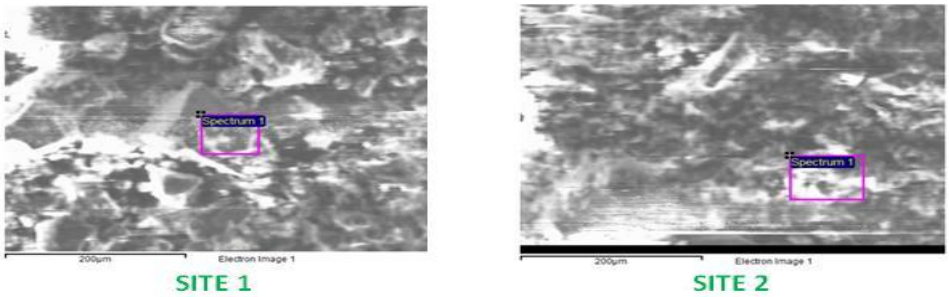

Location	C	O	S	Si	Na	Cl	V
Site 1	88.51	9.32	2.17	-	-	-	-
Site 2	91.81	5.74	2.45	-	-	-	-

EDS analysis of the n-pentane insoluble asphaltenes fraction of C11 crude oil.

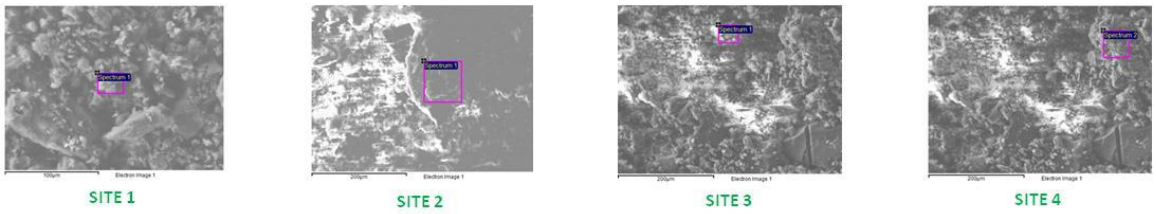

Location	C	O	S	Si	Na	Cl	V
Site 1	90.91	2.50	6.59	-	-	-	-
Site 2	90.13	3.53	6.34	-	-	-	-
Site 3	91.23	3.64	5.06	0.07	-	-	-
Site 4	89.50	4.36	6.15	-	-	-	-

EDS analysis of the n-heptane insoluble asphaltenes fraction of C11 crude oil.

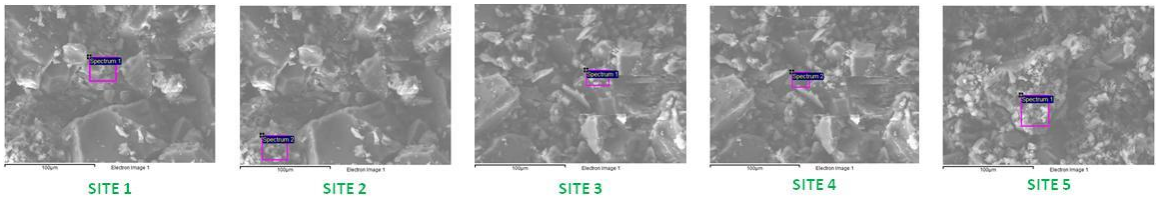

Location	C	O	S	Si	Na	Cl	V
Site 1	89.77	2.84	7.40	-	-	-	-
Site 2	90.99	3.57	5.45	-	-	-	-
Site 3	91.63	3.00	5.37	-	-	-	-
Site 4	90.77	3.26	5.97	-	-	-	-
Site 5	89.53	3.95	6.52	-	-	-	-

Appendix 3-C

Electrical Properties

Daily measurement of Total dissolved solids (TDS) for n-pentane and n-heptane insoluble asphaltenes fractions of 11 crude oil samples are given in Table 3C-1 and 3C-2, respectively.

Table 3C-1 – Total Dissolved Solids (TDS) within n-pentane asphaltenes fraction of crude oil.

Total Dissolved Solids							
Sample	**Day-1**	**Day-2**	**Day-3**	**Day-4**	**Day-5**	**Day-6**	**Day-7**
C1	4.89	5.97	6.56	7.34	7.39	7.58	7.83
C2	26.40	39.60	49.70	52.00	51.60	53.70	54.10
C3	0.76	0.90	0.87	0.88	0.93	1.05	1.31
C4	6.09	9.21	12.60	19.90	20.10	20.40	21.10
C5	5.89	13.80	15.70	16.10	16.20	16.30	16.70
C6	21.6	32.3	35.7	37.5	35.6	38.6	39.3
C7	2.21	2.94	3.84	3.92	4.38	4.28	4.62
C8	31.40	35.60	42.60	44.40	45.30	45.00	45.70
C9	34.10	37.20	40.10	41.60	43.60	42.60	42.80
C10	3.02	3.10	6.22	6.59	7.26	7.53	7.70
C11	3.08	3.93	4.40	4.62	4.75	5.11	5.26

Table 3C-2 – Total Dissolved Solids (TDS) within n-heptane asphaltenes fraction of crude oil.

Total Dissolved Solids							
Sample	**Day-1**	**Day-2**	**Day-3**	**Day-4**	**Day-5**	**Day-6**	**Day-7**
C1	11.30	33.20	39.40	44.10	45.80	56.10	60.80
C2	13.30	40.70	65.80	73.80	76.00	80.40	80.70
C3	1.52	1.62	2.22	2.27	2.53	2.63	2.78
C4	3.29	8.58	10.80	12.30	13.20	14.60	14.90
C5	1.94	2.02	2.06	2.15	2.36	2.56	2.65
C6	81.00	112.00	116.00	122.00	127.00	124.00	130.00
C7	3.28	6.90	7.15	7.66	7.67	7.92	7.98
C8	8.67	34.70	50.80	57.90	63.20	63.10	66.80
C9	50.80	64.60	68.00	68.90	68.10	70.90	72.10
C10	5.52	8.39	10.30	10.60	12.40	13.10	13.40
C11	2.27	3.75	2.79	2.90	3.13	3.18	3.56

Zeta potential and particle size analyses were carried out 4-6 times for each sample and the results for supernatant of n-pentane are presented in Table 3C-3.

Table 3C-3 – Zeta potential and particle size measurement for n-pentane asphaltenes.

C1 (n-Pentane insoluble asphaltenes)												
	Particle Size (nm)						Zeta Potential (mV)					
	Trial 1	Trial 2	Trial 3	Trial 4	Trial 5	Trial 6	Trial 1	Trial 2	Trial 3	Trial 4	Trial 5	Trial 6
Run 1	20174.7	1787.2	23922.1	3466.0	2096.6	2162.5	-31.35	-22.72	-24.28	-28.42	-34.04	-33.74
Run 2	33647.1	1440.4	6383.3	2936.2	1866.8	2179.1	-29.97	-30.38	-24.99	-27.72	-35.88	-34.01
Run 3	2311.6	1481.1	5264.7	4056.6	2028.9	1852.1	-28.98	-27.70	-23.44	-26.33	-36.22	-33.42
Run 4	3362.2	1198.3	7696.7	6587.2	1955.1	2527.6	-30.29	-25.15	-28.62	-23.69	-33.50	-34.14
Run 5	10377.2	4254.1	3174.7	3650.9	3292.1	1822.8	-25.52	-32.24	-27.23	-24.83	-34.62	-34.46
Combined Value	**10909.3**	**2117.7**	**8082.8**	**3861.0**	**2184.4**	**2119.7**	**-29.18**	**-27.58**	**-25.64**	**-26.18**	**-34.84**	**-33.95**
	4879.2						**-29.6**					

C2 (n-Pentane insoluble asphaltenes)												
	Particle Size (nm)						Zeta Potential (mV)					
	Trial 1	Trial 2	Trial 3	Trial 4	Trial 5	Trial 6	Trial 1	Trial 2	Trial 3	Trial 4	Trial 5	Trial 6
Run 1	11028.2	1911.0	8377.8	7876.9	1.8	1084.1	-28.84	-21.73	-28.49	-22.48	-19.33	-26.06
Run 2	1262.1	24753.7	12359.1	59170.1	0.0	1399.6	-31.29	-20.46	-21.15	-13.60	-22.34	-25.07
Run 3	1303.1	8090.9	737.5	8149.4	2.4	5947.6	-30.19	-17.45	-23.42	-21.25	-13.37	-19.89
Run 4	2048.7	2451.3	3722.8	7595.4	0.0	12882.9	-34.18	-16.67	-25.69	-43.03	-21.70	-13.13
Run 5	1858.6	1615.9	5409.5	11628.1	7427.4	2286	-26.55	-18.25	-31.05	-17.55	-24.90	-14.30
Combined Value	**1829.5**	**3055.2**	**11711.4**	**7728.7**	**1754.4**	**7675.9**	**-30.20**	**-18.76**	**-25.95**	**-23.48**	**-20.34**	**-19.33**
	5625.9						**-23.0**					

C3 (n-Pentane insoluble asphaltenes)												
	Particle Size (nm)						Zeta Potential (mV)					
	Trial 1	Trial 2	Trial 3	Trial 4	Trial 5	Trial 6	Trial 1	Trial 2	Trial 3	Trial 4	Trial 5	Trial 6
Run 1	7935.8	750.1	19612.8	1356.9	1207.6	-4.22	-10.94	-4.53	-3.95	-6.63	7935.8	750.1
Run 2	1007.6	690.2	1097.5	1092.4	1029.4	3.60	-6.52	-3.44	-12.35	-5.57	1007.6	690.2
Run 3	675.7	720.2	696.8	1386.3	1519.2	-4.68	-6.28	-5.34	-7.02	-7.45	675.7	720.2
Run 4	1245.2	571.4	724.5	1218.7	1059.0	-6.32	-10.35	-7.80	-7.46	-11.16	1245.2	571.4
Run 5	538.6	773.5	748.2	972.2	1004.5	-8.42	-9.02	-6.95	-9.49	-9.79	538.6	773.5
Combined Value	**5478.1**	**719.8**	**942.9**	**1171.9**	**1164.5**	**-4.05**	**-7.93**	**-3.28**	**-7.94**	**-7.89**	**5478.1**	**719.8**
	1895.4						**-6.2**					

Table 3C-3 cont. – Zeta potential and particle size measurement for n-pentane asphaltenes.

C4 (n-Pentane insoluble asphaltenes)												
	Particle Size (nm)						Zeta Potential (mV)					
	Trial 1	Trial 2	Trial 3	Trial 4	Trial 5	Trial 6	Trial 1	Trial 2	Trial 3	Trial 4	Trial 5	Trial 6
Run 1	12210.1	10398.1	9143.8	63117.9	23888.6	5356.9	-37.25	-38.54	-20.51	-11.54	-20.69	-19.36
Run 2	34037.0	8697.7	24647.4	13010.3	0.0	15985.9	-31.42	-36.34	-16.10	-15.88	-15.27	-25.79
Run 3	27786.1	20364.5	17051.1	2535.1	1834.9	755.1	-36.94	-39.19	-22.13	-23.69	-14.32	-24.44
Run 4	3539.1	3695.7	8553.0	3615.9	0.0	7007.1	-38.39	-36.61	-22.63	-19.79	-15.65	-26.86
Run 5	4397.2	11864.6	4560.6	11961.6	1625.5	1416.6	-36.91	-30.56	-14.23	-15.69	-17.28	-22.77
Combined Value	**18321.3**	**9404.8**	**14559.9**	**12561.9**	**24581.0**	**5099.3**	**-36.17**	**-36.22**	**-19.04**	**-17.12**	**-16.60**	**-23.86**
	14088.0						**-24.8**					

C5 (n-Pentane insoluble asphaltenes)												
	Particle Size (nm)						Zeta Potential (mV)					
	Trial 1	Trial 2	Trial 3	Trial 4	Trial 5	Trial 6	Trial 1	Trial 2	Trial 3	Trial 4	Trial 5	Trial 6
Run 1	27343.2	19862.6	20729.5	7588.4	20746.5	11869.1	-14.63	-7.55	-16.28	-18.98	-18.59	-21.69
Run 2	34333.0	6388.8	15163.9	2969.1	23952.8	2868.8	-16.00	-16.41	-17.78	-18.15	-19.81	-22.86
Run 3	8712.7	14405.6	19496.6	15036.0	2214.8	40740.0	-16.90	-16.49	-17.25	-12.85	-24.83	-18.49
Run 4	14351.2	6059.6	2978.7	13080.9	3712.2	66.0	-15.07	-16.79	-10.63	-18.59	-22.73	-18.10
Run 5	4590.4	13108.1	36995.5	12617.3	4808.6	1574.3	-17.15	-21.05	-17.55	-15.60	-22.19	-19.58
Combined Value	**23360.3**	**11185.1**	**18139.2**	**11343.1**	**8892.1**	**4166.7**	**-15.91**	**-15.60**	**-15.73**	**-16.61**	**-21.59**	**-20.13**
	12847.8						**-17.6**					

C6 (n-Pentane insoluble asphaltenes)												
	Particle Size (nm)						Zeta Potential (mV)					
	Trial 1	Trial 2	Trial 3	Trial 4	Trial 5	Trial 6	Trial 1	Trial 2	Trial 3	Trial 4	Trial 5	Trial 6
Run 1	3275.1	2741.8	5786.9	3549.7	3524.8	2895.2	-25.99	-27.89	-26.21	-25.06	-22.42	-29.19
Run 2	4144.7	2798.2	4838.9	5882.3	5312.7	2751.3	-24.39	-27.63	-26.91	-26.07	-24.81	-27.89
Run 3	13426.8	3768.7	3381.3	2745.6	3438.2	2515.1	-27.18	-27.57	-29.23	-24.11	-24.12	-25.92
Run 4	2482.7	2811.0	2677.8	5989.1	3337.4	3055.0	-26.14	-28.04	-26.48	-25.24	-26.33	-23.06
Run 5	2318.0	3615.4	2885.9	2898.7	3608.2	7540.5	-24.28	-26.43	-26.01	-26.53	-28.30	-24.96
Combined Value	**3896.2**	**3173.8**	**4032.4**	**4658.7**	**3831.9**	**3381.5**	**-25.58**	**-27.46**	**-26.95**	**-25.39**	**-25.22**	**-26.14**
	3829.1						**-26.1**					

Table 3C-3 cont. – Zeta potential and particle size measurement for n-pentane asphaltenes.

C7 (n-Pentane insoluble asphaltenes)												
	Particle Size (nm)						Zeta Potential (mV)					
	Trial 1	Trial 2	Trial 3	Trial 4	Trial 5	Trial 6	Trial 1	Trial 2	Trial 3	Trial 4	Trial 5	Trial 6
Run 1	0.0	1120.9	883.8	936.5	3087.8	1105.3	-14.94	-13.33	-19.21	-19.04	-16.51	-17.10
Run 2	1170.6	805.4	1069.2	967.3	1375.1	1358.2	-16.28	-12.63	-13.40	-19.87	-16.63	-17.56
Run 3	968.3	776.2	1128.5	805.5	1276.7	1122.1	-15.33	-16.57	-17.03	-18.31	-23.13	-19.47
Run 4	1039.0	1723.3	1197.2	1407.9	1543.5	37877.3	-12.87	-15.96	-17.59	-26.08	-19.40	-16.07
Run 5	936.4	1018.3	828.1	1489.5	980.0	972.0	-15.89	-14.76	-16.19	-20.07	-19.49	-14.40
Combined Value	**983.8**	**1047.5**	**1032.1**	**1088.7**	**1457.9**	**1936.3**	**-15.01**	**-14.58**	**-16.62**	**-20.67**	**-18.97**	**-16.90**
	1257.7						**-17.1**					

C8 (n-Pentane insoluble asphaltenes)												
	Particle Size (nm)						Zeta Potential (mV)					
	Trial 1	Trial 2	Trial 3	Trial 4	Trial 5	Trial 6	Trial 1	Trial 2	Trial 3	Trial 4	Trial 5	Trial 6
Run 1	847.0	3888.9	1257.6	4141.3	1165.4	-26.93	-32.80	-34.46	-19.09	-21.82	847.0	3888.9
Run 2	437.4	572.5	767.1	521.5	586.8	-25.87	-28.93	-28.90	-16.06	-38.30	437.4	572.5
Run 3	433.7	896.9	551.4	2254.2	517.0	-18.25	-27.57	-34.14	-20.79	-13.40	433.7	896.9
Run 4	1329.1	1339.3	456.3	368.7	28720.3	-13.66	-30.15	-24.49	-16.35	-14.85	1329.1	1339.3
Run 5	705.4	484.1	521.7	8403.5	746.8	-18.12	-34.05	-30.26	-22.03	-18.82	705.4	484.1
Combined Value	**666.1**	**796.8**	**717.7**	**5981.6**	**1237.8**	**-20.39**	**-30.68**	**-30.40**	**-18.75**	**-21.37**	**666.1**	**796.8**
	1880.0						**-24.3**					

C9 (n-Pentane insoluble asphaltenes)												
	Particle Size (nm)						Zeta Potential (mV)					
	Trial 1	Trial 2	Trial 3	Trial 4	Trial 5	Trial 6	Trial 1	Trial 2	Trial 3	Trial 4	Trial 5	Trial 6
Run 1	186.0	187.6	195.9	177.3	196.3	197.7	-40.17	-30.44	-42.06	-42.99	-39.39	-40.25
Run 2	179.4	196.3	186.9	172.4	184.9	184.6	-34.11	-35.38	-41.55	-35.25	-42.79	-35.04
Run 3	183.3	198.8	181.6	190.2	174.6	182.2	-35.80	-32.18	-36.88	-40.01	-37.51	-36.91
Run 4	209.9	195.4	177.5	216.8	176.2	189.3	-40.41	-24.43	-34.10	-41.87	-40.20	-36.31
Run 5	177.5	192.0	191.9	178.5	181.2	196.3	-33.09	-37.27	-31.72	-44.19	-44.03	-45.73
Combined Value	**187.6**	**194.1**	**187.2**	**185.8**	**183.3**	**190.3**	**-36.62**	**-31.91**	**-37.18**	**-40.84**	**-40.79**	**-38.83**
	188.1						**-37.7**					

Table 3C-3 cont. – Zeta potential and particle size measurement for n-pentane asphaltenes.

C10 (n-Pentane insoluble asphaltenes)												
	Particle Size (nm)						Zeta Potential (mV)					
	Trial 1	Trial 2	Trial 3	Trial 4	Trial 5	Trial 6	Trial 1	Trial 2	Trial 3	Trial 4	Trial 5	Trial 6
Run 1	1944.5	1665.1	3179.6	1519.3	1812.2	2347.1	-24.89	-23.59	-29.00	-28.24	-24.30	-23.73
Run 2	1872.0	2397.4	2118.6	1700.7	2207.1	1618.6	-24.17	-26.16	-26.05	-26.08	-24.46	-25.00
Run 3	3617.6	2186.9	2031.1	1534.5	1542.8	1757.2	-24.61	-24.76	-25.19	-25.05	-23.48	-23.77
Run 4	2242.8	1430.9	1892.8	1580.7	3550.2	1916.6	-22.97	-25.05	-25.72	-26.13	-24.96	-23.12
Run 5	2373.4	3873.3	2702.0	1514.9	1777.9	1986.2	-27.80	-24.64	-26.48	-26.16	-24.16	-21.42
Combined Value	**2165.5**	**2335.4**	**2287.2**	**1558.0**	**1938.1**	**1968.7**	**-24.87**	**-24.84**	**-26.72**	**-26.30**	**-24.18**	**-23.40**
	2042.2						**-25.1**					

C11 (n-Pentane insoluble asphaltenes)										
	Particle Size (nm)					Zeta Potential (mV)				
	Trial 1	Trial 2	Trial 3	Trial 4	Trial 5	Trial 1	Trial 2	Trial 3	Trial 4	Trial 5
Run 1	45427.0	9274.4	1097.2	21381.3	1437.0	-0.94	-22.76	-14.41	-21.99	-18.68
Run 2	1513.4	1423.7	660.3	18677.9	44621.1	-7.83	-23.72	-19.42	-22.36	-22.82
Run 3	3477.8	0.0	1535.1	20132.1	28200.6	-10.60	-16.65	-15.60	-21.02	-23.88
Run 4	357.2	22091.1	511.7	12595.7	0.0	-7.08	-18.04	-18.33	-23.93	-23.92
Run 5	12449.2	3635.1	1361.0	14706.6	1693.1	4.01	-18.41	-13.13	-19.68	-25.02
Combined Value	**15523.9**	**10562.3**	**1121.1**	**14547.5**	**27745.5**	**-3.60**	**-19.74**	**-15.92**	**-21.78**	**-22.83**
	13900.1					**-16.8**				

Similarly, zeta potential and particle size analyses data for the supernatant of n-heptane insoluble asphaltenes of all 11 samples is given in Table 3C-4.

Table 3C-4 – Zeta potential and particle size measurement for n-heptane asphaltenes.

C1 (n-Heptane insoluble asphaltenes)										
	Particle Size (nm)					Zeta Potential (mV)				
	Trial 1	Trial 2	Trial 3	Trial 4	Trial 6	Trial 1	Trial 2	Trial 3	Trial 4	Trial 6
Run 1	1190.0	812.5	1081.2	1577.0	2659.1	-21.22	-13.81	-9.13	-8.62	-17.88
Run 2	990.7	941.5	1101.1	996.5	917	-13.68	-17.06	-15.59	-11.92	-15.33
Run 3	1116.7	852.5	1159.2	2152.3	750.8	-20.21	-15.87	-10.66	-10.67	-13.40
Run 4	820.8	3774.9	1003.0	1357.6	5529.3	-13.96	-15.78	-7.52	-9.83	-10.92
Run 5	841.5	899.1	1534.0	1193.3	2244.8	-15.05	-17.21	-9.76	-18.48	-12.54
Combined Value	**945.0**	**1437.8**	**1209.6**	**1514.6**	**2377.1**	**-16.64**	**-15.59**	**-10.41**	**-11.68**	**-13.76**
	1496.8					**-13.6**				

C2 (n-Heptane insoluble asphaltenes)												
	Particle Size (nm)						Zeta Potential (mV)					
	Trial 1	Trial 2	Trial 3	Trial 4	Trial 5	Trial 6	Trial 1	Trial 2	Trial 3	Trial 4	Trial 5	Trial 6
Run 1	17225.9	25742.7	28498.4	2009.8	9532.1	39295.8	-46.10	-41.16	-60.17	-55.63	-13.00	-13.61
Run 2	19569.9	4831.5	4531.1	2118.3	0.0	24665	-45.64	-24.54	-63.93	-59.18	-18.28	-13.37
Run 3	13603.1	4952.6	11959.7	3684.2	1510.6	1149.7	-54.20	-29.57	-60.88	-58.73	-12.76	-22.60
Run 4	9741.3	2740.5	2253.8	3639.8	58741.5	587.1	-42.27	-28.96	-62.91	-59.95	-14.29	-12.42
Run 5	21225.4	2729.1	3486.0	2254.5	2056.6	1781.4	-59.08	-49.66	-60.15	-60.99	-20.12	-11.27
Combined Value	**17948.0**	**4466.5**	**5154.2**	**2952.6**	**10212.7**	**20679.3**	**-49.49**	**-34.77**	**-61.61**	**-58.90**	**-15.58**	**-14.61**
	10235.6						**-39.2**					

C3 (n-Heptane insoluble asphaltenes)												
	Particle Size (nm)						Zeta Potential (mV)					
	Trial 1	Trial 2	Trial 3	Trial 4	Trial 5	Trial 6	Trial 1	Trial 2	Trial 3	Trial 4	Trial 5	Trial 6
Run 1	739.7	677.9	723.0	910.9	1011.8	1063.8	-14.32	-14.37	-18.58	-17.51	-15.72	-13.91
Run 2	697.3	845.7	964.8	890.9	1100.6	11833.4	-10.10	-11.40	-14.91	-15.24	-15.43	-12.00
Run 3	628.7	665.4	770.9	912.5	897.7	1196.2	-9.18	-11.96	-15.08	-17.19	-12.84	-14.65
Run 4	22293.7	24224.9	1197.1	874.5	1068.5	1346.5	-10.13	-14.45	-16.81	-17.29	-11.53	-12.41
Run 5	777.0	676.7	864.9	766.1	1101.1	973.8	-9.42	-12.00	-15.02	-16.50	-17.25	-15.16
Combined Value	**18081.9**	**12638.2**	**894.6**	**878.7**	**1018.4**	**1182.7**	**-10.57**	**-12.78**	**-16.04**	**-16.74**	**-14.53**	**-13.59**
	5782.4						**-14.0**					

Table 3C-4 cont. – Zeta potential and particle size measurement for n-heptane asphaltenes.

C4 (n-Heptane insoluble asphaltenes)										
	Particle Size (nm)					Zeta Potential (mV)				
	Trial 1	Trial 2	Trial 3	Trial 4	Trial 5	Trial 1	Trial 2	Trial 3	Trial 4	Trial 5
Run 1	1659.7	1012.8	1940.0	12532.1	934.1	-9.45	-14.13	-2.05	-4.22	2.91
Run 2	13430.0	767.0	940.8	1603.9	107.3	-16.77	-13.60	1.53	-8.75	-1.26
Run 3	990.1	1396.0	963.8	1228.3	1459.7	-14.03	-7.05	-6.16	-7.86	-9.25
Run 4	1105.2	1344.4	944.6	1504.8	491.6	-11.95	-14.00	5.80	-1.59	-9.87
Run 5	604.2	37571.9	1097.6	1202.9	69.3	-14.71	-10.84	-2.60	-5.37	-9.22
Combined Value	**5127.2**	**1320.9**	**1230.1**	**2600.7**	**707.3**	**-13.03**	**-11.81**	**-2.76**	**-2.09**	**-4.49**
	2197.2					**-6.8**				

C5 (n-Heptane insoluble asphaltenes)												
	Particle Size (nm)						Zeta Potential (mV)					
	Trial 1	Trial 2	Trial 3	Trial 4	Trial 5	Trial 6	Trial 1	Trial 2	Trial 3	Trial 4	Trial 5	Trial 6
Run 1	4944.0	1857.8	27834.8	1151.2	1212.4	1307.0	-14.47	-15.78	-6.93	-1.26	-18.94	-9.91
Run 2	5264.3	1838.7	1592.3	1319.8	2004.3	1639.9	-17.24	-13.08	-6.05	-2.48	-16.46	-16.08
Run 3	2097.4	1833.8	1286.1	1665.0	1580.1	24297.5	-18.78	-16.93	3.88	3.07	-17.68	-17.47
Run 4	4236.3	1980.3	3176.6	1467.4	1153.6	1625.4	-19.19	-14.34	-3.43	-8.69	-17.39	-15.29
Run 5	2092.8	2273.1	1425.0	1654.0	18471.2	1382.6	-18.44	-11.53	-3.13	-8.68	-18.51	-16.88
Combined Value	**3103.9**	**1989.4**	**1885.5**	**1484.3**	**11051.7**	**15074.7**	**-17.61**	**-14.30**	**-3.96**	**-4.32**	**-17.78**	**-15.00**
	5764.9						**-12.2**					

C6 (n-Heptane insoluble asphaltenes)												
	Particle Size (nm)						Zeta Potential (mV)					
	Trial 1	Trial 2	Trial 3	Trial 4	Trial 5	Trial 6	Trial 1	Trial 2	Trial 3	Trial 4	Trial 5	Trial 6
Run 1	49561.7	7205.8	6503.2	4055.3	18778.3	13207.2	-4.99	-11.26	-11.23	-7.07	-10.61	-9.71
Run 2	0.0	59559.1	6371.0	4227.9	97011.5	14467.3	-4.86	-5.84	-9.36	-6.64	-11.01	-10.95
Run 3	23551.7	9532.2	23280.6	19998.3	8852.1	11880.5	-6.95	-7.40	-7.29	-5.26	-11.03	-11.42
Run 4	4186.1	50269.4	2829.1	3472.5	15432.7	22879.8	-5.03	-5.56	-10.75	-8.41	-9.25	-7.73
Run 5	2583.1	32194.8	1487.3	6122.8	8273.6	25725.1	-7.55	-5.89	-9.11	-9.83	-7.90	-9.89
Combined Value	**31995.7**	**30931.3**	**7236.5**	**10808.2**	**32478.1**	**17073.2**	**-5.05**	**-6.50**	**-9.51**	**-6.84**	**-9.86**	**-9.91**
	21753.8						**-7.9**					

Table 3C-4 cont. – Zeta potential and particle size measurement for n-heptane asphaltenes.

C7 (n-Heptane insoluble asphaltenes)												
	Particle Size (nm)						Zeta Potential (mV)					
	Trial 1	Trial 2	Trial 3	Trial 4	Trial 5	Trial 6	Trial 1	Trial 2	Trial 3	Trial 4	Trial 5	Trial 6
Run 1	14783.1	2165.8	1238.3	966.3	1053.1	1726.8	-0.77	-9.50	-13.91	-6.31	-15.66	-16.79
Run 2	5123.8	31643.5	48103.7	1769.3	1717.0	1973.0	-0.61	-8.43	-6.26	-6.31	-11.20	-12.14
Run 3	97916.8	1387.4	986.4	2138.8	1251.3	1828.2	-4.26	-11.33	-7.82	-4.32	-12.38	-18.31
Run 4	2599.0	2288.1	1390.0	1022.1	2701.2	942.2	-6.83	-12.63	-6.35	-9.37	-13.76	-11.26
Run 5	1579.6	1613.3	953.3	965.4	2188.9	33563.6	-5.22	-18.16	-11.47	-13.99	-16.58	-11.61
Combined Value	**7674.5**	**29255.6**	**11169.1**	**1421.1**	**1804.3**	**32640.2**	**-3.10**	**-11.86**	**-8.71**	**-7.65**	**-13.84**	**-13.76**
	13994.1						**-9.8**					

C8 (n-Heptane insoluble asphaltenes)						
	Particle Size (nm)			Zeta Potential (mV)		
	Trial 1	Trial 2	Trial 3	Trial 1	Trial 2	Trial 3
Run 1	2015.6	35392.8	43457.7	1.23	2.45	-13.21
Run 2	2112.5	15233.7	2415.1	-6.74	-10.95	-7.15
Run 3	3143.6	8734.0	5903.3	-5.63	4.27	-4.38
Run 4	4961.5	4392.5	6341.9	-8.09	-8.71	2.36
Run 5	4310.9	2084.6	1239.7	-8.55	-14.83	-3.94
Combined Value	**2825.3**	**6706.3**	**5965.8**	**-5.76**	**-6.88**	**-4.56**
	5165.8			**-5.73**		

C9 (n-Heptane insoluble asphaltenes)												
	Particle Size (nm)						Zeta Potential (mV)					
	Trial 1	Trial 2	Trial 3	Trial 4	Trial 5	Trial 6	Trial 1	Trial 2	Trial 3	Trial 4	Trial 5	Trial 6
Run 1	187.6	187.5	184.3	181.7	184.4	186.0	-55.01	-57.72	-49.85	-50.01	-55.73	-53.96
Run 2	177.1	188.8	185.7	174.2	188.0	179.9	-54.14	-57.06	-52.45	-50.41	-59.58	-45.47
Run 3	176.7	187.5	187.6	174.9	183.7	182.8	-52.58	-57.07	-48.54	-56.51	-57.47	-50.04
Run 4	175.4	186.3	184.1	184.6	187.7	183.8	-48.51	-50.07	-56.81	-54.26	-56.29	-53.43
Run 5	174.0	189.0	185.5	186.7	187.7	183.3	-47.75	-46.63	-51.17	-57.34	-58.15	-58.49
Combined Value	**178.3**	**187.7**	**185.6**	**180.3**	**186.3**	**183.3**	**-51.46**	**-53.61**	**-51.69**	**-53.66**	**-57.42**	**-52.24**
	183.6						**-53.3**					

Table 3C-4 cont. – Zeta potential and particle size measurement for n-heptane asphaltenes.

C10 (n-Heptane insoluble asphaltenes)												
	Particle Size (nm)						Zeta Potential (mV)					
	Trial 1	Trial 2	Trial 3	Trial 4	Trial 5	Trial 6	Trial 1	Trial 2	Trial 3	Trial 4	Trial 5	Trial 6
Run 1	5335.7	5783.5	26408.0	14043.4	45404.7	2388.1	-35.50	-36.01	-7.25	-9.99	-25.44	-23.24
Run 2	17660.5	12418.9	3393.6	20242.3	19809.0	5558.6	-35.84	-41.87	-15.57	-17.58	-24.77	-27.81
Run 3	3790.0	8029.8	3535.6	0.0	35492.3	3683.1	-39.21	-39.43	-13.50	-11.71	-24.54	-25.02
Run 4	6059.1	10015.8	0.0	48689.9	30600.3	7397.6	-34.31	-36.28	-6.12	-16.95	-21.48	-26.99
Run 5	8394.0	5662.6	1595.9	0.0	23215.7	5358.3	-34.52	-31.49	-3.22	-8.69	-21.25	-23.26
Combined Value	**6906.7**	**10080.3**	**8931.6**	**21919.9**	**30609.5**	**6482.8**	**-35.87**	**-37.00**	**-9.17**	**-12.96**	**-23.39**	**-24.91**
	14155.1						**-23.9**					

C11 (n-Heptane insoluble asphaltenes)												
	Particle Size (nm)						Zeta Potential (mV)					
	Trial 1	Trial 2	Trial 3	Trial 4	Trial 5	Trial 6	Trial 1	Trial 2	Trial 3	Trial 4	Trial 5	Trial 6
Run 1	0.0	1249.4	1569.6	1895.8	0.0	44575.8	-15.51	-20.12	-8.33	-5.81	-19.02	-16.21
Run 2	1148.4	22878.3	15261.5	12776.0	7989.8	1960.2	-10.85	-12.60	-0.68	-4.84	-14.56	-22.09
Run 3	7278.4	17236.4	36362.2	0.0	2534.8	1241.8	-17.97	-12.33	-8.38	-3.16	-19.41	-17.36
Run 4	10033.8	966.3	76901.7	9173.0	0.0	14526.8	-17.65	-7.07	-9.24	3.45	-21.67	-15.37
Run 5	2053.5	8645.7	18550.9	88722.0	10288.6	1389.4	-9.45	-11.92	-3.93	-4.55	-16.00	-18.84
Combined Value	**41903.5**	**22389.4**	**34504.3**	**13237.6**	**18807.9**	**14101.8**	**-13.84**	**-12.64**	**-5.30**	**-3.48**	**-18.08**	**-19.95**
	24157.4						**-12.2**					

Appendix 3-D

Statistical Analysis of Particle Size and Zeta Potential Data

Furthermore, to analyze the significance of each measured data point on the average particle size and zeta potential result, a statistical approach of regression and determination of p-value is carried out. It should be noted that a p-value of less than 0.05 represents statistical significance. Table 3D-1 enlists the p-values for particle size and zeta potential of both n-pentane as well as n-heptane insoluble asphaltenes samples.

Table 3D-1 – P values for particle size and zeta potential results signifying the contribution of all the data points.

Trial #	Particle Size		Zeta Potential	
	nC5 asphaltenes	nC7 asphaltenes	nC5 asphaltenes	nC7 asphaltenes
Trial 1	9.62E-05	2.81E-03	8.32E-04	4.84E-05
Trial 2	3.32E-07	3.02E-03	1.76E-03	1.64E-05
Trial 3	2.59E-02	7.46E-03	2.60E-05	4.10E-04
Trial 4	8.22E-06	3.59E-02	3.05E-04	8.35E-05
Trial 5	2.99E-04	1.36E-02	3.80E-04	2.10E-03
Trial 6	1.24E-01	8.99E-02	3.75E-04	2.82E-03

Appendix 4-A

Capacitor Design Calculations

According to Gauss' law, the area integral of the electric field over any closed surface is equal to the net charge enclosed in the surface divided by the permittivity of space. Mathematically this law can be represented by Eq. 4A-1.

$$\oint \vec{E}.\overrightarrow{dA} = \frac{Q}{\varepsilon_0} = \frac{\lambda L}{\varepsilon_0} \qquad (4A\text{-}1)$$

Where dA is an elemental area of closed Gaussian surface placed within an electric field of potential E, Q denotes the net charge enclosed in the surface, $\lambda = Q/L$ is the charge per unit length, and ε_0 represents permittivity of space (8.85×10^{-12} F/m).

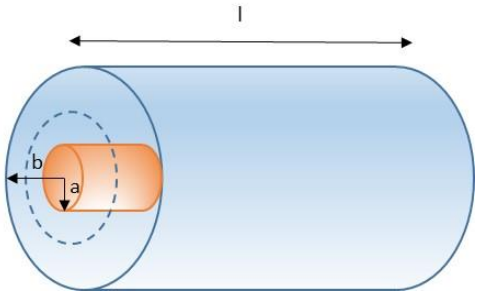

Fig. 4A-1 – Schematic diagram of a cylindrical capacitor.

For a coaxial solid cylindrical capacitor having length 'l' m, inner radius 'a' m, and outer radius 'b' m (as a shown in Fig. 4A-1), such that l is much greater than (b-a), gauss law is modified as given by Eq. 4A-2.

$$\oint \vec{E}.\overrightarrow{dA} = E.(2\pi rl) = \frac{\lambda l}{\varepsilon_0} \quad \Rightarrow E = \frac{\lambda}{2\pi r \varepsilon_0} \qquad (4A\text{-}2)$$

It should be noted that the electric field is significant only in the radial region between the inner and outer radii (i.e. $a < r < b$). For $r < a$, the enclosed charge is 0,

because in all the electric charge in a conductor must reside on its surface. Similarly, for r > b, the enclosed charge is λl - λl = 0, since the Gaussian surface encloses equal but opposite charges from both coaxial cylindrical solid conductor surfaces. Therefore, the potential difference is given by a close integral of charge distribution within the radial region between 'a' and 'b'. Mathematically, it is expressed by Eq. 4A-3.

$$\Delta V = V_b - V_a = \oint_a^b E\, dr = \frac{\lambda}{2\pi\varepsilon_0}\oint_a^b \frac{dr}{r} = \frac{\lambda}{2\pi\varepsilon_0}\ln\left(\frac{b}{a}\right) \tag{4A-3}$$

Therefore, the overall capacitance is

$$C = \frac{Q}{\Delta V} = \frac{\lambda l}{\frac{\lambda}{2\pi\varepsilon_0}\ln\left(\frac{b}{a}\right)} = \frac{2\pi\varepsilon_0 l}{\ln\left(b/a\right)} \tag{4A-4}$$

For a material with dielectric constant ε, Eq. 4A-4 is modified as follows:

$$C = \frac{2\pi\varepsilon_0\varepsilon l}{\ln\left(b/a\right)} \tag{4A-5}$$

If the annulus between the cylindrical radii is empty is filled with air (ε=1), then Eq. 4A-5 can be reduced to an expression yielding dimensional constraints for the capacitor, as given by Eq. 4A-6.

$$\frac{l}{\ln\left(b/a\right)} = \frac{C}{2\pi\varepsilon_0} = \frac{10*10^{-12}\ F}{2*3.14*10*10^{-12}\ F/m} = 0.15955\ m \tag{4A-6}$$

Therefore, the dimensions of the fabricated capacitor are optimized (length = 0.78 cm, inner radius = 2 cm, outer radius = 2.1 cm) to follow the correlation constraints highlighted by Eq. 4A-6 and have an annulus volume of 1 cm^3.

Appendix 4-B

Mathematical Representation of Tested Analytical Correlations

1. Lowry (1929) Correlation

$$\varepsilon_m = v_1\varepsilon_1 + v_2\varepsilon_2 \tag{4B-1}$$

2. Bruggeman (1935) Correlation

$$v_2 = 1 - \frac{\varepsilon_2 - \varepsilon}{\varepsilon_2 - \varepsilon_1}\left(\frac{\varepsilon_1}{\varepsilon}\right)^{1/3} \tag{4B-2}$$

3. Böttcher (1952) Correlation

$$v_2 = \frac{(\varepsilon - \varepsilon_1)(2\varepsilon + \varepsilon_2)}{3\varepsilon(\varepsilon_2 - \varepsilon_1)} \tag{4B-3}$$

4. Looyenga (1965) Correlation

$$\varepsilon_m = \left[({\varepsilon_2}^{1/3} - {\varepsilon_1}^{1/3})v_2 + {\varepsilon_1}^{1/3}\right]^3 \tag{4B-4}$$

5. Maxwell-Garnett Correlation (Borhen and Huffman 1983)

$$\varepsilon_m = \varepsilon_1 + 3v_2\varepsilon_1 \frac{(\varepsilon_2 - \varepsilon_1)}{\varepsilon_2 + 2\varepsilon_1 - v_2(\varepsilon_2 - \varepsilon_1)} \tag{4B-5}$$

6. Lichtenecher Correlation (Wu et al. 2004)

$$log\varepsilon_m = v_1 log\varepsilon_1 + v_2 log\varepsilon_2 \tag{4B-6}$$

Where ε and v denotes the dielectric constant and volume fraction, respectively. Both the parameters are dimensionless. Subscript 'm' signifies crude oil mixture, 1 and 2 represents properties corresponding to DAO and asphaltenes fraction, respectively.

Appendix 4-C

Asphaltenes Density Measurement

Asphaltenes are defined as a solubility class of the crude oil, which is insoluble in n-alkanes and soluble in aromatic solvents (Speight 1991). Due to the polydispersity of the crude oil molecules, various fractions such as saturates, aromatics, resins, and asphaltenes comprises of numerous chemical compounds having distinct physical properties (Speight 1991; Yen and Chilingarian 1994). Therefore, accurate determination of molecular weight, density, chemical composition, and chemical structure of these fractions is very difficult (Barrera et al. 2013). In addition to the molecular polydispersity, the self-association tendency between asphaltenes molecules also makes estimation of these properties difficult (Mullins and Sheu 1998; Birdi 2008). Furthermore, entrapment of air bubbles and irregular molecular surface of asphaltenes cluster also increase the uncertainty associated with the estimation of these physical properties.

Density of asphaltenes affects various solubility and polarity parameters. Thus, it is important to accurately measure or estimate the density values of the 11 different asphaltenes analyzed in this study. Several procedures using different test fluids such as water, n-pentane, and toluene were carried out to experimentally measure the density of asphaltenes samples. Additionally, material balance based on the weight fractions of asphaltenes and maltenes (deasphalted oil) within the crude oil sample was also conducted. Chemical interactions between the test fluid and asphaltenes or incomplete accessibility of test fluid due to entrapped air bubbles resulted in inaccurate

measurement of the volume occupied by asphaltenes clusters. Consequently, the error associated with the volumetric estimation led to lower measured density of asphaltenes as compared to its real value. Following section provide the values of asphaltenes density obtained by using different test fluids and procedures.

Asphaltenes-Toluene Mixture

Procedure developed by Barrera et al. (2013) was followed to determine asphaltenes density using asphaltenes-toluene mixtures. Since asphaltenes are soluble in toluene, mixtures of varying concentration of asphaltenes were prepared. Density of each mixture was measured using an Anton Paar DMA4100 density meter at room temperature (22°C). Assuming that the mixture of asphaltenes and toluene form regular solution, then the density of the solution can be estimated using equation 4C-1.

$$\frac{1}{\rho_{mix}} = \frac{w_1}{\rho_1} + \frac{w_2}{\rho_2} \qquad \text{(4C-1)}$$

Where ρ is density (g/cm^3), w represents the weight fraction, and subscripts mix, 1, and 2 denote the mixture, solvent, and asphaltenes, respectively. Thus, density of asphaltenes can be indirectly determined from the plot of specific volume (inverse of mixture density) and asphaltenes weight fraction. Density obtained through this process for n-pentane and n-heptane asphaltenes fractions of all the 11 asphaltenes are tabulated in Table 4C-1. The plots between specific volume and asphaltenes weight fractions are shown in Fig. 4C-1.

Table 4C-1 – Density of asphaltenes determined by analyzing asphaltenes-toluene mixture.

Asphaltenes	n-pentane Asphaltenes Density (g/cm^3)	n-heptane Asphaltenes Density (g/cm^3)
C1	1.16	1.21
C2	1.12	1.44
C3	0.95	0.89
C4	1.18	1.16
C5	1.16	1.17
C6	1.21	1.10
C7	1.08	1.20
C8	1.15	1.17
C9	1.05	1.16
C10	1.16	1.12
C11	1.28	1.12

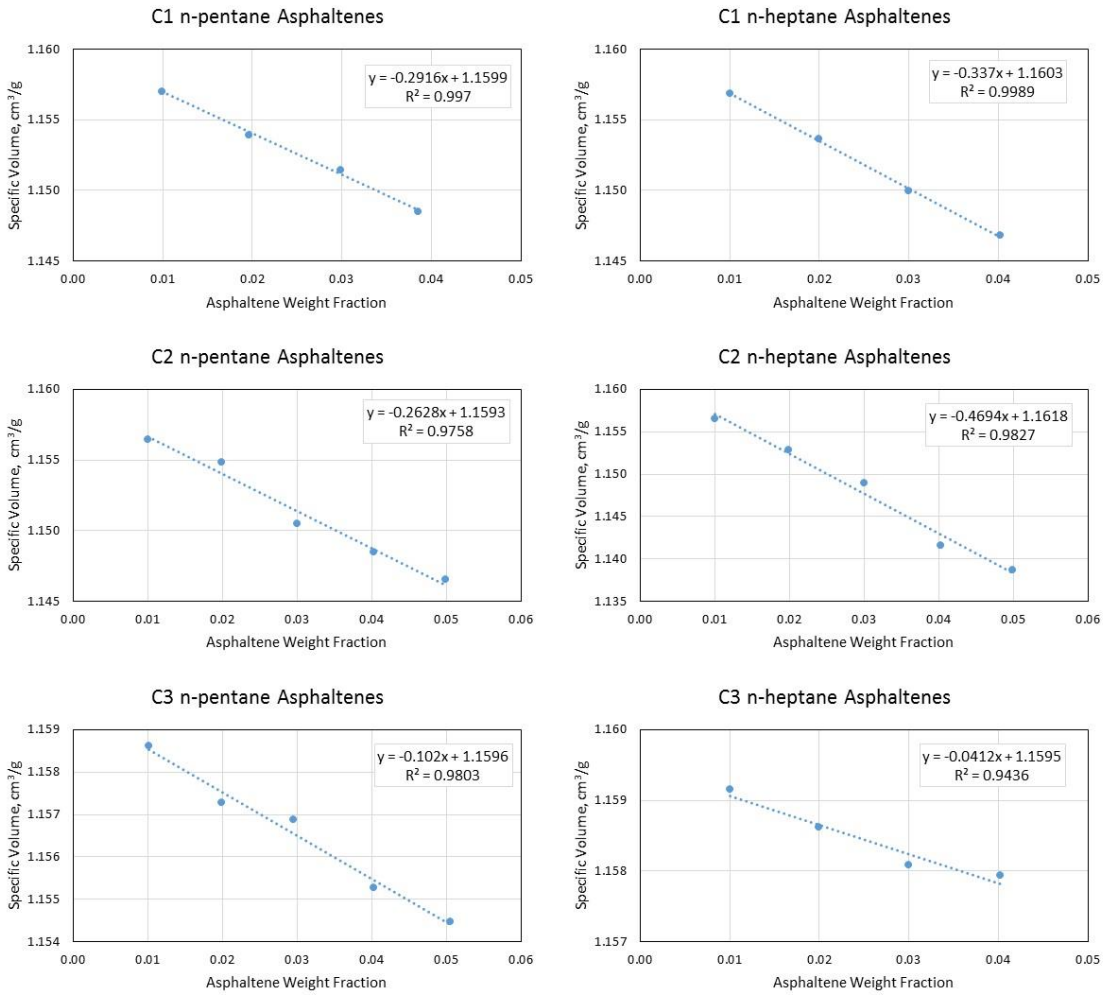

Fig. 4C-1 – Density of n-pentane and n-heptane asphaltenes determined by analyzing asphaltenes-toluene mixture.

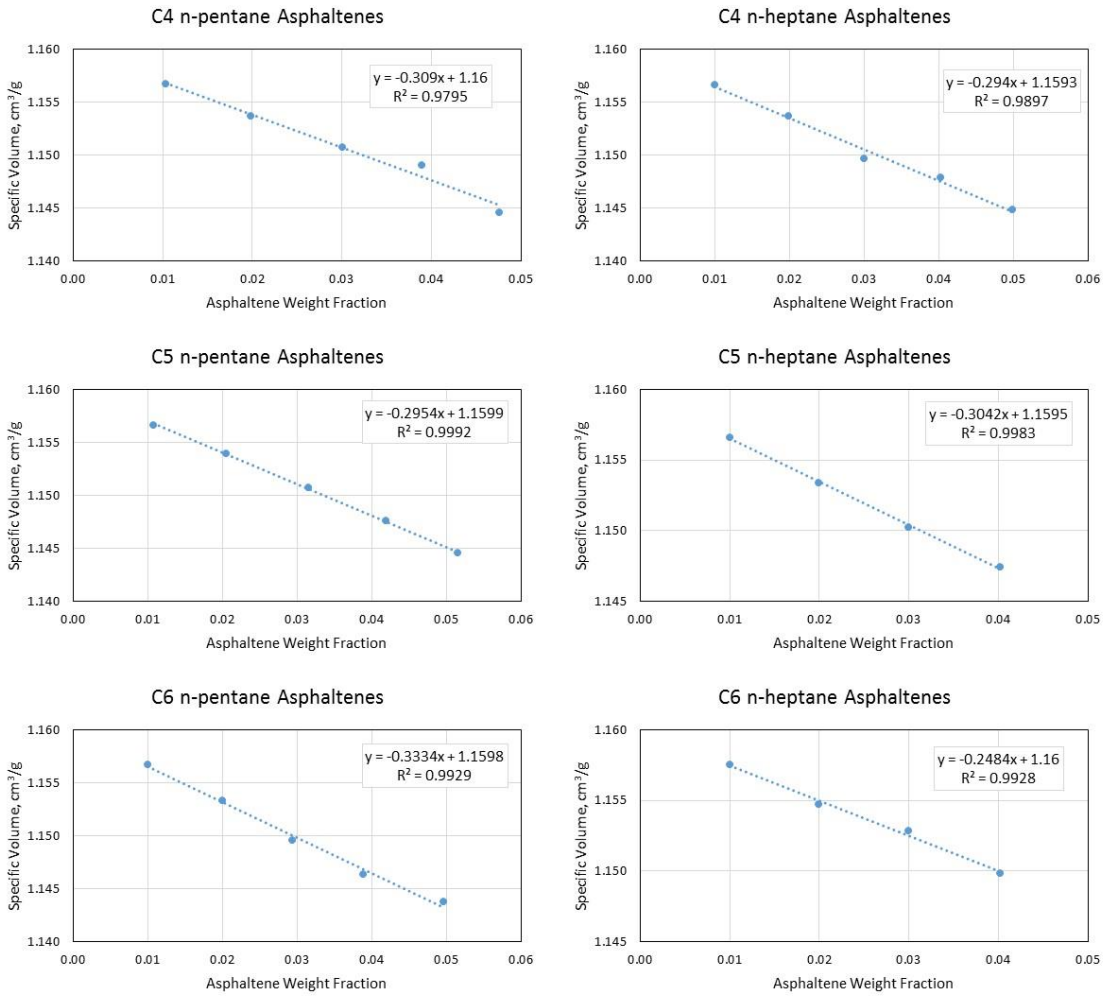

Fig. 4C-1 cont. – Density of n-pentane and n-heptane asphaltenes determined by analyzing asphaltenes-toluene mixture.

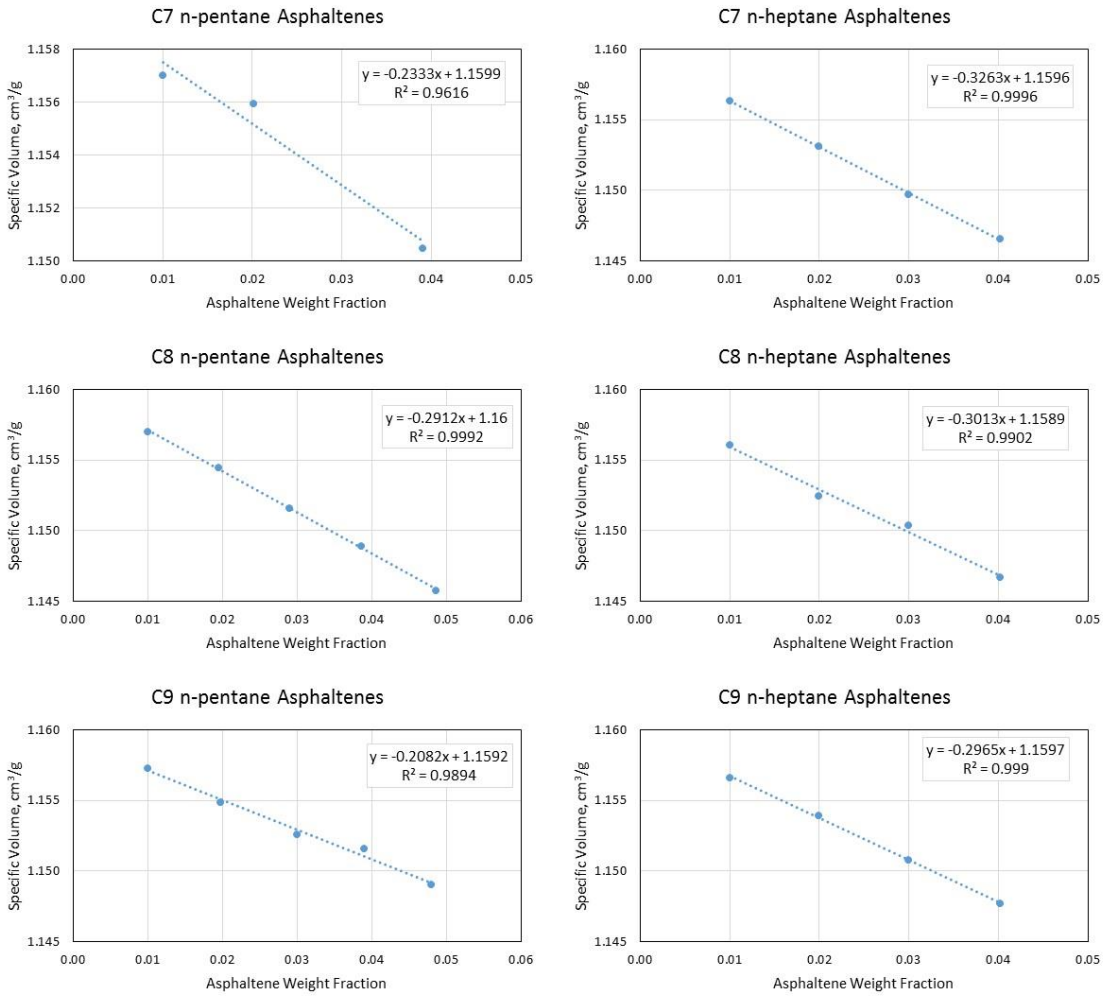

Fig. 4C-1 cont. – Density of n-pentane and n-heptane asphaltenes determined by analyzing asphaltenes-toluene mixture.

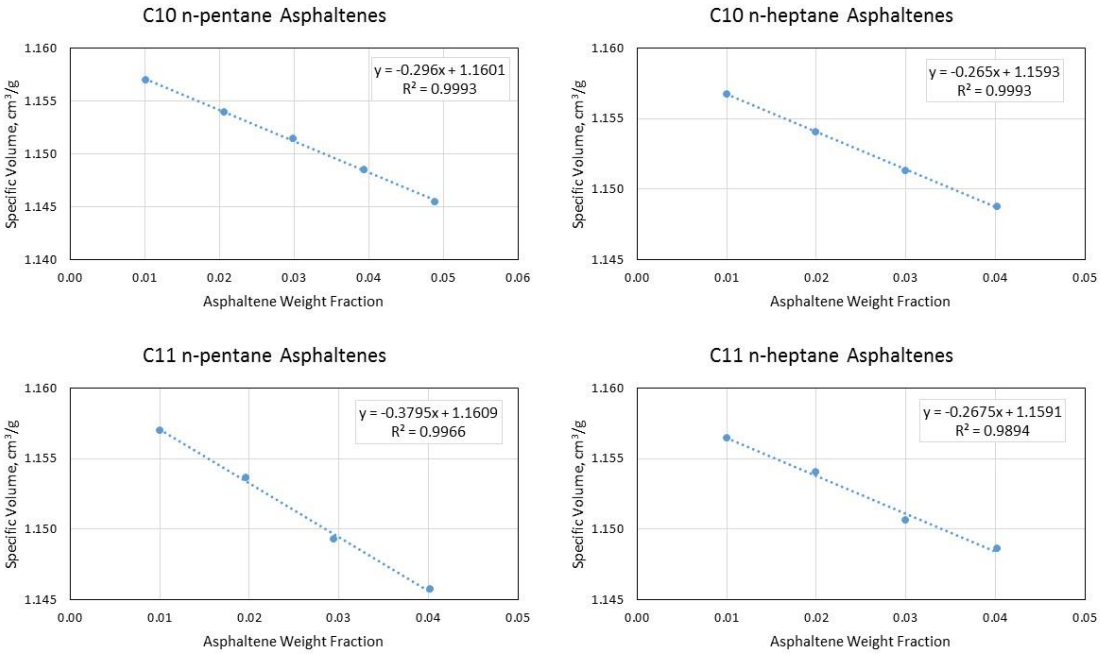

Fig. 4C-1 cont. – Density of n-pentane and n-heptane asphaltenes determined by analyzing asphaltenes-toluene mixture.

Asphaltenes-Water Mixture

Another approach used in this study to determine the density of asphaltenes is through preparation of asphaltenes-water mixtures. Specific mass of asphaltenes is measured and mixed with known mass (and volume) of water. The mixture is allowed to interact for a week to enable complete expulsion of air bubbles from the asphaltenes clusters. Weight and volume of the mixture are measured and the volumetric increase of mixture is measured. This incremental volume is considered to be the volume of asphaltenes clusters and accordingly density is estimated as the ratio of known mass of asphaltenes to its measured volume. Results corresponding to asphaltenes density measured from this method are given in Table 4C-2.

Table 4C-2 – Density of asphaltenes determined by analyzing asphaltenes-water mixture.

Asphaltenes	Density (g/cm^3)
C1	0.21
C2	1.52
C3	0.35
C4	1.55
C5	2.11
C6	0.33
C7	0.30
C8	1.11
C9	1.00
C10	1.06
C11	0.89

Appendix 4-D

Analyses to Test Statistical Significance of Analytical Correlations with Measured Mixture Dielectric Constant

To understand whether the analytically computed crude oil dielectric constant have any statistical significance with the experimentally measured values, simple regression procedure is carried and p-value were determined. It should be noted that a p-value of less than 0.05 represents statistical significance between the two parameters. In this section, the difference between crude oil dielectric constant computed from each of the analytical models as compared to the experimental values (using the data provided in Table 4.4) were compared with the experimental values. Table 4D-1 shows that the p-values for this comparison is less than 0.05, thus indicating statistical significance between the models and the measured values. It can also be observed that Lowry (1929) model has least p-value and therefore is most significantly related to the experimentally measured dielectric constant of crude oil.

Table 4D-1 – P values highlighting the significance between analytically computed and experimentally measured crude oil dielectric constant values.

Sample	Lowry (1929)	Bruggeman (1935)	Böttcher (1952)	Looyenga (1965)	Bohren and Huffman (1965)	Wu et al. (2004)
C1	0.55	0.51	1.72	0.51	0.51	0.49
C2	0.48	0.46	2.4	0.46	0.46	0.45
C3	1.59	1.39	3.98	1.41	1.36	1.32
C4	0.54	0.51	1.47	0.51	0.51	0.5
C5	0.71	0.7	2.79	0.7	0.7	0.7
C6	0.29	0.24	0.74	0.24	0.23	0.22
C8	1.93	1.93	5.21	1.93	1.93	1.93
C10	0.64	0.61	1.65	0.61	0.6	0.59
C11	1.03	0.94	2.15	0.95	0.94	0.92
p-value	**0.0029**	**0.0048**	**0.0088**	**0.0045**	**0.0053**	**0.0059**